Doctoral Theses at NTNU 2005:84

Pavel Liferov

First-year ice ridge scour and some aspects of ice rubble behaviour

NTNU
Norwegian University of
Science and Technology
Doctoral thesis
for the degree of doktor ingeniør
Faculty of Engineering Science and Technology
Department of Civil and Transport Engineering

NTNU

ABSTRACT

This thesis deals with two separate but closely connected subjects, namely: the process of first-year ice ridge scour with an emphasis on physical modelling and the mechanical behaviour of ice rubble. When drifting into shallow waters, ice ridges may scour the seabed and create a significant threat to all seabed installations such as pipelines, cables, wellheads etc. Better understanding of the scour process will enable to determine the pipeline burial depth more accurately.

Field experiments, examination of previous research and numerical work have been performed. Two in-situ medium scale ice ridge scour tests and one keel shear-off test have been carried out in the Van Mijen fjord on Spitsbergen. The tests on ice rubble that have been conducted during the last three decades have been reviewed and compared with respect to characteristic behaviour, mechanical properties and scaling. Laboratory punch tests on ice rubble have been analysed using finite element method to assess rubble behaviour and to derive its mechanical properties. A pseudo-discrete continuum model has been developed to simulate the micro-mechanical behaviour of ice rubble.

The two ice ridge scour tests revealed, under given conditions, the steady state scour process, i.e. when the scour depth does not change significantly along the scour track. This agrees well with resent laboratory tests on ice scour and, that is most important, with observations from seabed mapping in the areas that are of interest for the oil industry. Experiments showed that there are two main competing mechanisms that result in the steady state scour. They are the heave of the ridge and the destruction of the keel. Another mechanism, the compaction of the keel, could also be of importance though it is less in magnitude. Keel failure appeared to be not simultaneous, but progressive. The shear-off test has been specially designed to test the keel in the shear mode under natural conditions. The strength properties of the keel in terms of the Tresca and the Mohr-Coulomb material models were evaluated.

A number of different tests on ice rubble were done during the last three decades. An extensive review and analysis of some of these tests have been performed to examine the characteristic features of ice rubble behaviour. Particular attention has also been focused on scaling of the ice rubble strength in the reviewed tests. The primary and the secondary failure modes were outlined. The primary failure mode is associated with breakage of the initial rubble skeleton and was studied with the custom-developed pseudo-discrete continuum model. It enabled to study the correlation between the freeze bond strength in the discrete model and the equivalent cohesion in the continuum model. A non-linear Mohr-Coulomb failure envelope has been proposed to describe the rubble strength in the secondary failure mode that is associated with significant deformations and mobilization of frictional resistance.

Finite element analysis of the laboratory punch tests on ice rubble has been used to simulate the tests conducted in the laboratory and to derive the material properties. The simulations showed that the bending effect and consequently the tensile strength of ice rubble are of importance in punch tests the way they were performed in the laboratory. Direct comparison of the laboratory and the in-situ punch tests is thus not entirely correct and requires accounting for the complex deformation modes under certain boundary conditions at the laboratory testing.

ACKNOWLEDGEMENT

The time I spent working on my doctoral thesis has been the best period of my life since I left behind the ideas of establishing a fast-food kiosk and entered the university. There are four Gentlemen who made this work possible and I am very thankful to them for giving me this opportunity. Professor Karl Shkhinek from the St. Petersburg State Technical University (SPTU) first made me interested in offshore engineering and after supervised throughout my university years, including those at the University Centre on Svalbard (UNIS) and the Norwegian University of Technology (NTNU). Professor Ove Tobias Gudmestad from Statoil ASA and the Stavanger University College (HIS) supported and encouraged my first steps into the field of Arctic Offshore Engineering in Norway. Mr. Truls Mølmann, a managing director of Barlindhaug AS, has brought me to Norway despite significant resistance from immigration authorities and let me to leave (partly) the company to work on my dissertation. My supervisor Professor Sveinung Løset from NTNU has motivated the Norwegian Research Council to provide the finances for my project. He did not let me do what I now realize should not have been done and fully supported the ideas I did not even hope he would. No in-situ tests on Svalbard would have been done without him. I would also very much like to thank the following people who have made my strive easier and less lonely:

Associate Professor Knut Vilhelm Høyland from UNIS and Dr. Arnor Jensen from Barlindhaug Consult, who have been my gurus for the last four years. They also introduced my to ice rubble testing by allowing me to participate in experiments at The Hamburg Ship Model Basin (HSVA), Germany.

I learned a lot from Per Olav Moslet and Basile Bonnemaire. They made Svalbard field experiments feasible and changed my general opinion about Norwegians and French from good to best. Rune Nilsen, Sergey Vernyaev and Rinat Kamalov made me to believe that impossible is possible during the field season 2003 on Svalbard.

My co-advisor Professor Lars Grande and Professor Steinar Nordal from NTNU have tried to transfer some knowledge about soil into my head. If their efforts have been in vain it is my fault but not theirs.

Morten Bjerkås, Alex Klein Paste and Ronny Winther opened my mind by introducing me to another forms of water below the freezing point rather than ice rubble. Svetlana Shafrova has helped me with modelling when I was quite tired of it.

The Norwegian Research Council has paid my scholarship for three years. Financial supports from Statoil, Store Norske Spitsbergen Gruvekompani (SNSG), UNIS, Norwegian Polar Institute and Barlindhaug Consult AS are greatly appreciated.

CONTENTS

1 INTRODUCTION

1.1 General

Exploration, production and transportation of hydrocarbons in ice-infested waters have been an issue for engineers since the early sixties. Offshore pipelines have often been considered necessary to transport the hydrocarbons onshore and a number of potential hazards caused by the arctic environment were identified. Ice scouring of the seabed was among the major ones and a question "How deep do we have to trench the pipeline" has become crucial. Some parts of the Beaufort Sea and off the East Coast of Canada have received considerable attention with respect to the scouring phenomena. Extensive surveys were conducted resulting in statistical description of the parameters associated with ice scoring, i.e. gouge depth, width, length, orientation and frequency.

During the last decade offshore hydrocarbon fields in Northwest Russia, North American Arctic, North Caspian Sea and offshore Sakhalin have been subjected to increasing interest from the oil industry. Several pipeline projects involving crossing of areas subjected to ice scouring have also been considered, e.g. the Millennium Pipeline Project and the Baltic Pipeline System crossing respectively Lake Erie and the Baltic Sea as well as the pipeline across the Baydaratskaya Bay. In most of the above areas only the first-year ice ridges are the features that cause scouring.

Recent technological innovations yield to augmentation of the cost-effective solutions in development of the oil and gas fields. A combination of a main production, process and storage platform with simple wellhead platform or subsea production systems for the satellite fields may reduce the overall development costs. Determination of the burial depth for pipelines and seabed installations thus becomes an important issue. Reducing the risk of subsea facilities damage by ice ridges to an acceptable level and at the same time avoiding excessively conservative estimation of the burial depth requires solid knowledge about the processes associated with the ice ridge scouring.

1.2 Scope and organisation of the thesis

The intent of this thesis has been to gain increased knowledge about the first-year ice ridge scour process in general and to examine the keel-soil interaction in particular. Special attention has been focused on studying the keel-composing material further named as ice rubble or simply rubble. To accomplish this, a combination of in-situ experiments, examination of previous research and numerical modelling has been performed. The main objectives were:

(1) In-situ experiments:

- To investigate the process of ice ridge scour in-situ with focus on keel-soil interaction
- To estimate the strength of medium scale ice rubble in-situ
- To study temporal development of the internal structure of a first-year ice ridge by observing the ridge throughout its lifetime.

(2) Examination of previous research:

- To analyse and to compare the results from different tests on model and in-situ ice rubble
- To outline the characteristic rubble failure mechanisms and the material properties associated with them
- To assess scaling of ice rubble strength.

(3) Numerical work:

- To study the behaviour and to derive the mechanical properties of ice rubble from the laboratory punch tests
- To develop a numerical model that allows simulating the micro-mechanical behaviour of ice rubble.

The present work on ice rubble behaviour is a follow up of more than a decade research on first-year ice ridges and ice rubble at the department of Structural Engineering at NTNU. Prof. Sveinung Løset has initiated it in 1992 by conducting experimental program on mechanical behaviour of fresh water ice rubble. Dr. Knut V. Høyland has followed it up with respect to consolidation in first-year sea ice ridges and Dr. Arnor Jensen continued in the area of mechanical tests on ice rubble.

The content of the thesis is represented by an introductory chapter and eight papers submitted to or accepted in international journals and conference proceedings.

Chapter 2 gives an overview of the challenges associated with the design of pipelines in the areas subjected to ice scouring. Existing approaches in assessment of the pipeline burial depth are briefly discussed.

Chapter 3 describes and discusses the in-situ ice ridge scour experiments that were conducted in the Van Mijen fjord on Spitsbergen during the years 2002 and 2003. This chapter consists of three papers and Dr. Knut V. Høyland is the principal author of one of them that deals with consolidation and physical properties of ice ridges.

Chapter 4 deals with analysis of behaviour and strength of ice rubble. This chapter consists of five papers. It gives a review of the ice rubble testing methods with emphasis on interpretation of results and approaches to describe and constitute its characteristic behaviour. Punch tests on ice

rubble conducted basically in the Large Ice Tank at the Hamburg Ship Model Basin (HSVA) in Hamburg, Germany were analysed. Finite element modelling was used to simulate the rubble behaviour and to derive its equivalent continuum strength properties. Dr. Arnor Jensen is the principal co-author of the two papers on analysis of punch tests as the initiator and the leader of the testing program at HSVA.

Chapter 5 concludes the study and makes recommendation for further work within the realm of first-year ice ridge scour and ice rubble mechanics.

1.3 Readership

The present work deals with ice scouring - one of the environmental phenomena that may significantly affect the design of submarine pipelines in the ice-infested waters. A large piece of attention has been given to studying ice rubble as there was (and still is) incomplete knowledge about its mechanical properties. The primary readership targets for this thesis as a whole and for some particular parts are engineers and scientists working with:

- Hydrocarbon field development in ice-covered waters
- Submarine pipeline design in the areas subjected to ice scouring
- Design of any kind of structures subjected to loads from ice rubble
- Ice research with focus on first-year sea ice ridges
- Operations that involve field activities on the ice.

2 REVIEW OF DESIGN ISSUES FOR SUBMARINE PIPELINES IN THE AREAS SUBJECTED TO FIRST-YEAR ICE RIDGE SCOUR

2.1 Introduction

Submarine pipelines in ice-covered seas have been under consideration for more than 25 years, but very few have actually been built. One reason for this is that petroleum prices have not increased as fast as had been expected, but another is that it has turned out to be several technical difficulties associated with ice scour, strudel scour, marine permafrost, upheaval buckling, leak detection and possible repair (Palmer, 2000). Nevertheless, in the recent years a number of pipeline projects in the areas subjected to ice scour have been accomplished. The design of the recently built Northstar offshore pipeline in the Alaskan Beaufort Sea has been presented by Nogueira and Paulin (1999). A strategy for the pipeline burial depth determination for the pipeline to the Piltun-Astokhskoe field off the Sakhalin Island has been described by Alekseev et al. (2001). At the moment, there are more pipeline projects to be realized in the ice-scoured areas. The following sections give a brief overview of the items that are of importance for the design of submarine pipelines in the areas subjected to first-year ice ridge scouring.

2.2 First-year ice ridges

A characteristic feature of ice-covered waters is the presence of ice ridges. They are formed by compression or shear in the ice cover and are often found in the shear zone between the landfast ice and the drift ice. A high ridging intensity may also be found in straits and sounds with strong currents. Ice ridges are in general long and curvilinear, i.e. they are three-dimensional features. Ridges often exist in combination with rafted ice and this combination is named a ridge field. When a ridge or a ridge field becomes grounded it forms a stamukha. Normally, there are substantially less stamukhas than ice ridges in the ice cover. The most common method to categorize ridges is based on the age of the ridge – either first-year or multi-year ridges. In the present review only the first-year ice ridges will be addressed. When drifting into the shallow waters, ice ridges may scour the seabed and create a significant threat to all seabed installations such as pipelines, cables, wellheads etc.

A typical section of the first-year ice ridge is schematically shown in Fig. 2.1. Morphology and shapes of the first-year ice ridges is given by e.g. Leppäranta and Hakala (1992), Timco and Burden (1997), Bonnemaire et al. (2003). One of the most extensive published studies of ice ridges and stamukhas is given by Astaf'ev et al. (1997) based on the data from the Sea of Okhotsk off the

Sakhalin Island. A first-year ice ridge consists of the sail, the consolidated layer and the keel. The keel is a part of a ridge that may scour the seabed if the contact occurs.

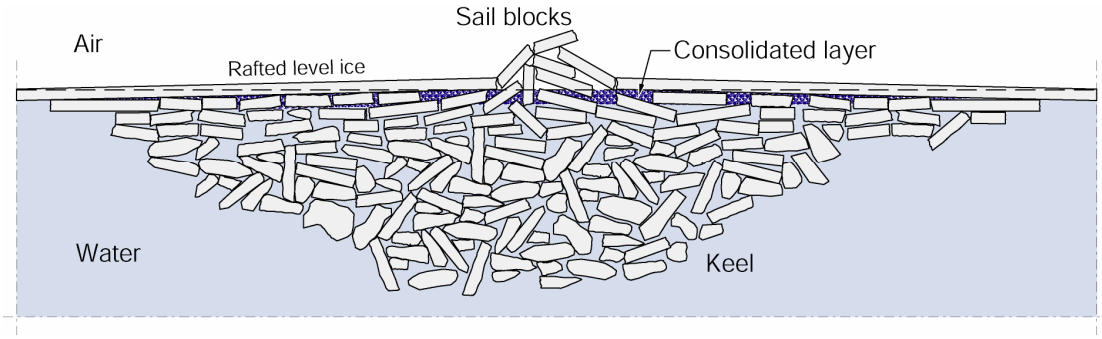

Fig. 2.1. Schematic section of cross-section of a first-year ice ridge.

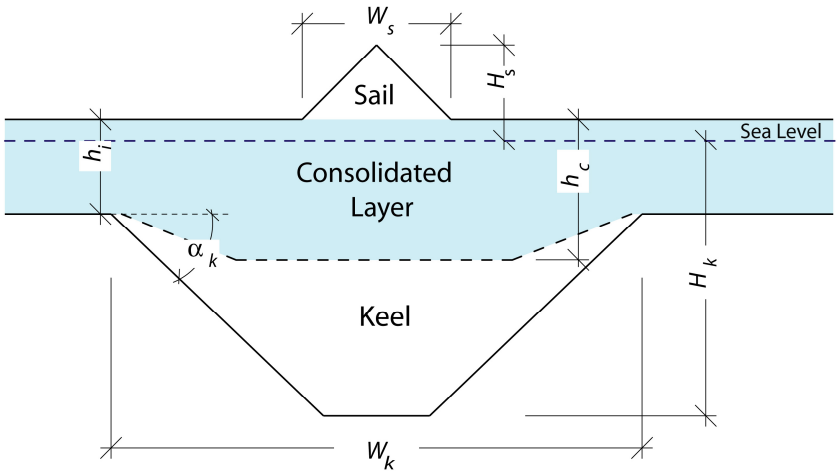

Fig. 2.2. Geometric parameters describing a typical first-year ice ridge.

The basic geometrical parameters that describe the shape of a typical first-year ice ridge are illustrated in Fig. 2.2. Timco and Burden (1997) reported the following best-fit linear relationships between the keel depth H_k, the sail height H_s and the keel width W_k based on analysis of 112 first-year ice ridges:

$$H_k = 3.95H_s \tag{2.1}$$

$$W_k = 3.91H_k \tag{2.2}$$

The keel angle α_k has a mean value of 26.6º (Timco and Burden, 1997). Surkov (2001) reported that a mean keel angle for the triangular ridges and trapezoidal ridges off the Sakhalin Island is 24º and 26º, respectively. Several well known distribution functions such as lognormal, Weibull, Gumbel and Gamma are often used to describe distributions of the geometric parameters of ice ridges.

Information on ridge frequency has important implication for determining the number of keels that will scour a seabed during a certain period of time. A large number of investigations have been made to measure ridge spacing, primarily using laser profilers, upward-looking laser and stereo photographic methods. Analysis of this data has suggested that negative exponential and lognormal distributions fit well for the distribution of keel spacing (Wadhams et al. 1985; Davis and Wadhams, 1995).

The keel of a first-year ice ridge consists of ice rubble – ice blocks with water/slush-filled voids. Fig. 2.3 gives a photo of ice rubble in the keel of a ridge in the Barents Sea taken by the underwater camera.

Fig. 2.3. Ice rubble in the keel of a ridge in the Barents Sea (year 2002).

There have been a few direct measurements of the macro-porosity of the sail and the keel parts of first-year ice ridges. Porosity of the keel has a direct influence on the strength of ice rubble and consequently on the scour process. Porosity of the keel was reported in a range between 0.25 and 0.45. Grishenko (1988) reported that porosity depends on the thickness of ice blocks composing the rubble. Summarizing his results, the following relationship between the porosity η and the block thickness T [m] can be outlined:

$$\eta = 0.11 \ln T + 0.37 \tag{2.3}$$

Surkov (2001) also reported that the linear porosity, i.e. based on the drilling measurements, is 15 - 25 % less than the volumetric porosity. Porosity, as well as the thickness of pores tends to increase towards the bottom of the keel (Bonnemaire et al., 2003). The same study reports the internal morphology of the ridge. The purpose was to investigate the dimensions of ice blocks in the rubble. Along the sail of the ridge, 80 blocks were randomly chosen and observed. The length, width, thickness and angle of vertical inclination were measured. Looking at the repartition of the blocks thickness shown in Fig. 2.4, three groups can be distinguished; around 0.3, 0.6 or 0.9 m thick blocks; 40 % of the observed blocks were 0.30 to 0.35 m thick, 24 % 0.5 to 0.7 m and 21 % 0.8 to 1.0 m. Most of the sail blocks were observed to come from rafting of 0.3 m thick level ice. Fig. 2.5 shows the average width, length and inclination for the different groups of blocks. On average the blocks were 0.57 m thick, 1.6 m wide, 2.5 m long and inclined of 39.8º to the horizontal plane. This gives us a *L*/*W*/*T* ratio (Length/Width/Thickness ratio) of 4.4:2.1:1. This ratio varies from 5:3.7:1 for the "0.3 m thick" group, to 5:2.9:1 for the "0.6 m thick" group and to 3.7:2.3:1 for the bigger blocks. It is seen also that the bigger blocks are, the less inclined they are.

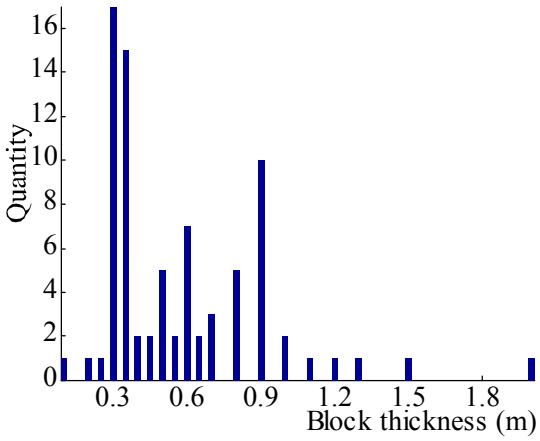

Fig. 2.4. Thickness frequency of the chosen blocks (Bonnemaire et al., 2003).

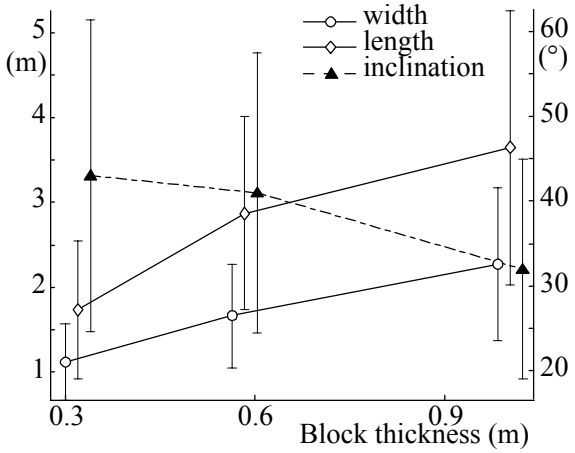

Fig. 2.5. Width, length and inclination for the different thickness groups (Bonnemaire et al., 2003)

The strength of ice rubble, including overview of testing methods and modelling approaches, is addressed in Chapter 4 of this thesis. Generally, the rubble strength is treated using soil mechanics concepts as derived for granular materials which leads to a strength description based on friction angle and cohesion (Timco et al., 2000). The Mohr-Coulomb relation is thus frequently used to describe the ice rubble properties:

$$\tau = \sigma \tan \varphi + c \tag{2.4}$$

where τ and σ are the shear and normal stresses on the failure plain respectively, φ is the angle of internal friction and c is the cohesion. Sometimes, ice rubble is described as the Tresca, or frictionless Mohr-Coulomb material implying that φ is zero. In turn, cohesionless description is also used so that c is zero.

2.3 Ice Scour

Ice scour is a phenomenon that occurs when an ice body moves while in contact with the bed of a water basin. This is a widespread feature of most of the coastal regions and interior water basins of the northern continents. During the scour process deep gouges in the seabed can be formed. Their depth, depending on the type of scour, may exceed 5 m. Fig. 2.6 shows an image of the Beaufort Sea seabed to illustrate the result of the scour processes. Ice scour poses one of the main threats to the bottom-based facilities and is therefore one of the key design issues.

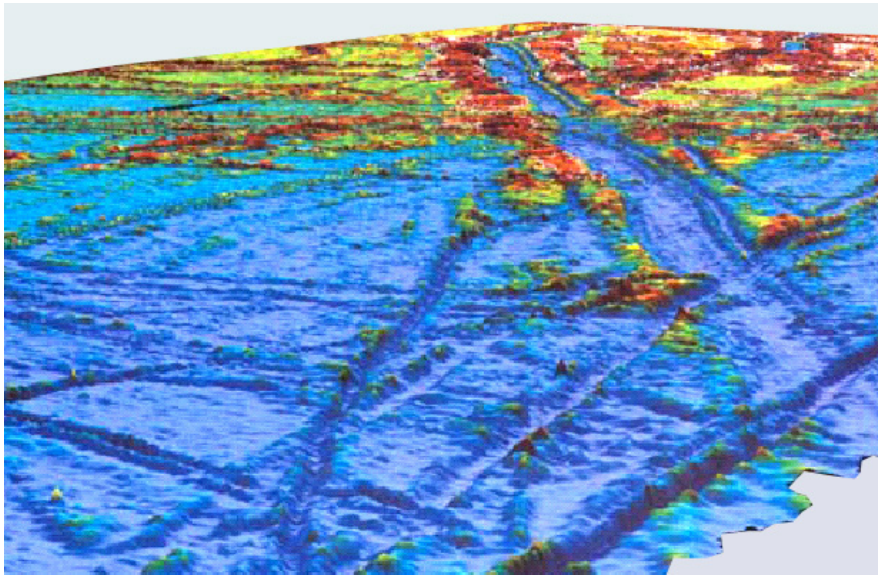

Fig. 2.6. Multi-beam in the Beaufort Sea (Image source: Ibrahim Konuk, Geological Survey of Canada).

An iceberg, an ice ridge, or individual ice floes may represent such an ice body. There is a certain distinction between scouring of the seabed (this name will be used further to refer the bed of any water basin) by the different types of ice features. Scouring of the seabed by individual ice floes and rafted ice may take place in the near-shore areas during the ice storms in the winter and the break-up period. This phenomenon shall be particularly evaluated when considering the pipeline shore crossing.

In those areas where iceberg invasion is possible the iceberg scour is the major threat to the seabed installations. Typical iceberg shapes and sizes presented by Chari (1979) show that iceberg scouring occurs in water depths beyond 40 m. Icebergs travel at relatively small velocities but because of their huge mass, the kinetic energy is high. Grounding of an iceberg and dissipation of its kinetic energy can occur in either of the following two ways or their combination. One is by a conservation of the kinetic energy to the potential energy when the berg contacts a hard, sloping seabed and travels along the slope. The second is by a horizontal ploughing action when it meets a slope of soft sediments. The strength of icebergs is high compared to that of the typical seabed sediments. The berg can therefore be considered as a solid indentor in the scour process.

Ice ridge scour, as illustrated in Fig. 2.7, is a phenomenon that takes place in water depths up to 45 m. It can be distinguished by the type of ice ridges that scour the seabed to be either first-year or multi-year. This distinction is done because of the following two reasons: first of all, from the morphological and mechanical points of view multi-year ice ridges are more likely to be regarded as small icebergs (i.e. solid body) due to their high degree of smoothness and consolidation (Kovacs, 1983). First-year ice ridges and their keels in particular are much less consolidated than multi-year ridges and this makes them to behave differently during scouring. And secondly, in many areas that are of interest for the oil industry only first-year ice ridges exist.

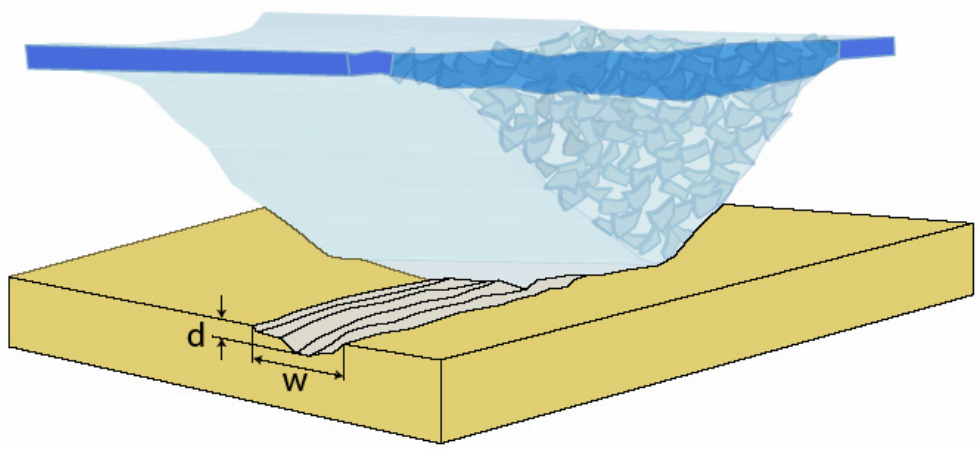

Fig. 2.7. Ice ridge scour illustration.

Among a variety of different scour scenarios, it is possible to distinguish between the following two general cases:

Case 1: A separate ice ridge scours the seabed. After grounding and slowing down, it will most likely be contacted by the surrounding ice floes.

Case 2: An ice ridge is confined within large ice field. During the process of grounding, the ice ridge is slowed down and the surrounding ice field pushes it forward. As a matter of fact, the

presence of the surrounding ice field may also play an important role in controlling the heave of the ice ridge during scouring process. This effect has been accounted for in the model developed by Been et al. (1990). Three scenarios of further process may be proposed (adopted from the ice – structure interaction diagram after Løset et al., 1998):

Limit Momentum - Ice ridge and the surrounding ice floe are stopped; no more kinetic energy is available.

Limit Force - Failure takes place on the border between the ridge and the surrounding ice floe. Ice ridge is grounded and the ridging process continues.

Limit Stress – soil or/and keel undergo deformation and the process continues until one of the above two scenarios takes place or the ice drift changes direction such that the ridge gets off the ground.

Surkov (2000) discusses the two general cases as indicated above with respect to the ice scouring of the north-eastern shelf off the Sakhalin Island and observed that Case 1 is typical for the spring period when ice ridges have reached their maximum dimensions. Case 2 is more usual in the beginning of the ice season. However, at this time the ice ridges are far below their maximum dimensions.

On the other hand, Case 2 may be more representative for the areas with multi-year ice. Shearer et al. (1986) describe observations done during the late summer of 1983, when a large number of vast, thick, second-year ice features known as hummock fields were driven into the southern Canadian Beaufort Sea. One particular ice feature designated as E1 was observed and the scour track made by E1 was later surveyed. E1 was a multi-year hummock contained in a larger first year ice sheet and it produced a 13 km scour with a maximum depth of 3 meters.

The main method to protect pipelines and other seabed installations from moving bodies of ice is to bury them down into the seabed. A design of subsea installations in the areas subjected to scouring therefore has to involve a determination of the necessary burial depth. This depth shall minimize the risk of pipeline damage by ice to an acceptable level. Principal issues related to determination of the safe burial depth are briefly discussed in the subsequent sections.

2.4 Scour depth prediction

There exist three alternatives to predict the main scour characteristics (depth, width, length, orientation as well as spatial and temporal frequencies) for a given location:

Repetitive mapping of the seabed

Ice scour modelling

A combination of those above.

Determination of the main scour characteristics from the seabed mapping, though attractive, requires a multi-year survey and may yield unreliable results in case when significant backfilling of scours exists, i.e. their residence time is short. McKenna et al. (2003) addressed the key elements of the ice scour depth prediction from the repetitive mapping and major challenges associated with this method.

The second alternative is based on the imitational modelling (probabilistic) of scour events for an area under consideration. An ice scour model (deterministic) is a core of this method. Whether it is realistic or not will to a large extent govern the accuracy of the obtained results.

The third alternative exists as none of the first two are reliable enough. The repetitive mapping and the ice scour modelling shall therefore supplement each other to achieve the best possible results.

One of the most well known methods for computing scour depths was given in the pioneering work of Weeks et al. (1983). After examining ice gouge data collected by the U.S. Geological Survey between 1972 and 1979 they found that the probability distribution of gouge depths in the Alaskan Beaufort Sea is well approximated by a negative exponential function. It was later found that the negative exponential distribution fits well the data from other regions as well, e.g. the Sea of Okhotsk (Alekseev et al., 2001). That is, the probability density function of scour depths can be given in the following form:

$$p(x) = \lambda \, \mathrm{e}^{-\lambda(x-c)} \;\; ; \;\; \mathrm{x} > \mathrm{c} \tag{2.5}$$

where x is scour depth, λ is the distribution parameter and c is the system resolution/cutoff for measuring scour depth (for Weeks' data c = 0.2 m). The "best estimator" for the exponential parameter is simply the reciprocal of the sample mean minus cutoff:

$$\lambda = 1/(\overline{x} - c) \tag{2.6}$$

Weeks et al. (1983) also obtained a formula for computing design gouge depths for pipelines. For a given linear route with a length L having linear scour encounter rate of G gouges per km per year, one would expect, on average, GLT new gouges along this route in T years. The exceedence probability for scour depth d corresponding to a return period T is:

$$E(d) = 1/GLT \tag{2.7}$$

Assuming an exponential distribution, the design scour depth for any particular pipeline segment or zone is:

$$d = c + \ln(GLT)/\lambda \tag{2.8}$$

Some modifications and refinements to the above approach have been done by e.g. Wang (1990), Lever (2000) and Surkov (2001).

Similar approach to predict the design scour depth can be used when such parameters as the gouge depth distribution and frequency are determined from the imitational modelling. Chari (1979) has proposed the first deterministic model for iceberg scour. The basic idea of this energy model is the following: the work done by motion against soil resistance F_s equals to the iceberg's kinetic energy E_k dissipated plus the work done on the iceberg by wind and current drag forces F_d as the iceberg is slowed down:

$$E_k = \int_o^l (F_s - F_d) dl \tag{2.9}$$

From Eq. 2.9 it is possible to determine the scour length l and hence the scour depth d for a given pipeline segment. Ice scour models and modelling, both physical and numerical, have been later addressed by e.g. Abdelnour and Graham (1984), Been et al. (1990), Kioka and Saeki (1995), Yang and Poorooshasb (1997), and Barker and Timco (2002). All deterministic scour models are very sensitive to how the soil resistance is computed. Idealization of the keel shape, boundary wedges and speed effects are among the items that require particular attention.

Imitational modelling requires information about bathymetry, geotechnical and metocean condition. Probability distribution functions for the following key parameters must be available:

Speed and direction of ice drift

Size of drifting ice formation (mass characteristics)

Sail height (keel depth)

Keel sheltering (when several keels may be present within the same ice floe and only the deepest can contact the seabed).

Liferov (1999) used simplified probabilistic modelling to predict the scour depths in the Eastern Barents Sea and Surkov (2001) used the complex imitational modelling to determine the pipeline burial depth in the Sea of Okhotsk.

2.5 Sub-scour soil deformations

It has been relatively recently realized that a pipeline trenched below the maximum scour depth is not necessarily safe. Scouring by an ice keel results in large sub-scour horizontal and vertical soil deformations, and these deformations will transmit loading to any buried structure that is stiffer than the surrounding soil (Nixon et al., 1996). Subgouge soil deformations will therefore play a significant role in determination of a safe pipeline burial depth. Forces transmitted through the soil

and soil displacements around the pipeline could load the pipeline to failure if not taken into account in design as illustrated in Fig. 2.8.

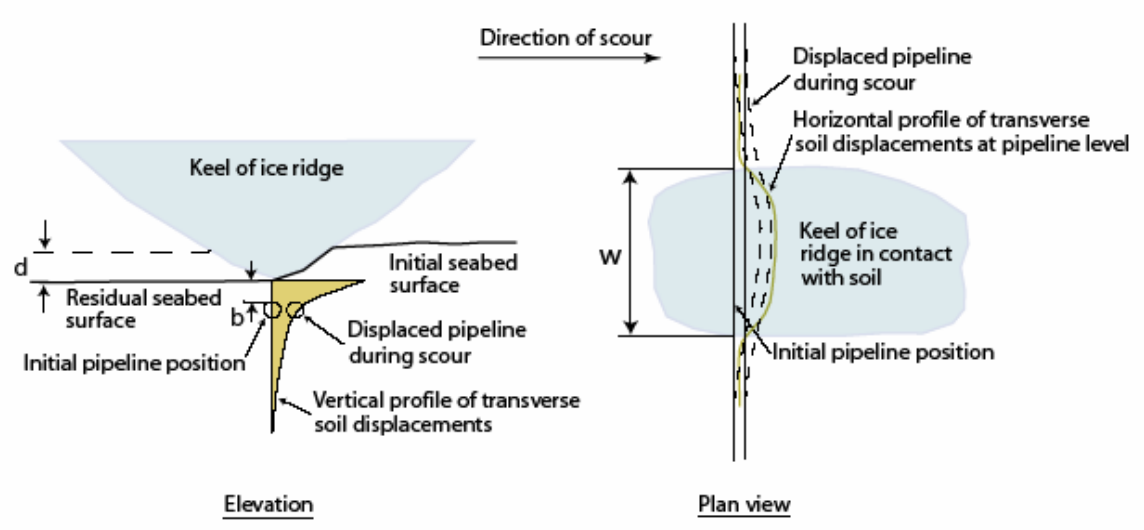

Fig. 2.8. Illustration of sub-scour soil deformations and pipeline response.

The subject of sub-scour soil deformations and pipeline response has been addressed in several studies (Palmer et al., 1990; Clark et al., 1994; Nixon et al., 1996; Woodworth-Lynas et al., 1996; Kenny et al., 2000; Konuk and Gracie, 2004). The pipeline response model was derived to establish functional relationships between the pipeline state and the gouge characteristics. The agreement on the magnitude of sub-scour soil deformations is, however, quite incomplete so far. More efforts should be focused on determining the effect of different soils on sub-scour deformations. Pipeline response and effect of the trench infill material also require further investigations.

2.6 Pipeline burial depth

Having known the scour depth d and width w distributions as well as the frequency for a given pipeline route and the pipeline response to the scour event, it is then possible to determine the optimal pipeline burial depth D_b as:

$$D_b = d + b \tag{2.10}$$

where d is the scour depth and b is the cover depth.

Significant factors in pipeline design include cost minimization and the satisfaction of target safety levels. These can be achieved through optimum route selection and optimum cover depth along various sections of the route (Kenny et al., 2000). Through knowledge of economic and

geotechnical data, the overall risk of pipeline failure for a proposed route can be apportioned to minimize trenching costs.

The probability of exceedence p for gouge depth and width can be estimated either from the seabed survey or from the imitational modelling as was discussed in Section 2.4. The annual probability of exceedance P is then determined by combining the corresponding distributions with the scour encounter rate for a given pipeline section g:

$$P(d,w) = g \cdot p(d,w) \tag{2.11}$$

The pipeline response model defines a relationship between the pipeline strain ε and stress σ, the gouge depth and width and the cover depth, i.e. $\varepsilon,\sigma(d,\ w,\ b)$. This allows relationships to be established for annual probability of exceedence of pipeline strain and stress for given cover depth, i.e. $P(\varepsilon,\sigma \mid b)$. The final step is an iterative process to determine the appropriate cover depth, where the computed pipeline strain or stress responses equal the allowable limits as defined by the appropriate design codes and standards.

2.7 References

Abdelnour, R. and Graham, B., 1984. Small scale tests of sea bottom ice scouring. Proceedings of the 7th Ice Symposium. Hamburg, Germany, Vol. ?, pp. 267-279.

Alekseev, J.N., Afanas'ev, V.P., Litonov, O.E., Mansurov, M.N., Panov, V.V. and Truskov, P.A., 2001. Ice aspects of offshore oil and gas field development. Gidrometeoizdat, St.Petersburg, Russia, 356 p. (in Russian)

Astaf'ev, V.N., Surkov, G.A. and Truskov, P.A., 1997. Ice ridges and stamukhas of the Okhotsk Sea. Rosneft-Sakhalinmorneftegaz, 197 p. (in Russian)

Barker, A and Timco, G., 2002. Laboratory experiments of ice scour processes: buoyant ice model. Cold Regions Science and Technology, 36: 103-114.

Been, K., Kosar, K., Hachey, J., Rogers, B.T. and Palmer, A.C., 1990. Ice Scour Models. Proceedings of the Ninth International Conference on Offshore Mechanics and Arctic Engineering Conference. Huston, USA, Vol. 5, pp. 179-188.

Bonnemaire, B., Høyland, K.V., Liferov, P. and Moslet, P.O., 2003. An ice ridge in the Barents Sea, Part I: Morphology and physical parameters in-situ. Proceedings of the 17th International Conference on Port and Ocean Engineering under Arctic Conditions. Trondheim, Norway, Vol. 2, pp. 559-568.

Chari, T.R., 1979. Geotechnical aspects of iceberg scours on ocean floors. Canadian Geotechnical Journal, Vol. 16, No. 2: 379-390.

Clark, J.I., Paulin, M.J., Lach, P.R., Yang, Q.S. and Poorooshasb, H., 1994. Development of a design methodology for pipelines in ice scoured seabeds. Proceedings of the 13th International

Conference on Offshore Mechanics and Arctic Engineering Conference. Houston, USA, Vol. 5, pp. 107-125.

Clark, J.I., Phillips, R. and Paulin, M.J., 1998. Ice scour research for safe design of pipelines. Proceedings of the 13th International Symposium on Okhotsk Sea & Sea Ice. Mombetsu, Japan, pp. 1-8.

Davis, N.R. and Wadhams, P. 1995. A Statistical Analysis of Arctic Pressure Ridge Morphology. Journal of Geophysical Research 100, pp. 10915-10925.

Grishenko, V.D., 1988. Morphological characteristics of ice ridges in the Arctic basin. Proceedings of the AARI, Vol. 401, Leningrad, pp. 46-55. (in Russian)

Kenny, S., Phillips, R., McKenna, R.F., Clark, J.I., 2000. Response of buried arctic marine pipelines to ice gouge events. Proceedings of ETCE/OMAE2000 Joint Conference. New Orleans, USA, pp. 1-8.

Kioka, S. and Saeki, H., 1995. Mechanisms of ice gouging. Proceedings of the fifth International Offshore and Polar Engineering Conference. The Hague, Netherlands, pp. 398-402.

Konuk, I. and Gracie, R., 2004. A 3-Dimensional eulerian FE model for ice scour. Submitted to the International Pipeline Conference. Calgary, Alberta, Canada.

Kovacs, A., 1983. Characteristics of multi-year pressure ridges. Proceedings of the 7th International Conference on Port and Ocean Engineering under Arctic Conditions. Helsinki, Finland, Vol. 3, pp. 173-182.

Lever, J.H., 2000. Assessment of the Millennium Pipeline Project, Lake Erie Crossing. USA Cold Regions Research and Engineering Laboratory, ERDC/CRREL Report TR-00-13.

Leppäranta, M. and Hakala, R., 1992. The structure and strength of first-year ridges in the Baltic Sea. Cold Regions Science and Technology, 20: 295–311.

Liferov, P., 1999. Pechora Sea – Pipeline Study. M.Sc thesis. Statoil, Stavanger, Norway.

Løset, S., Shkhinek, K. and Høyland, K.V., 1998. Ice physics and mechanics. Norwegian University of Science and Technology, Trondheim, Norway, 101 p.

McKenna, R., King, T., Brown, R., Bruce, J. and Phillips, R., 2003. Ice gouge risk to offshore pipelines – making the most of available data. Proceedings of the 17th International Conference on Port and Ocean Engineering under Arctic Conditions. Trondheim, Norway, pp. 689-698.

Nixon, J.D., Palmer, A. and Phillips, R., 1996. Simulations for buried pipeline deformations beneath ice scour. Proceedings of the 15th International Conference on Offshore Mechanics and Arctic Engineering Conference. Florence, Italy, Vol. 5, pp. 383-392.

Nogueira, A.C. and Paulin, M., 1999. Limit state design for Northstar offshore pipeline. Offshore magazine, September 1999, pp. 146-…196.

Palmer, A.C., 2000. Are we ready to construct submarine pipelines in the Arctic? Proceedings of the Offshore Technology Conference. Huston, USA, paper No. OTC 12183.

Palmer, A.C., Konuk, I., Comfort, G. and Been, K., 1990. Ice gouging and safety of marine pipelines. Proceedings of the 22nd Annual Offshore Technology Conference. Huston, USA, pp. 235-244.

Shearer, J., Laroche, B. and Fortlin, G., 1986. Canadian Beaufort Sea 1984 repetitive mapping of ice scour. Environmental Studies Revolving Fund Report 032, ? p.

Surkov, G.A., 2001. Scientific-methodological basis of determination of loads on offshore structures from ice ridges. Doctor of Science dissertation. VNIIGAZ, Moscow, Russia, 383 p. (in Russian)

Timco, G.W., Croasdale, K. and Wright, B., 2000. An overview of first-year sea ice ridges. PERD/CHC report 5-112, 159 p.

Timco, G.W. and Burden, R.P., 1997. An analysis of the shapes of sea ice ridges. Cold Regions Science and Technology, 25: 65–77.

Wadhams, P., McLaren, A.S. and Weintraub, R. 1985. Ice Thickness Distribution in Davis Strait in February from Submarine Sonar Profiles. Journal of Geophysical Research, 90(C1), pp. 1069-1077.

Wang, A.T., 1990. Numerical simulations of rare ice gouge depths. Journal of Cold Regions Science and Technology, 19: 19-32.

Weeks, W.F., Barnes, P.W., Rearic, D.M. and Reimnitz, E., 1983. Statistical aspects of ice gouging on the Alaskan Shelf of the Beaufort Sea. USA Cold Regions Research and Engineering Laboratory, CRREL Report 83-21.

Woodworth-Lynas, C.M.L., Nixon, J.D., Phillips, R. and Palmer A.C., 1996. Subgouge deformations and the safety of Arctic marine pipelines. Proceedings of the 28th Annual Offshore Technology Conference. Huston, USA, pp. 235-244.

Yang, Q.S. and Poorooshasb, H.B., 1997. Numerical modelling of seabed ice scour. Computers and Geotechnics, Vol. 21, No. 1: 1-20.

3 IN-SITU ICE RIDGE SCOUR TESTS

3.1 Introduction

This chapter describes the in-situ medium scale ice ridge scour experiments. They have been conducted in the Van Mijen fjord on Spitsbergen during the years 2002 and 2003. The main reasons that motivated the field activities described in this chapter are summarised below:

1. *Lack of any field experimental database on first-year ice ridge scour.* There are evidences of gouges in the seabed, three decades of theoretical work on ice scouring and a number of small scale tests done with artificial solid indenters, but not anything that could closely resemble the natural first-year ice ridge scour process.

2. *To study the keel behaviour during the scour process.* Historically, iceberg scour has first been addressed in the research programmes. Icebergs were considered as non-deformable bodies at the interaction with the seabed. Keels of the multi-year ridges were also treated as solid indenters while scouring the seabed. Similar approach has naturally passed over to the first-year ice ridge scouring that is not entirely correct and may result in excessively conservative estimate of the gouge depth. There are areas where one might expect deeper scours, but nothing significant is seen, e.g. offshore Sakhalin and Melville Island (note by Dr. A. Palmer at the discussion session at the 2nd Ice Scour & Arctic Marine Pipelines Workshop in Mombetsu, Japan, 2000). One of the reasons for this is, as the author believed, the partial destruction of the keel during the scour process.

3. *To study temporal development of the first-year ridge in-situ from the day of creation with focus on the initial phase of consolidation.*

This chapter consists of three papers, each composing a section. Dr. Knut V. Høyland is the principal author in one of them that deals with consolidation and physical properties of ice ridges. Sections 3.2 and 3.4 are identical to the reviewed papers. Section 3.3 is essentially based on the referred paper with minor corrections present.

Publication references:

(3.2) Liferov, P. and Høyland, K.V. (2004). In-situ ice ridge scour tests: Experimental set-up and basic results. Journal of Cold Regions Science and Technology, 40/1-2: 97-110.

(3.3) Liferov, P., Løset, S., Moslet, P.O., Bonnemaire, B. and Høyland, K.V. (2002). Medium scale modelling of ice scouring, Part I: Experimental set-up and basic results. Proceedings of the 16th

International Symposium on Ice (IAHR'02), Dunedin, New Zealand, December 2002, vol. 2, pp. 86-94.

(3.4) Høyland, K.V. and Liferov, P. (2004). On the initial phase of consolidation. Journal of Cold Regions Science and Technology, 41/1: 49-59.

3.2 In-situ ice ridge scour tests: Experimental set up and basic results

Pavel Liferov[1,2] and Knut V. Høyland[3]

Abstract

An in-situ program was carried out in the Van Mijen fjord on Spitsbergen during the 2002 and 2003 winter seasons to investigate the ice ridge scour process. Two ice scour tests and one shear off test were performed. Ice ridges with dimensions of up to 4.0 × 4.0 × 2.45 m were artificially made by cutting the level ice into pieces to produce ice rubble. The ridges were left to consolidate for up to four weeks and then pulled towards the beach scouring the seabed that consisted of clayey sediments (ice scour tests). The ice ridge for the shear off test was built up in a pre-excavated trench in hard moraine. During pulling the keel of the ice ridge was sheared off by the sidewall of the trench. The pulling force, displacements, failure of the keel and resulting plough marks were measured. This paper provides a description of the test arrangement and the basic experimental results.

Keywords: Ice scour, first-year ice ridge, keel, ice rubble.

1. Introduction

First-year ice ridges are one of the major obstacles to offshore operations in ice-infested waters. They may control design load levels for sea ice interactions with offshore structures as well as be a significant impediment to shipping. In addition, first-year ice ridges can scour the seafloor in relatively shallow waters, e.g. offshore Sakhalin island, Eastern Barents Sea, Beaufort Sea, etc. This has significant implication on the design of pipelines and other subsea facilities (Timco et al., 2000). The phenomenon of interaction between the ice features and the ocean floor is named ice scouring. It has been quite extensively studied for the last 30 years particularly in respect to the iceberg and multi-year ridge scouring (Chari, 1979; Woodworth-Lynas et al., 1996; Palmer, 1998). Icebergs and multi-year ice ridges have been treated as solid bodies that are not destroyed while scouring the seabed. First-year ice ridges and particularly their keels are much looser and weaker. This makes it reasonable to assume that they may be partly destroyed during the contact with the seabed soil. The reader is referred to Leppäranta and Hakala (1992), Bowen and Topham (1996) and Høyland (2002) for description of morphology and consistency of the first-year ice ridges and

[1] Norwegian University of Science and Technology
[2] Barlindhaug Consult AS

their variation in different seas. A number of investigations and studies have also been carried out to estimate the mechanical properties of ice rubble – the material that composes the keel of the first-year ice ridge. The results were summarized by Ettema and Urroz (1989) and Timco and Cornet (1999) followed by more recent studies (Jensen et al., 2001; Lemée and Brown, 2002; Heinonen, 2002; Liferov et al., 2003).

Basically, ice scouring of the seabed by first-year ice ridges may involve the following three basic components: Gouging of the seabed, Destruction of the keel and Heave/Pitch of the ice ridge. The last and particularly the first components have been addressed in several studies (Been et al., 1990; Kioka and Saeki, 1995; Barker and Timco, 2002). The approach accounting for possible keel destruction during scour process has not been studied yet, although it seems to differ from the "solid body" type of scouring. This may be primarily due to the lack of solid knowledge about the ice rubble mechanical properties, which are needed to solve the problem of contact between the ice ridge and the seabed soil.

In the year 2001 it was decided to conduct the in-situ ice scour test, and during the spring 2002 one pilot test was done as described by Liferov et al. (2002) and Høyland et al. (2002). Having the experience from the first experiment, two more tests were conducted during the winter/spring 2003. The rational for the experiments was the following:

- To study the keel destruction
- To investigate the process of scouring
- To observe the ice ridges throughout their lifetime.

It was intended that the collected data would be used for verification and justification of existing first-year ice ridge scour models as well as for development of the improved ice ridge scour model.

2. Experimental

2.1 General

The experiments were conducted in the Van Mijen fjord a few kilometres away from the coal mining community Svea on Spitsbergen (78°N, 16°E). The ice conditions are fairly stable during winter and spring thus posing no danger for the ice ridge to drift away. The precise location of the experimental site has been chosen after extensive bathymetry survey and evaluation of access for heavy machines that would be needed during the fieldwork.

Altogether three tests were conducted: two scouring tests R1 (pilot test, 2002) and R2 (2003) and one shear-off test R3 (2003). All tests were conducted similarly using the same equipment and

[3] The University Centre in Svalbard

instrumentation. The principal difference between the ice scouring tests and the shear-off tests was the following:

- The ice ridges for the scouring tests were built at such water depth that there always was a gap between the keel and the seabed at low tide. Then the ice ridges were towed towards the shore in the open channel scouring the seabed, which consisted of relatively soft clayey sediments.
- The ice ridge for the shear-off test was built in a more shallow area. It was built in the trench excavated in very stiff and hard moraine. The depth of the trench was sufficient to prevent grounding of the ridge at low tide. The wall of the trench has further provided the boundary against which the ice ridge was sheared-off. The main goal of the shear-off test was to estimate the strength of the keel.

A description of the basic actions performed throughout the test program is given in the following sections.

2.2 Soil conditions and testing

No precise information about soil conditions in the near-shore area was available prior to the tests. It was thus decided to conduct a mechanical weight sounding of the seabed to determine stratigraphy of the upper part of the seabed. Soil samples were also taken from the test area and subsequent laboratory testing was conducted. The results are shown in Table 1.

Table 1. Soil properties.

Parameter		Silty clay
Density (kg/m^3)		1880
Water content (%)		43.7
Undrained shear strength* (kPa)		11.2
Mohr-Coulomb parameters**	φ (º)	32
	c (kPa)	3.1

*Average from the falling cone test
**From the undrained triaxial test

2.3 Ice Ridge Production

The ice ridges were artificially produced from the parent level ice. They were produced in mid/late March when the ice thickness reached about 0.9 m. The production of the ice ridges was essentially similar regardless of the type of test. The practical procedure included the following operations. Primarily, the snow was removed from the testing area (approximately 100 m by 70 m). In the year 2002 the team experienced severe difficulties with flooding of the ice (negative

freeboard up to 0.4 m) from the beginning of April caused by the snow drift. Therefore in the year 2003 it was decided to clean the snow from the testing area on a regular basis.

The initial openings in the ice with dimensions of up to 3.7 × 3.7 m were made where the ice ridge had to be built. Firstly, the ice was chain-sawed in the net pattern of approximately 1m by 1m. Both hydraulic and petrol driven chain saws were used. In some places additional 125-mm drilling was required in order to free the blocks. Then the blocks were lifted up either by the shovel of a digger (Komatsu PW95) or by drilling the 125-mm holes in the pre-cut ice blocks, inserting the anchor and lifting it with the forks of the tractor (Massey Ferguson).

Having the opening ready, large ice blocks (approx. 1 m^3) were chain-sawed into smaller blocks with dimensions of about 0.15 m × 0.25 m × 0.45 m. The amount of ice required to be sawed in pieces was estimated based on the expected shape and porosity of the ridge. The small blocks were then manually thrown into the opening, layer by layer, i.e. after the first layer covered the water surface the next layer was thrown on top of the first layer. Many of the blocks broke in two-three parts during this operation. After approximately one meter of rubble was placed in the opening, the new layers thrown on top did not cause its further submersion. This is believed to be due to the initial consolidation and the freeze-bonding with the surrounding ice. The shovel of the tractor was then used two-three times to push down the rubble. The consequence of it could be somewhat reduced porosity of the ridge.

After the ridges were produced they were left to consolidate. None of the ridges was under external pressure during the consolidation period. This may not entirely resemble the boundary conditions at the consolidated layer under the natural ridge building process while the boundary conditions at the keel are believed to be fully resembled. The above statements are not valid for stamukhas (grounded ice ridges) as they are not an object of the present research. The consolidation time was two to four weeks for the different ridges. Table 2 gives a summary of the ridge dimensions. Morphology, physical properties and consolidation of the ice ridges are described in the accompanying paper (Høyland and Liferov, 2004).

Table 2. Summary of the ridge dimensions.

Test	Length (m)	Width (m)	Keel depth (m)	Sail height (m)	Consolidated layer thickness (m)
(R1)	3.7	3.7	1.1	0.2	0.7
(R2)	4.1	4.1	2.15	0.4	0.7
(R3)	3.0	3.0	1.95	0.4	0.55

2.4 Channel opening and ridge towing

Channels in the ice cover were made in the same way as the openings for ridge production. In nature, an ice ridge is exposed to driving forces of current, wind, waves as well as it can interact

with the surrounding ice. Moreover, an ice ridge that scours the seabed is likely to be a part of a large ice floe. A complicated driving mechanism such as this is not possible to simulate in an in-situ "laboratory" environment. In the present tests it was decided to provide a constant displacement driving force along the back of the ice ridge. Towing of the ridges was done by pushing them from behind by the parent ice sheet, called the towing floe. The towing floe and the ice ridge were merged together on the day of ridge production. Ice anchors installed into the towing floe were connected by chain links to the main pulling chain that was powered by a pneumatic winch. In the pilot test R1 the ridge was pulled by a heavy loader Volvo L90. Figs. 1 and 2 show the general plan views of the R2 and R3 tests respectively. The ridges were manually towed back to their original position after the tests at high tide.

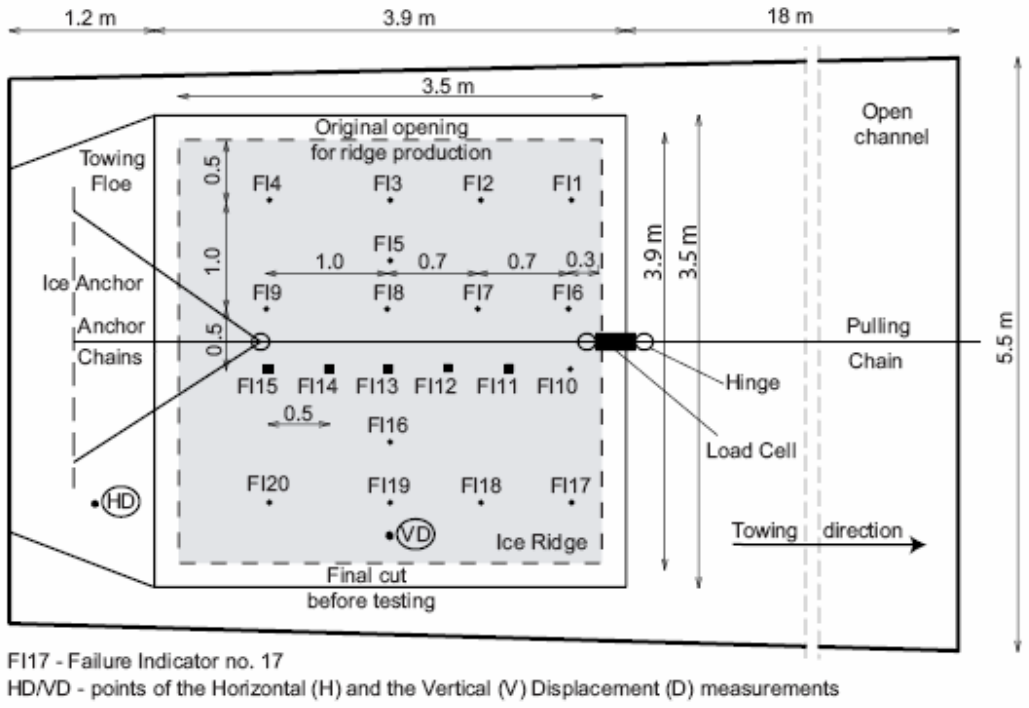

Fig. 1. Plan view of the R2 test.

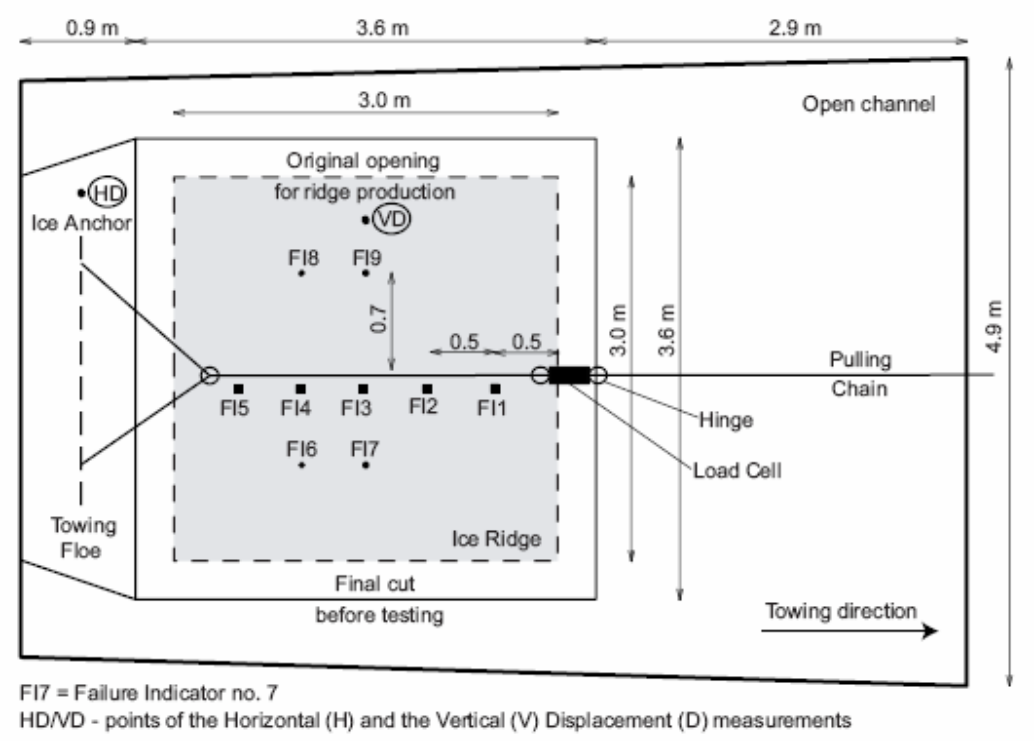

Fig. 2. Plan view of the R3 test.

2.5 Instrumentation and measurements

One of the key objectives in these experiments was to study failure of the keel during scour process. For this purpose the failure indicators (FI) were designed. Thin Plexiglass plates were cut into bars that were 1.25 m long, 6 mm wide and 2 mm thick. An electrical cable was glued inside a longitudinal micro-notch in the bar to indicate its failure by measuring change in electrical resistance. The resolution of the failure indicators was 0.25 m, i.e. they were able to indicate the region where the major failure slip took place inside the keel of the ice ridge. They were extended with bamboo sticks to achieve the length required for convenient installation. The indicators were installed into the ice ridge a few days before the experiment that provided their freezing into the consolidated layer of the ridge. To install the failure indicators 50-mm holes were drilled in the ice ridge. The indicators were placed into the casing pipe and inserted into the ice ridge ensuring that their bottom end coincided with the bottom of the keel. The casing pipe was used in order to secure the failure indicator during the installation and was lifted up after the indicator was installed. The plan of the failure indicators installed in the ridges is given in Figs. 1 and 2 for R2 and R3 tests, respectively. Only five failure indicators were used as dynamic indicators (shown with squares), i.e. recording the keel failure in the time domain during the test. They could indicate keel failure up to 0.5 m from the bottom of the keel. The amount of the dynamic indicators as well as their resolution was limited by available number of channels on the data acquisition device. The remaining failure

indicators could characterize the failure that took place inside the ridge during the experiment by residual reading from them after the test.

The horizontal translation and the heave of the ice ridge were measured by the displacement sensor IS-375 (Russian). In its original configuration this sensor can measure translations up to 1.5 m and vertical angles in a range of ±70º. In order to increase the range of horizontal measurements a reducer (1:32) was used. The points where horizontal and vertical displacements of the ice ridge were measured are shown in Figs. 1 and 2 for R2 and R3 tests, respectively. A 20-t load cell (T20 from Waage Instruments) measured axial force in the towing line.

The data acquisition system recorded the analog signals from all of the instrumentation. The signals were sampled and digitized by the Datascan 7221 data logger. The digitalized signals were recorded on a PC using the Labtech software package. All equipment was calibrated at the beginning of the test program to ensure reliable and accurate performance. Simulations of the test were also conducted indoors to test the performance of the entire measuring system. A special tester was used to ensure the integrity of failure indicators before the tests as well as to conduct the residual readings after the test. A summary of the measurements and observations conducted before, during and after the tests is given in Table 3.

Table 3. Summary of measurements and observations.

No.	Description
	Before testing
1	Temperature, salinity and hardness of the ice
2	Temperatures in the ice ridge (thermistor string)
3	Mechanical drilling (thickness of the consolidated layer, initial keel profile, porosity and consistency of the keel)
4	Underwater (UW) video of the ridge
5	Initial seabed profile along the scouring path
6	Seabed sounding (depth to the moraine)
7	Soil sampling and subsequent testing
	During testing
1	Pulling force by 20-t load cell at 3Hz
2	Horizontal and vertical displacements of the ridge at 3Hz
3	Failure of the ridge (five dynamic FI) at 3Hz
4	Overview, side view and UW video (UW video for scouring test only)
	After testing
1	Residual seabed profile along the scouring path
2	Residual ice ridge profile by means of mechanical drilling
3	Residual reading from all failure indicators
4	UW video of the scouring path

3. Results and analysis

3.1 Basic measurements and observation

The basic results of the experiments are outlined in this section. Figs. 3 and 4 show slides from the overview camera video record and Figs. 5 and 6 show the pulling force (10 moving average trendline), the vertical displacement (10 moving average trendline) and the failure in the keel recorded by the dynamic failure indicators versus the horizontal displacement for the R2 and R3 tests, respectively. Failure indicators are denoted as FI#, where # and corresponding location are given in Figs. 1 and 2 and failure depth is measured from the bottom of the keel upwards. The ice ridge was manually towed a few meters from its original position before the test R2 has started. The ice ridge was not in contact with the seabed during the pre-test towing. Table 4 gives a summary of test measurements.

Fig. 3. Test R2, overview slide.

Fig. 4. Test R3, overview slide.

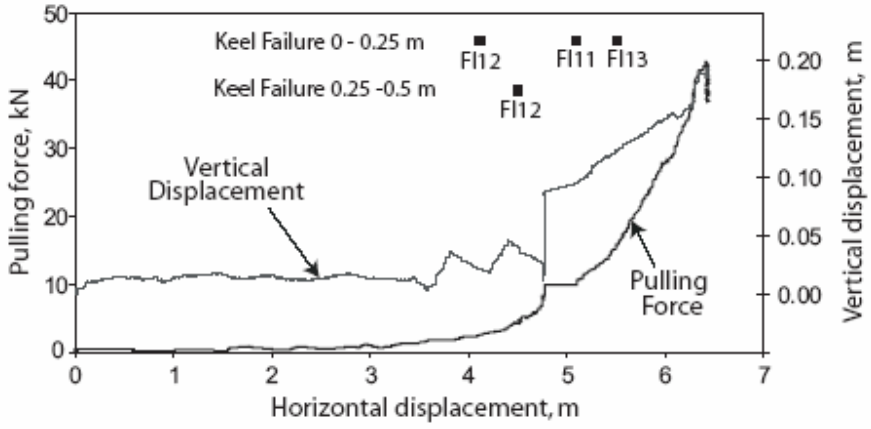

Fig. 5. Pulling force and heave of the ridge, test R2.

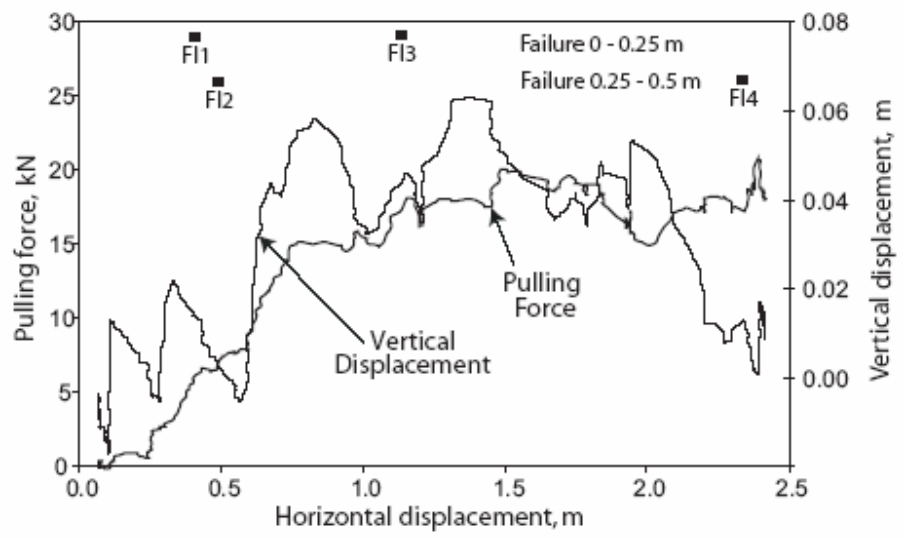

Fig. 6. Pulling force and heave of the ridge, test R3.

Table 4. Summary of test results.

	(R1)	(R2)	(R3)
Max. scour depth (m)	0.12	0.25	-
Max. heave of ice ridge (m)	0.29	0.20	0.06
Max. keel destruction (m)	0.2	0.45	0.45
Max. keel compaction (m) *	0.10	0.17	-
Average keel destruction (m)	0.09	~0.17	0.34
Average keel compaction (m) *	~0.04	~0.07	-
Max. force (kN)	32.7	42.7	21.3
Average velocity** (m/s)	0.1	0.02	0.02

* In case the entire out of balance value (x) from Fig. 10 is attributed to compaction

** The velocity oscillated significantly about average value (±50%)

Both scouring tests R1 and R2 behaved in the same manner. At the beginning of each test, the ice ridge was free-floating. After the first contact with the seabed the ice ridge began to heave slowly. A number of very shallow plough marks were observed on the seabed in this area. Initial compaction of the ice rubble in the keel could have taken place at this stage of the scour process. The ice ridge began to slightly pitch and the so-called “galloping” behaviour was observed, similar to as described by Barker and Timco (2002). The failure of the keel began to propagate from the area that contacted soil. In the final stage of the test when the ice ridge moved into even more shallow area, the scour magnitude increased, the keel continued to fail and significant heave of the ice ridge as well as significant increase in the pulling force was observed. A number of ice blocks were observed behind the ridge in the water right after the test. After the ridge was towed back at high tide, a few ice blocks were seen stuck in the seabed.

The R3 test behaved quite differently. After the ice ridge was cut free from the surrounding ice before the test, it was also free-floating. However, the walls of the trench prevented its movements at a distance of more than 0.3 m in the horizontal plane. As the ice ridge contacted the wall of the trench it began to pitch such that the front edge of the ridge was lower than the back edge of the towing floe. Significant "galloping" behaviour was observed throughout the entire test. No scouring took place in the area where the ice ridge interacted with soil. After the test significant amount of ice rubble from the keel was observed in the water around the ice ridge.

3.2 Keel failure and keel strength

As it was already mentioned, failure of the lower part of the keel was observed in all of the tests. Initial and residual ice ridge profiles for tests R2 and R3 are shown in Figs. 7 and 8, respectively. Results from the residual mechanical drilling and the residual reading from all failure indicators (the latter were taken before towing the ridge back to the original position) correlated well for all tests in the front part of the ridge. In the back part of the ridge the mechanical drilling seems to underestimate the magnitude of keel destruction. The results of residual reading from failure indicators for test R3 are presented in Table 5. They show that the ultimate global failure plane could have propagated as deep as up to one meter inside the keel. This discrepancy between different types of measurements can be explained as following. It could have happened that a part of ice rubble that disintegrated from the keel during shearing did not "escape" permanently, i.e. it could have accumulated beneath the towing floe after the test. When the ridge was towed back to its original position at high tide, this rubble could move back under the keel.

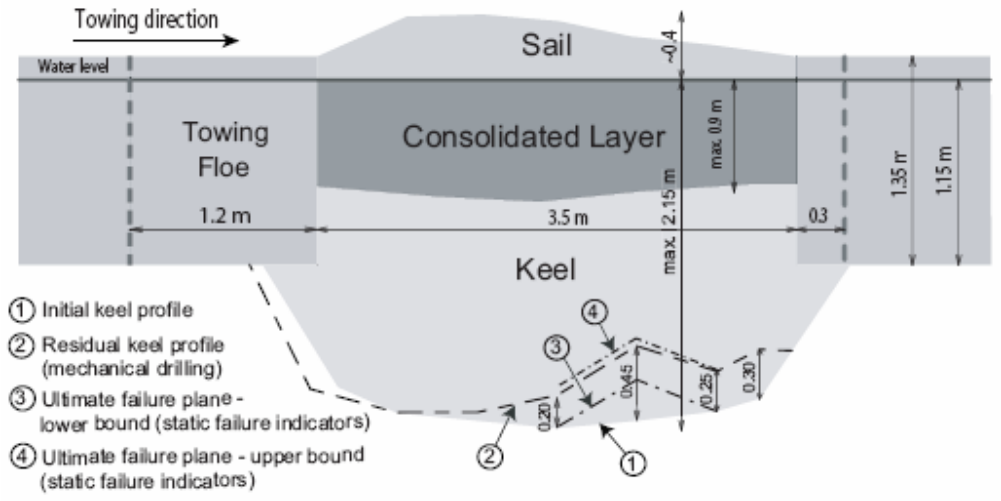

Fig. 7. Cross-section of the ice ridge (along centreline), test R2.

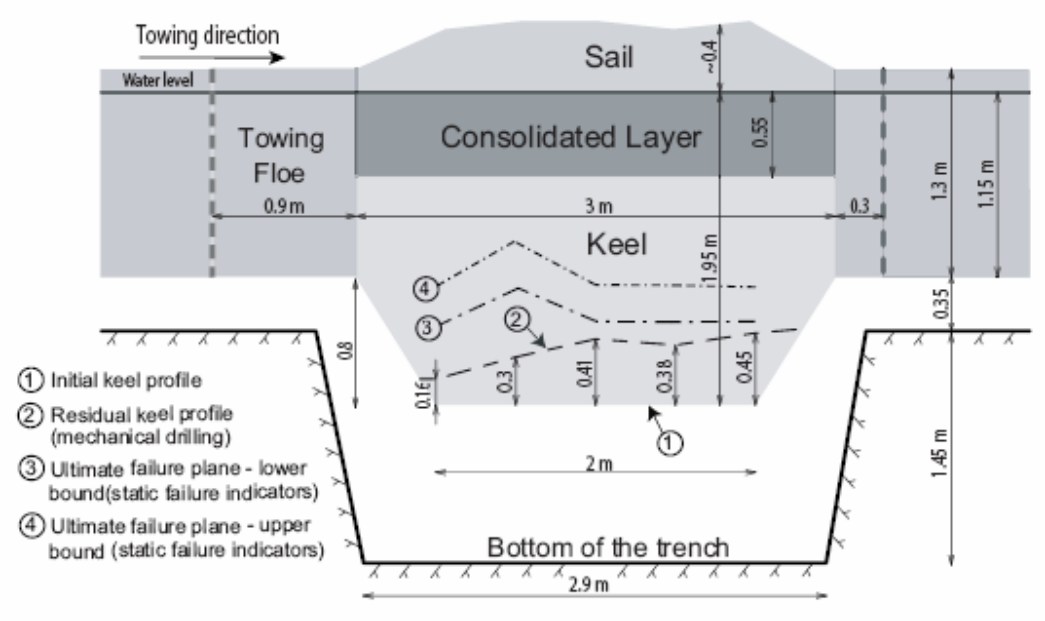

Fig. 8. Cross-section of the ice ridge (along centreline), test R3.

Table 5. Residual readings from failure indicators, test R3.

FI	Distance from bottom of the keel (m)			
#	0-0.25	0.25-0.50	0.50-0.75	0.75-0.1
1	×	○	×	○
2	○	×	×	○
3	×	○	×	○
4	○	×	○	×
5	○	○	×	○
6	×	×	×	○
7	×	○	×	○
8	×	×	×	○
9	×	○	×	○

× broken; ○ not broken

Failure of the keel was observed to be not simultaneous, but progressive, occurring while the ice ridge translated forward. In addition to the ultimate global failure plane there could form several secondary local failure planes as the ice ridge moved forward. Analysis of the entire data set, i.e. heave of the ridge, keel destruction and scour depth from tests R1 and R2 has also shown that the keel of ice ridge could have been temporarily (elastically) compacted. Additional discussion on this issue follows in Section 3.4.

Strength of the keel was estimated based on the data from test R3 and the results are shown in Table 6. Strength parameters of ice rubble were evaluated from the 2D finite element (FE)

simulations of test R3 conducted in Plaxis (2002). The material strength parameters in the numerical model were adjusted such as to fit the experimentally measured towing force. Three different material models were used to describe the ice rubble, namely: cohesionless Mohr-Coulomb (model 1):

$$\tau = \sigma \tan(\varphi) \tag{1}$$

Tresca/frictionless Mohr-Coulomb (model 2):

$$\tau = c \tag{2}$$

and standard Mohr-Coulomb (model 3):

$$\tau = c + \sigma \tan(\varphi) \tag{3}$$

where τ is the shear strength, σ is the normal stress on plane of shearing, c is the cohesion and φ is the angle of internal friction. The latter model does not give a unique answer about the rubble strength but only reflects one of the possible combinations of the Mohr-Coulomb parameters that provide the measured resistance (towing force). The above material models are fairly simple but at present these are the only models for ice rubble that have been experimentally validated.

Table 6. Strength parameters of the keel, test R3.

	φ (°)	c (kPa)
Model 1*	47	0
Model 2	0	4.5
Model 3**	32	1.5

*Associated plasticity, i.e. φ = ψ (dilatancy angle)
**Arbitrary combination of material parameters

3.3 Scour profiles

The seabed profile was measured before and after the test. The survey density was 1 m in longitudinal direction (parallel to towing direction) and 0.5 m in transversal direction (perpendicular to towing direction). Profiling was done manually by a long meter-stick and the accuracy of measurements was not high. It was estimated to be ± 0.02 m after the raw data was processed. Visual observations of the plough marks in the seabed were also done. The view and the distribution of the plough marks were similar for the R1 and R2 tests. From the place of first contact between the ice ridge and seabed a number of "scratch" looking plough marks was observed. As the scouring continued and ice ridge moved into shallower waters, the plough marks became wider and deeper. At the end of scour the plough marks more or less merged together forming one plough mark of trapezoidal shape. The initial and residual seabed profiles from test R2 are shown in Fig. 9.

In case of the R3 test significant permanent deformations in the soil were neither observed nor measured.

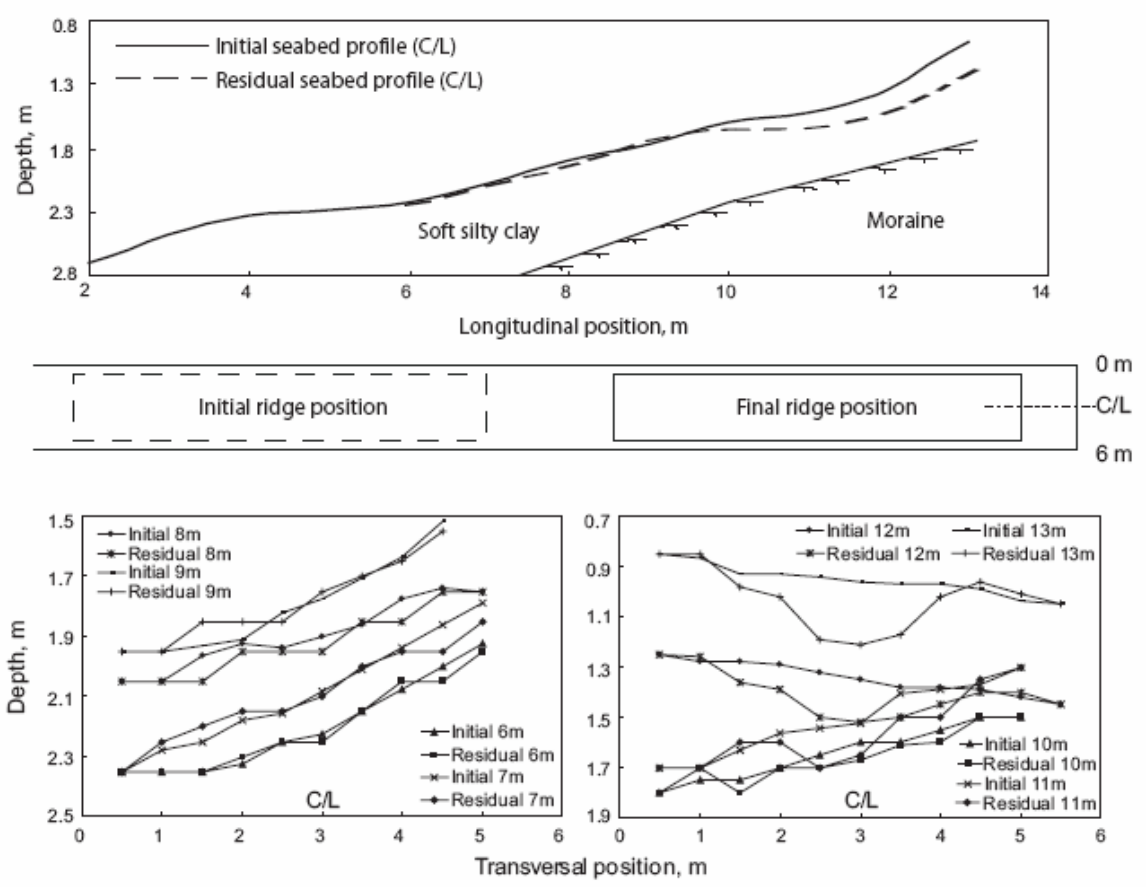

Fig. 9. Seabed profiles taken for test R2.

3.4 Overall ridge behaviour in test R2

To better understand the overall behaviour of the ridge scouring the seabed in test R2, a step-by-step illustration of the scour process is presented in Fig. 10. This figure shows the ridge in four positions: the initial (beginning of towing), two intermediate and the final (end of towing). The magnitude of the final keel destruction was taken from the mechanical drilling data. At the end of the scour track, below the initially deepest part of the ridge, a point was chosen to compare different approaches of the gouge depth prediction. The line (1) in Fig. 10 shows the trajectory of the bottom of the keel in case there was neither heave nor destruction. This line also shows how deep the scour depth would be predicted using simple scour models. The line (2) shows the scour depth that would be predicted in case the heave of the ridge was taken into account (assuming the absolute agreement between the observations and the prediction). And finally, the line (3) shows the measured scour depth at the same point. Given the values that are shown in Fig. 10, the ratio between the measured scour depth (3) and the ones predicted using approaches (2) and (1) are 2 and 3 times accordingly.

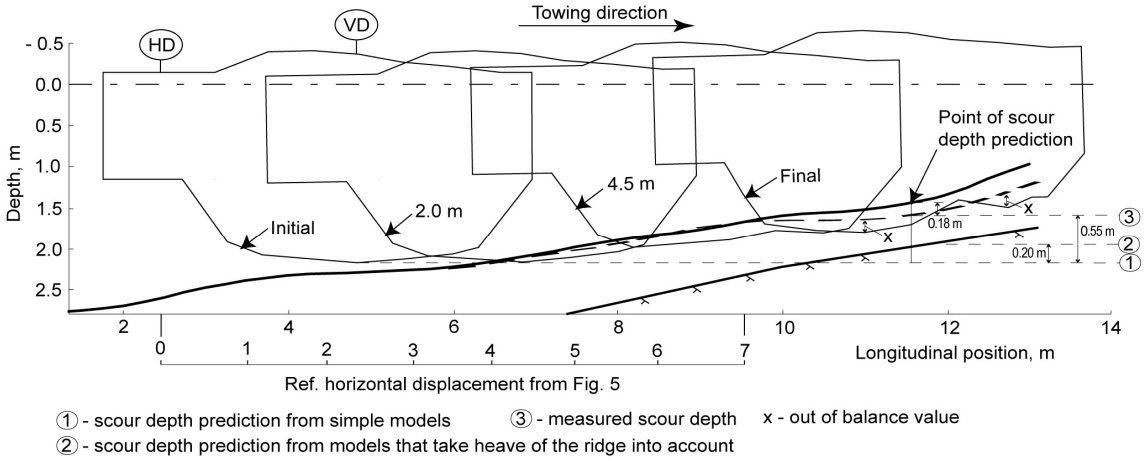

Fig. 10. Step-by-step illustration of the scour process, test R2.

As major consequence, the scour length and depth will be respectively under- and overestimated using scour models that do not account for the keel destruction. This has to be further verified for the full-scale ridge properties. Nevertheless, observations from the conducted scour tests agree well with those from seabed mapping in the Beaufort Sea. There it was observed that after a relatively short transient phase, the scour process reaches steady state conditions, in the sense that the scour depth does not change significantly (Konuk and Gracie, 2004). The basic contributors to the steady state scour process are believed to be the ridge heave and the keel destruction.

Apparently, the following relationship should be valid:

$$d = W_{initial} - (W_{final} + H + D) \tag{4}$$

where d is the scour depth, $W_{initial}$ and W_{final} are respectively the initial and the final water depths; H is the heave of the ridge and D is the destruction of the keel. The relationship 4 did not hold for scour tests R1 and R2. The out of balance value x as shown in Fig. 10 could be attributed to either the temporary (elastic) compaction of the keel (NB: the residual drilling was conducted when the ridge was free-floating at high tide) or to the redeposition of seabed material in the scour trench. Elastic response of the seabed material could also be a reason for that, however, it is unlikely.

3.5 Towing force in test R2

After the ridge in test R2 has moved about 4.5 – 5 m, it has reached steady state conditions, i.e. the gouge depth did not change significantly the last 1.5 – 2 meters of scour. The analysis and discussion on the contributors to the towing force at the end of the scour are given further.

The interaction between the ice ridge and the soil is a contact problem between two deformable bodies: the seabed soil and the ridge keel. As the ridge has been moving, the measured towing force reflected the resistance corresponding to failure of the weakest of two bodies as:

$$F_{tow} = \min\left\{R_{soil}, R_{keel}\right\} \tag{5}$$

where F_{tow} is the measured towing force; R_{soil} is the soil resistance and R_{keel} is the keel resistance. The soil resistance consists of the frontal resistance R_{front} and the one due to friction between the bottom of the keel and the seabed R_{bottom}:

$$R_{soil} = R_{front} + R_{bottom} \tag{6}$$

The bottom friction contribution to the towing force becomes particularly significant when the ice ridge heaves and loses its buoyancy. When neglecting the complicated interaction mechanism between the bottom of the keel and the seabed, a simple estimate of the bottom friction resistance can be made as:

$$R_{bottom} = \mu_K B_{loss} \tag{7}$$

where μ_K is the coefficient of kinetic friction and B_{loss} is the loss of buoyancy of the ridge that was estimated from the heave measurements as well as from the pitch observations with respect to the point where the heave of the ridge was measured. The kinetic friction coefficient may be estimated from assumption that both contact surfaces consisted of the remoulded soil. The coefficient of static friction may thus be defined by the friction angle of the soil. The kinetic effect is accounted for by introducing a reduction factor of 0.7 as can be estimated from Takeuchi et al. (2003).

The frontal resistance of the soil and the keel resistance were estimated by conducting the (FE) analysis (2D) as shown in Fig. 11. A simple upper bound estimate of the horizontal component of the gouging force as proposed by Palmer et al. (1990) has also been used. Their estimate was based on treating the soil as an ideal plastic material, with the cutting face of the ice at a 30º angle to the horizontal and is given as:

$$R_{front} / kbd \approx 4 \tag{8}$$

where k is the shear strength of the soil, b is the scour width and the scour depth assumed small compared to the width.

The FE analysis consisted of two parts. In each part one of the contacting bodies was considered as a solid indenter and was pushed against the other. The subdivision of the analysis in such a way was done to avoid instabilities caused by the "bi-directional gravity" in the case studied, in the sense that the floating ridge ("gravity" in the keel acts upwards) and the soil are a lot easier to model separately. The soil was assumed to behave undrained and an updated Lagrangian plastic analysis was used to account for large deformations. It was modelled as a Mohr-Coulomb material with the strength properties as given in Table 1. Interface elements with zero strength were used outside the contact face to simulate the stress-free slip between the keel bottom and the soil. The keel in test R2 was assumed to have similar properties to the keel in test R3 and Model 3 from Table 6 was used to simulate its behaviour. Additional confining pressure was also applied to the bottom of the keel to account for the ridge uplift.

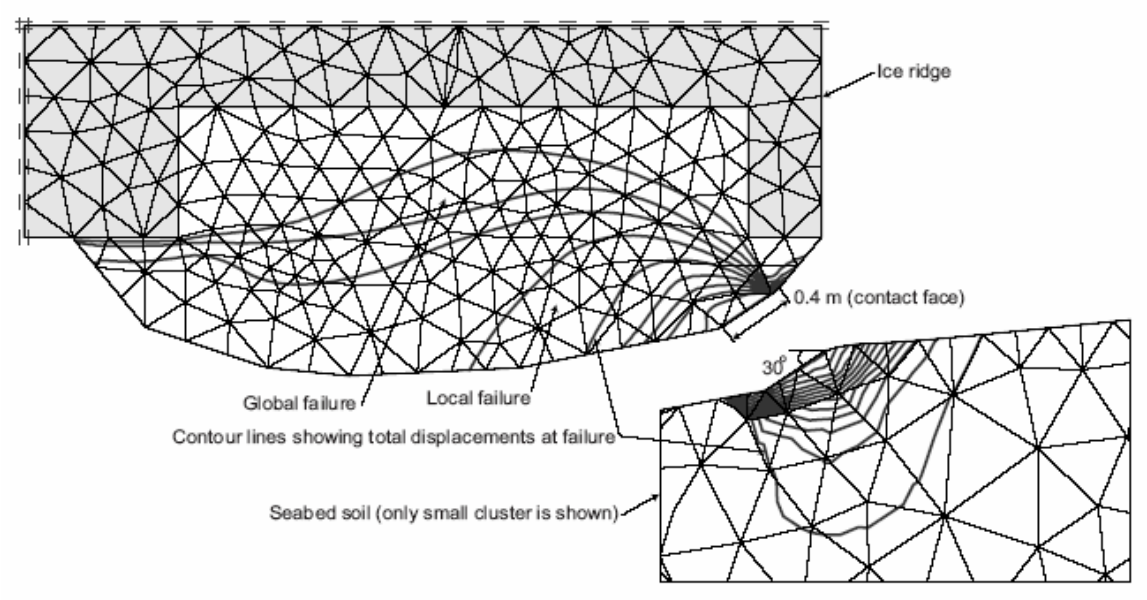

Fig. 11. FE modelling of the keel – soil interaction, test R2.

The resistance estimates and the corresponding towing force measured are summarized in Table 7. The least resistance at that particular moment was associated with the soil failure. The keel resistance, however, was not much higher and, if the ridge would penetrate into the soil and the average gouge depth would increase from 0.20 m to 0.24 m, the keel resistance would become less than that of the soil.

Table 7. Measured vs. estimated resistance, test R2.

Input / Measured		Evaluated	
d^* (m)	0.2	R_{keel} (kN)	39.1
b^* (m)	2.0	R_{front} (kN)	20.4 (17.9)†
H (m)	0.2	R_{bottom} (kN)	13.5
F_{tow} (kN)	32 - 42	R_{soil} (kN)	33.9

*equivalent
†from Eq. 8

4. Conclusions

A field program has been performed to examine the ice ridge scouring process. Two ice scour tests and one shear off test provided some interesting results, both qualitatively and quantitatively. In both ice scour tests (R1 and R2) a clear evidence of the keel destruction during the scour process was observed. The magnitude of the keel destruction was in the order of the scour depth and the heave of the ridge. The failure of the keel was observed to be not simultaneous, but progressive, occurring while the ice ridge translated forward.

The ice ridge in both tests moved in such a manner so as to reduce the overall scouring force. This observation is similar to the one done by Kioka and Saeki (1995) and Barker and Timco (2002) in their laboratory experiments on ice scouring. This also experimentally confirms the steady state scour observations from the Beaufort Sea.

Evaluation of the keel strength from the shear-off test (R3) showed that it was slightly less than the strength of the silty clay that the keel had scoured. This is with a good agreement with the magnitude of the keel destruction relative to the scour depth and the given boundary conditions.

The major conclusion from the conducted field program is an evidence of the second component in addition to heave of the ridge, e.g. keel destruction that makes an ice ridge follow the way of the least resistance while scouring the seabed. There is no doubt that the conducted experiments cannot be directly compared to the full-scale conditions. The present results suggest that this aspect of ice ridge scouring shall be evaluated and simulations of the full scale ice ridge scouring are needed based on the carefully evaluated material parameters for the full-scale ice ridges.

Acknowledgements

The authors would like to thank Per Olav Moslet, Rune Nilsen, Sergey Vernyaev and Rinat Kamalov for their crucial assistance during the field operations. The encouragement and help from Sveinung Løset and Karl Shkhinek are also greatly appreciated. We are thankful to Anatoly Alekseev for design and manufacturing of failure indicators, displacement sensors and intelligent boxes that enabled to establish a link between the old Russian and the modern Western equipment.

Particular acknowledgement is given to the Store Norske Spitsbergen Gruvekompani (SNSG) and Leonhard Nilsen Store Norske for their help with the heavy machines and logistics. And finally we would like to thank those who have financially supported the project, namely: Statoil ASA, the Norwegian Research Council, the Norwegian Polar Institute and the University Centre in Svalbard.

References

Barker, A and Timco, G., 2002. Laboratory experiments of ice scour processes: buoyant ice model. Cold Regions Science and Technology, 36: 103-114.

Been, K., Kosar, K., Hachey, J., Rogers, B.T. and Palmer, A.C., 1990. Ice scour models. Proceedings of the 9th International Conference on Offshore Mechanics and Arctic Engineering Conference, Houston, USA, Vol. 5, pp. 179–188.

Bowen, R.G. and Topham, D.R., 1996. A study of the morphology of a discontinuous section of a first year arctic pressure ridge. Cold Regions Science and Technology, 24: 83–100.

Chari, T.R., 1979. Geotechnical aspects of iceberg scours on ocean floors. Canadian Geotechnical Journal 16(2): 379–390.

Ettema, R. and Urroz, G.E., 1989. On internal friction and cohesion in unconsolidated ice rubble. Cold Regions Science and Technology, 16: 237–247.

Heinonen, J., 2002. Continuum material model with shear-cap yield function for ice rubble. Proceedings of 15th Nordic Seminar on Computational Mechanics. Aalborg, Denmark, pp. 87-90.

Høyland, K. V., 2002. The consolidation of first year ice ridges. Journal of Geophysical Research, 107/C6, 10.1029/2000JC000526, pp. 15,1 – 15,15.

Høyland, K.V., Liferov, P., Moslet, P.O., Løset, S. and Bonnemaire, B., 2002. Medium scale modelling of ice ridge scouring of the seabed, Part II: Consolidation and physical properties. Proceedings of the 16th International Symposium on Ice, Dunnedin, New Zealand, Vol. 2, pp. 94–100.

Høyland, K.V. and Liferov, P., 2004. On the initial phase of consolidation. Submitted to the Cold Regions Science and Technology.

Jensen, A., Løset, S., Høyland, K.V., Liferov, P., Heinonen, J, Evers, K.-U. and Maattanen, M., 2001. Physical modelling of first-year ice ridges, Part II: Mechanical properties. Proceedings of the 16th Conference on Port and Ocean Engineering under Arctic conditions. Ottawa, Canada, Vol. 3, pp. 1493–1502.

Kioka, S. and Saeki, H., 1995. Mechanisms of ice gouging. Proceedings of the 5th International Offshore and Polar Engineering Conference. The Hague, Netherlands, pp. 398–402.

Konuk, I. and Gracie, R., 2004. A 3-Dimensional eulerian FE model for ice scour. Submitted to the International Pipeline Conference. Calgary, Alberta, Canada.

Lemée, E. and Brown, T., 2002. Small-scale plain strain punch tests. Proceedings of the 16th International Symposium on Ice. Dunedin, New-Zealand, Vol. 2, pp. 1–8.

Leppäranta, M. and Hakala, R., 1992. The structure and strength of first-year ridges in the Baltic Sea. Cold Regions Science and Technology, 20: 295–311.

Liferov, P., Løset, S., Moslet, P.O., Bonnemaire, B. and Høyland, K.V., 2002. Medium scale modelling of ice ridge scouring of the seabed, Part I: Experimental set-up and basic results. Proceedings of the 16th International International Symposium on Ice. Dunnedin, New Zealand, Vol. 2, pp. 86–93.

Liferov, P., Jensen, A. and Høyland, K.V., 2003. 3D finite element analysis of laboratory punch tests on ice rubble. Proceedings of the 17th Conference on Port and Ocean Engineering under Arctic conditions. Trondheim, Norway, Vol. 2, pp. 599–610.

Palmer, A.C., 1998. Alternative paths for determination of minimum burial depth to safeguard pipelines against ice gouging. Proceedings of the 13th International Symposium on Okhotsk Sea & Sea Ice. Mombetsu, Japan, pp. 9–16.

Palmer, A.C., Konuk, I., Comfort, G. and Been, K., 1990. Ice gouging and safety of marine pipelines. Proceedings of the 22nd Annual Offshore Technology Conference, pp. 235-244.

PLAXIS, 2002. Plaxis v. 8.1. Finite Element Code for Soil and Rock Analyses. www.plaxis.nl.

Takeuchi, T., Sasaki, M., Miura, K., Sanbe, H. and Takahashi, A., 2003. Coefficients of friction of sea ice on sand. Proceedings of the 13th International Offshore and Polar Engineering Conference. Honolulu, USA, Vol. 1, pp. 461–464.

Timco, G.W. and Cornet, A.M., 1999. Is φ a constant for broken ice rubble? Proceedings of the 10th Workshop on River Ice Management with a Changing Climate. Winnipeg, Manitoba, Canada, pp. 318–331.

Timco, G.W., Croasdale, K. and Wright, B., 2000. An overview of first-year sea ice ridges. PERD/CHC report 5-112, 159 p.

Woodworth-Lynas, C.M.L., Nixon, J.D., Phillips, R. and Palmer A.C., 1996. Subgouge deformations and the safety of Arctic marine pipelines. Proceedings of the 28th Annual Offshore Technology Conference, Huston, Texas, pp. 235–244.

3.3 Medium scale modelling of ice ridge scouring of the seabed, Part I: Experimental set-up and basic results

P. Liferov[1,2,3], S. Løset[1,2], P.O. Moslet[2], B. Bonnemaire[1] and K.V. Høyland[2]

[1]Norwegian University of Science and Technology
[2]University Centre in Svalbard
[3]Barlindhaug Consult AS

Abstract

An ice ridge with dimensions of 3.7 × 3.7 × 1.4 m was artificially produced close to the beach in Svea in the Van Mijen fjord on Svalbard. An opening was made in the ice and the level ice was cut into pieces and thrown in the opening to form a ridge. The ridge was left to consolidate for a month and then pulled towards the beach to investigate first year ice ridge - sea bed interaction. The pulling force as well as horizontal and vertical displacements of the ridge were measured. Keel failure indicators were installed in the ridge for measuring the destruction of the keel when it contacts the seabed. Profiling of the seabed was done before and after the experiment.

1. Introduction

Icebergs and ice ridges are one of the major obstacles to offshore operations in the Arctic. In particular, they may cause a danger to bottom installations like submarine pipelines, wellheads, etc. It may happen when an ice feature contacts the sea-bottom being driven by environmental forces into the shallow areas. The phenomenon is named ice scouring and has been quite extensively studied for the last 30 years particularly in respect to the iceberg and multi-year ridge scouring (Chari, 1979; Palmer et al., 1990; Woodworth-Lynas et al., 1996; Palmer, 1998). Icebergs and multi-year ice ridges have been treated as solid indenters, which cannot be destroyed while scouring the seabed. First year ice ridges and particularly their keels are much looser and weaker which means that they may be partly destroyed during the contact with the seabed soil. The reader is referred to e.g. Leppäranta and Hakala (1989, 1992), Eranti et al. (1992), Bowen and Topham (1996) for description of consistency of the first year ice ridges and its variation in the different seas. The approach accounting for possible keel destruction was not, however, studied yet although it seems to differ from the “solid indentor” type of scouring.

Ice scouring of the seabed by the first-year ice ridges may involve the following three basic components: *Gouging of the seabed, Destruction of the keel and Heave/Rotation of the ice ridge*.

The last and particularly the first components have been addressed in several studies (Been et al., 1990; Kioka and Saeki, 1995) while very little is known about possible destruction of the ridge keel. This is primarily due to a lack of knowledge about the ice rubble properties (Timco and Cornet, 1999), which are needed to solve the problem of contact between the ice ridge and the seabed soil. Experimental modelling and particularly scaling is also difficult.

Nevertheless, an attempt to conduct the in-situ modelling of the first year ice ridge scouring process was undertaken. The rational for the experiment was the following:

- Investigation of the process of keel destruction during the scouring
- Observation of the ice ridge consolidation throughout its life.

The results of the experiment could be used for justifying the numerical/analytical model of the scouring process. Material parameters of the in-situ modelled ice ridge can also be estimated based on modelling of the ridge-soil contact and fitting it with the experimental data. And finally, the idea was to design an in-situ test on the artificially produced ice ridge, which would closely approximate the real scouring process.

2. Description of experiment

The experiment was conducted in the Van Mijen fjord a few kilometres away from the coal mining community Svea on Svalbard (78° N). Seabed sounding from the rubber boat in the fall, 2001 showed that the near-shore bathymetry and the seabed consistency would make the planned experiment feasible. The ice conditions are fairly stable during winter and spring thus posing no danger for the ice ridge to drift away. The description below will include both the originally planned the actually performed actions throughout the experiment.

2.1 Ridge production

Originally planned

It was planned to produce the ice ridge from a newly refrozen ice of about 15 cm thickness. The original wanted ridge dimensions are shown in Fig. 1. For this purpose a channel of 15 m × 5 m should have been opened to freeze the new ice. Production of the ridge from the naturally formed ice would have given us an opportunity to obtain a “thermodynamically” correct ice ridge. However, the meteorological conditions and the time schedule did not let us to conduct this operation and another solution had to be found.

Actually performed

The alternative solution was to produce the ridge from the original level ice on the site. At that time (week 11) the ice was 0.85 m thick. In order to build the ridge from the "realistic ice blocks", 0.15 m thick ice blocks would be cut from the 0.85 m thick ice blocks. No blocks were produced from the lowest part of the level ice, as this layer was very weak. The uppermost part of the level ice was very cold, drained from brine (low salinity) and thus very hard. The blocks were therefore made out of the layer between -0.40 m and -0.75 m of the level ice. Part II of the present paper (Høyland et al., 2002) gives more details. The practical procedure included the following operations. Firstly, about 0.25 m of the hard blown snow had to be removed from the site. After having defined the position of the opening (Fig. 2), some pre-cuts were done with the petrol-driven chainsaw on which 0.9/1.5 m blade was mounted. The chainsaw itself was mounted on a trolley to make the vertical cutting easier (Fig. 3).

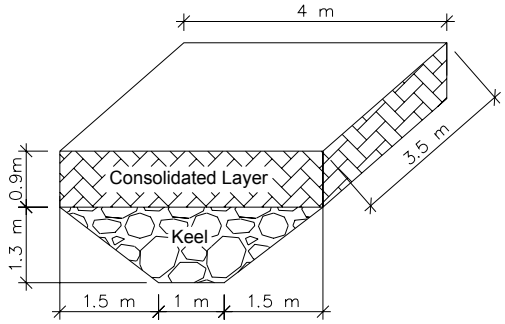

Figure 1. Originally planned ridge.

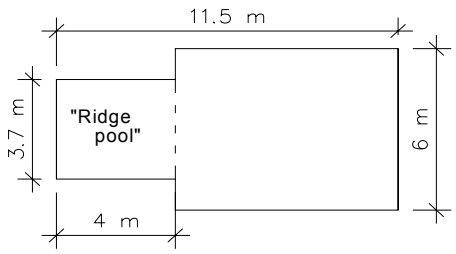

Figure 2. Geometry of the first opening

Square slots of approximately 1 m^2 were cut from three sides and then the digger broke the big ice blocks free from the level ice and lifted them up (Fig. 4). As soon as the "ridge pool" was free of ice, a net, shaped as the originally wanted ridge (but bigger, the net was 2.5 m deep) was placed in the opening, fixed on 3 sides on the level ice and on one side on a beam transverse to the opening. The role of the net was to prevent the ice blocks from going away from the ridge area. The knitting of the net was designed to be easily released, as the net should have been removed. Unfortunately, after consolidation of the ridge it was not possible to remove the net. But, as it was seen on some underwater pictures, there was a substantial gap (at least 1 m) between the rubble and the net. It thus produced no artificial confinement to the ice rubble during the scouring phase.

Figure 3. Cutting the level ice.

Figure 4. Digger in operation.

When a big ice block was cut free from the level ice it was put aside and several small blocks were chain sawed from the layer mentioned earlier. Dimensions of the blocks were about 0.15 m × 0.30 m × 0.45 m (see Fig. 5). However, many blocks broke being thrown in the "ridge pool". Unfortunately, mechanical problems with chain saws did not let us to build the ridge with wanted dimensions. It was neither not possible to continue next morning as the low temperatures (down to –30 °C) made the ridge consolidation quite fast. The final ridge dimensions are shown in Fig. 6. Part II of the present paper (Høyland et al., 2002) gives more details about the ridge dimensions.

Figure 5. Ice ridge is being produced.

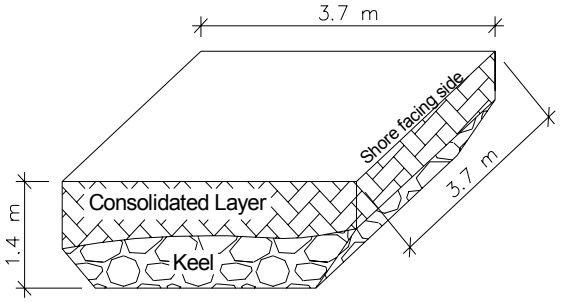

Figure 6. Final dimensions or the ridge.

2.2 Channel opening and ridge towing

Originally planned

It was planned to tow the ridge in the direction perpendicular to the shoreline. However, water flooding (negative freeboard of about 0.2 – 0.4 m) particularly in the area of the planned towing made us to change the direction of towing.

Actually performed

The ridge had to be rotated by about 30° from the original towing direction. Then a new channel (6 m wide and approximately 26 m long) was opened and cleaned from the slush. Towing of the ridge was done by pushing it from behind by the 2 m × 3.5 m parent ice sheet. A net of the reinforcement bars frozen into the ice was connected to the pulling wire via three chains and the hinge. Pulling was provided by a 12-t Volvo L90 loader with approximately constant speed of 0.1 m/s. It was done one month after the ridge was built. Fig. 7 shows the final stage of the channel opening and Fig. 8 shows the ridge in the final grounded position.

Figure 7. Channel is being opened.

Figure 8. Grounded ice ridge.

2.3 Instrumentation and measurements

One of the key issues in this experiment was the indication of the keel failure in the time domain together with the pulling force and ridge displacements. For this purpose the failure indicators were designed. They were made out of the brittle plastic bars (7 mm × 2 mm cross-section) with an electrical cable inside. Resolution of the failure indicators was 25 cm. They were installed in the ridge one night before the experiment as shown in Fig. 9. Only five indicators were used as dynamic indicators (black dots), i.e. recording the keel failure in the time domain. This was due to limited number of channels on the data acquisition device.

Both initial and residual ice ridge profiling was also done manually by 50-mm drilling. Pulling force was measured with a 5-t load cell (at 1 Hz) located between the hinge and the pulling wire. Both horizontal and vertical displacements of the ridge were measured (at 1 Hz). The vertical displacement of the ridge was not, however, measure accurately due to the construction of the displacement sensor, experimental set-up and relatively small heave of the ridge. Initial (before the scouring took place) and residual sea bottom profiling was conducted. Seabed sounding was done in order to determine the thickness of the sediments lying on the bedrock. A special care was taken of

the tidal variation (up to 1.6 m) and all measurements were finally adjusted to the mean sea level (MSL). After the experiments a soil sample was taken and two tri-axial tests were conducted.

3. Results

Basic results of the experiment are shown in figures below. Fig. 10 shows the geometric notations that are further used.

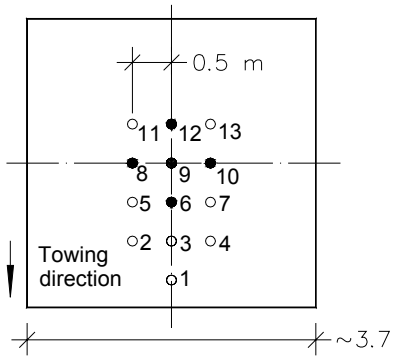

Figure 9. Scheme of the failure indicators installed in the ridge.

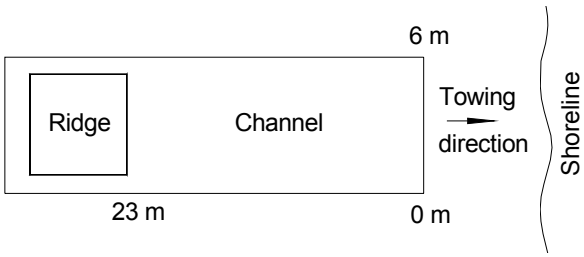

Figure 10. Geometric notations.

The time series of the pulling force is shown in Fig. 11. Pulling force, vertical translation of the ridge and records from dynamic failure indications versus horizontal translation are shown in Fig. 12. Points on the plot indicate the failure of the dynamic failure indicators (FI). In all cases the failure took place in the lower 0.25 m of the keel. Destruction of the keel was also indicated by the static failure indicators number 1, 7 and 13. Fig. 13 gives the longitudinal initial and residual profiles of the seabed along the centreline of the channel. The experiment was conducted at the lowermost sea level (LSL). The difference between the MSL and the LSL was 0.69 m for the day of experiment.

The tri-axial tests on soil sample showed that the seabed soil (silty clay) has the following strength properties (uniformly distributed over the depth): angle of internal friction (φ) = 32° and cohesion (c) = 3.1 kPa.

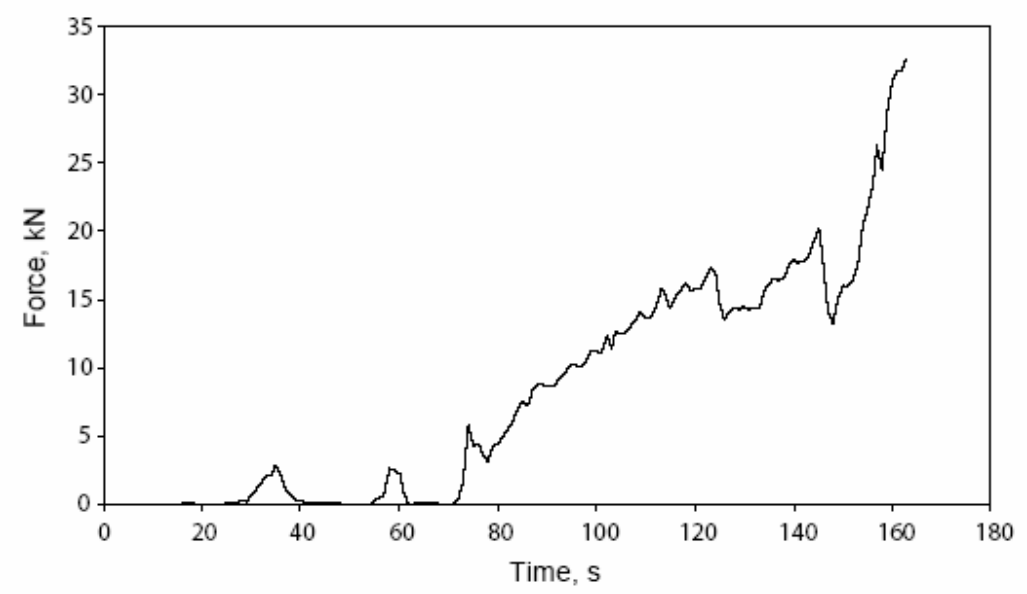

Figure 11. Time series of the pulling force.

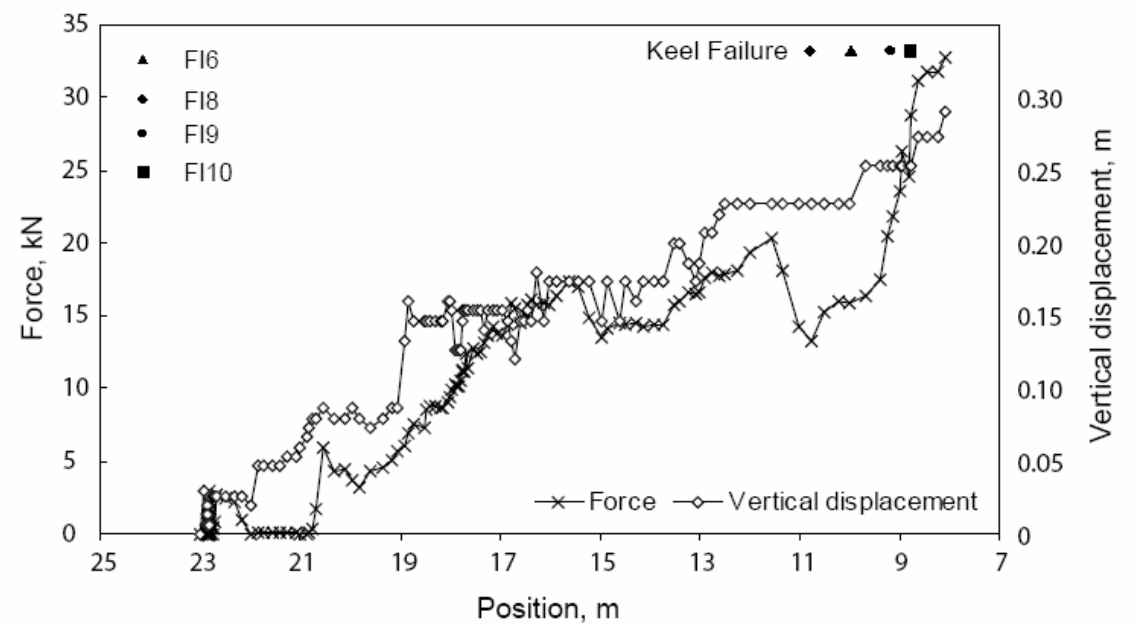

Figure 12. Pulling force, vertical translation and keel failure vs. horizontal translation.

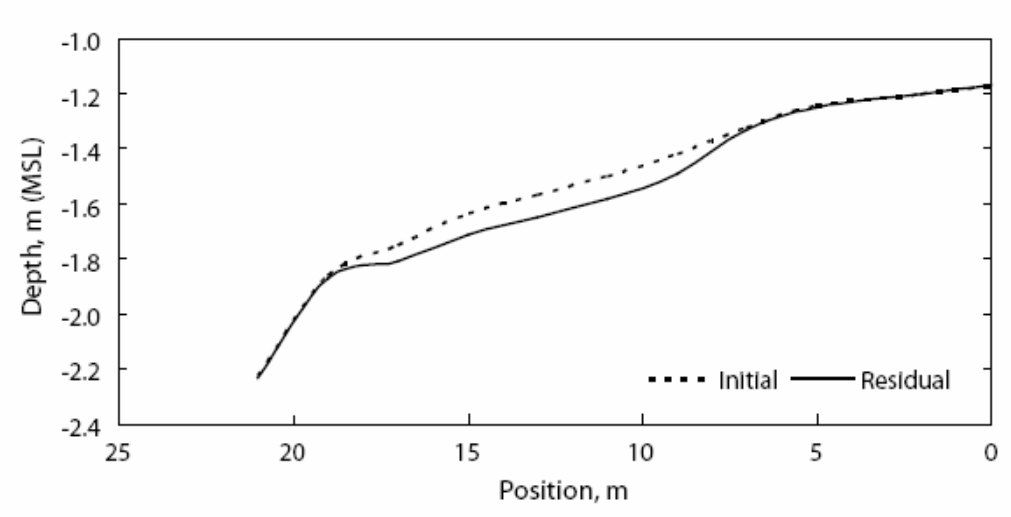

Figure 13. Longitudinal seabed profiles.

Examples of the transversal initial and residual seabed profiles are shown in Fig. 14.

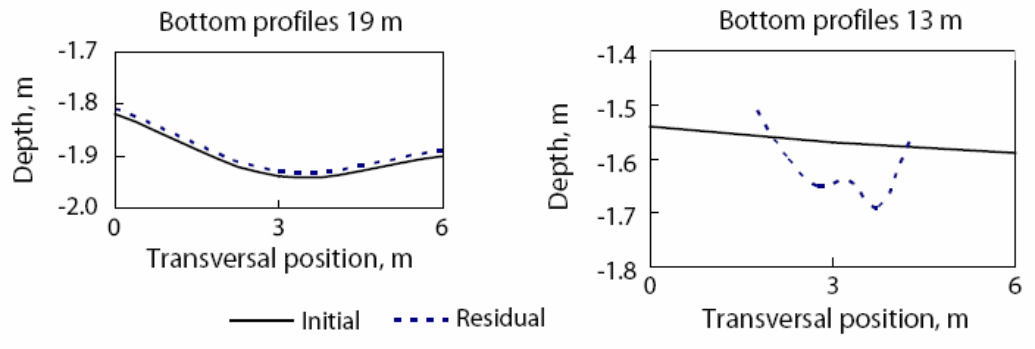

Figure 14. Transversal seabed profiles.

Longitudinal and transversal ice ridge profiles before and after scouring event are shown in Fig. 15.

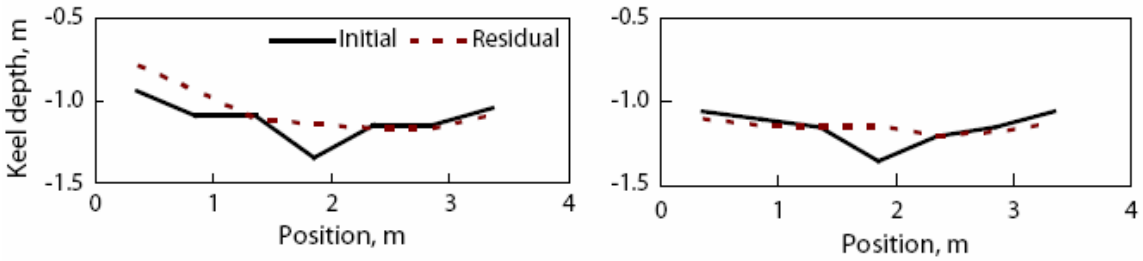

a) Longitudinal (zero position indicates the front of the ridge)

b) Transversal

Figure 15. Ice ridge profiles.

4. Discussion

The experiment described above was planned as the first trial of the in-situ ice scouring modelling. Unfortunately we did not succeed to build the ice ridge with wanted dimensions and then the towing direction has been changed. The failure indicators neither functioned well as some of them did not register the failure while it clearly took place as this was found later by the residual ridge profiling. Nevertheless, the experiment was finalized and valuable results and experience were gathered. A clear evidence of the keel destruction during the scouring process was seen and its value was proportional to the depth of the plough mark in the seabed. Significant heave of the ridge was also observed. This confirms that the simplified scouring models, which neglect the heave of the ridge, may significantly overestimate the scouring depth. This is particularly true if the ridge is drifting along being surrounded only by a small level/rafted ice field.

The experimental results will further be analysed. Better solution for the ridge production will be found in order to conduct the second trial more successfully. An attempt to avoid water flooding will be done by keeping the entire experimental area free of snow. All this will allow us to produce bigger ice ridge/ridges and conduct the scouring in the best direction. The failure indicators will also be modified thus giving better information about the keel destruction during the scouring process.

Acknowledgement

The authors would like to thank professor Karl Shkhinek for the original idea, Anatoly Alekseev for design and manufacturing of the failure indicators and Rudiger Biedorf for his crucial assistance in the fieldwork. We would also like to thank the Store Norske Spitsbergen Gruvekompani (SNSG) for the great assistance with the heavy machines and logistics. And finally we would like to thank all those who helped us a lot during the field season full of contingency operations.

References

Been, K., Kosar, K., Hachey, J., Rogers, B.T. and Palmer, A.C. Ice scour models. In Proceedings of the Ninth International Conference on Offshore Mechanics and Arctic Engineering (OMAE ’90) Conference, Vol. 5, Houston (1990) 179–188.

Bowen, R.G. and Topham, D.R. A study of the morphology of a discontinuous section of a first year arctic pressure ridge. Cold Regions Science and Technology 24: 83–100 (1996).

Chari, T.R. Geotechnical aspects of iceberg scours on ocean floors. Canadian Geotechnical Journal 16 (N2): 379–390 (1979).

Eranti, E. et al. First year ice ridge characteristics and loads on offshore structures. In Proceedings of the Second International Offshore and Polar Engineering Conference, San Francisco, USA, June 14-19 (1992) 681–687.

Kioka, S. and Saeki, H. Mechanisms of ice gouging. In Proceedings of the 5th International Offshore and Polar Engineering Conference, The Hague, June 11-16 (1995) 398–402.

Leppäranta, M. and Hakala, R. Field measurements of the structure and strength of first-year ice ridges in the Baltic Sea. In Proceedings of the Eighth International Conference on Offshore Mechanics and Arctic Engineering, The Hague, March 19-23 (1989). 169–174

Leppäranta, M. and Hakala, R. The structure and strength of first-year ridges in the Baltic Sea. Cold Regions Science and Technology 20: 295–311 (1992).

Palmer, A.C., Konuk, I., Comfort, G. and Been, K. Ice gouging and safety of marine pipelines. In Proceedings of the 22nd Annual Offshore Technology Conference (1990) 235–244.

Palmer, A.C. Alternative paths for determination of minimum burial depth to safeguard pipelines against ice gouging. In Proceedings of the 13th International Symposium on Okhotsk Sea & Sea Ice (1998) 9–16.

Timco, G.W. and Cornet, A.M. Is φ a constant for broken ice rubble? In Proc. 10th Workshop on River Ice Management with a Changing Climate, J.C. Doering ed., Winnipeg, Mantioba, Canada, 8-11 June (1999) 318–331.

Woodworth-Lynas, C.M.L., Nixon, J.D., Phillips, R. and Palmer A.C. Subgouge deformations and the safety of Arctic marine pipelines. In Proceedings of the 28th Annual Offshore Technology Conference (1996) 235–244.

3.4 On the initial phase of consolidation

Knut V. Høyland[1] and Pavel Liferov[2,3]

Abstract

Three ice ridges have been artificially produced close to Svea in the Van Mijen fjord on Svalbard, Norway; one in the year 2002 (R1) and two in the year 2003 (R2 and R3). The temperature development in R1 and R2 was monitored for about four weeks and ice was sampled for measurements of salinity and hardness (of the rubble). The initial thickness of the consolidated layer in R1 and R2 respectively was 0.10 and 0.32 m, the duration of the initial phase was 16 hours and 96 hours and the final thickness of the consolidated layer was about 0.70 m for R1 and about 0.72 m for R2. A simple model to calculate the oceanic flux during the initial phase is explained and the oceanic flux was about 230 W/m2 for R1 and 63 W/m2 for R2. The larger keel in R2 was the main reason for the longer duration of the initial phase and the lower average oceanic flux.

Key words: Ice ridges, consolidation, initial phase, oceanic flux, mechanical properties

1. Introduction

Sea ice ridges are formed by compression or shear in the ice cover and do in many cases give the design load for arctic marine structures, such as platforms, ships and pipelines. The loads from first-year ice ridges on various structures are not clear, and one of the major deficiencies is that the mechanical properties, in time and space, of first-year sea ice ridges are not well known. Ice ridging is also important in large scale geophysical models as it affects the heat transfer between the ocean and the atmosphere. The oceanic heat is increased for two reasons; firstly a ridging event leaves open water from which the heat flux is higher than through the ice, and secondly, as we argue for in this paper, the oceanic flux into a newly formed ridge is substantially higher than into the level ice.

An ice ridge consists of ice blocks and water and during the growth season the air above is cold and removes heat from the top surface, whereas the water below is warm, at or above the freezing point ($T_w \geq T_f$) and adds heat to the ridge from below. The lifetime of a first-year ice may be divided in three phases: the initial phase, the main phase and the decay phase, and different energy fluxes are important in three phases.

[1] University Centre in Svalbard
[2] Norwegian University of Science and Technology
[3] Barlindhaug Consult AS

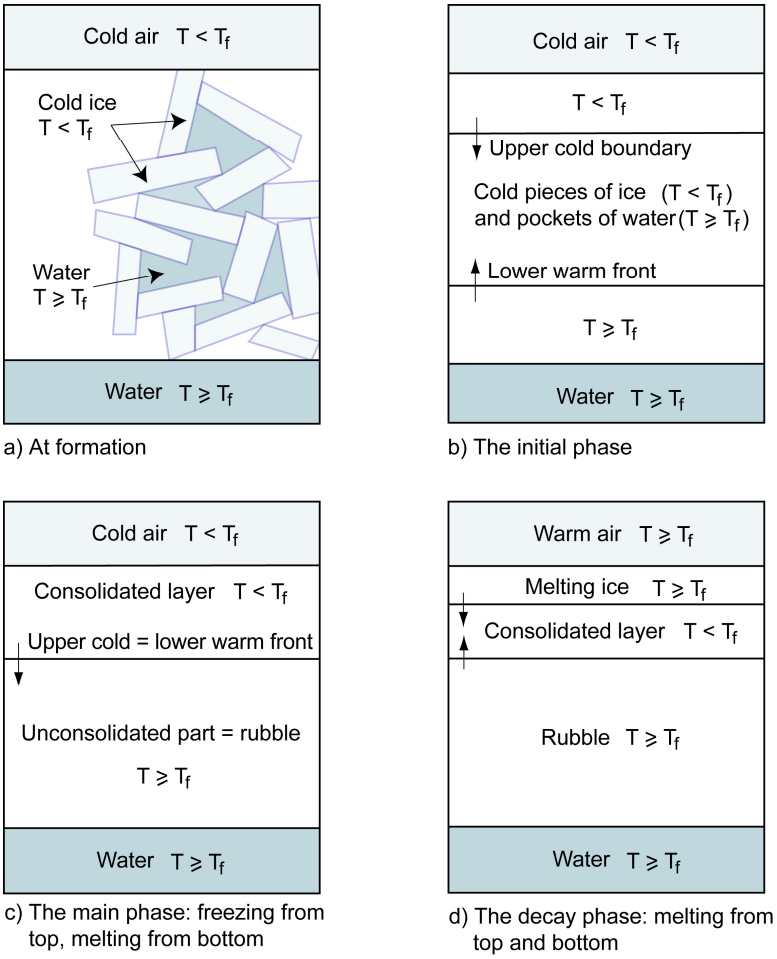

Fig. 1. The lifetime of a first-year ice ridge.

The initial phase starts during the formation when the ice blocks are solid pieces of ice with their initial temperature (Fig. 1 a)). An internal heat flux between the water pockets and the ice blocks gradually evens out the temperatures. As the top surface is cooled down by the surrounding cold air the water pockets gradually freeze up. An upper, cold boundary above which everything is frozen is created and this cold front moves down in the ridge. At the bottom of the ridge heat is added from the water, this is called the oceanic flux (q_{ocean}) and it creates a lower, warm front below which the temperatures are at or above the freezing point (Fig. 1 b)). This warm front moves upwards in the ridge and at some point it meets the downwards advancing cold front. This defines the end of the initial phase and starts the main phase (see Fig. 1 c)). Now the keel of the ridge consists of two different parts clearly defined by temperatures; a cold refrozen upper layer called the consolidated layer where the temperatures everywhere are less than the freezing point ($T < T_f$), and a lower part called the rubble in which the temperature is at the freezing point. Now the upper and the lower

fronts are merged into one thermal boundary in the ridge defining the thermal transition between the consolidated - and the unconsolidated parts of the keel. The thickness of the consolidated layer is defined as the size of frozen layer (h_c). The main phase is characterized by the growth of h_c as a function of the meteorological conditions, and has been discussed by several authors see e.g. Høyland (2002b); Beketsky et al. (1997); Veitch et al. (1991); Croasdale et al. (1990). The deterioration phase starts when the ice ridge is heated also from above, usually late in the season (Fig. 1 d)). But in the rubble the deterioration and the consolidation goes on parallel in the main phase, the upper part of the rubble freezes up and the lower parts is subjected to erosion from the ocean.

When ice rubble deforms the ice blocks may firstly rotate and slide and secondly they may break and crush. In the first case there is also some ice breaking as the freeze bonds between the blocks have to be broken before the blocks can move. These mechanisms can in principle be modelled in a discrete element model, but more common are the continuum models. An elastic-plastic continuum model such as the Mohr-Coulomb model is often used in analytical and numerical models. Much effort has been put into finding the appropriate cohesion (c) and the angle of internal friction (φ), see Liferov and Bonnemaire (2004), Timco and Cornet (1999) and Ettema and Urroz-Aguirre (1989) for overviews. However, as the consistency of the ice rubble changes substantially during its lifetime (Leppäranta et al., 1995; Høyland, 2002a) it is likely that the mechanical parameters also change. The development of the consistency of the unconsolidated parts of a first-year ice ridge is governed by a number of factors: the temperature, the thickness and the salinity of the initial ice, the velocity, the temperature and the salinity of the surrounding water and finally the ridge keel permeability. When the initial phase ends all the negative energy (cold) of the ice blocks is gone and the direct effect of the initial conditions stops. Thereafter in the main phase the oceanographical conditions govern the thermal and mechanical erosion and thus the development of the consistency of the rubble. This means that the freeze bonds in-between the ice blocks (which is often linked to the cohesion of the material) increase in volume and strength during the initial phase and thereafter decrease. The individual blocks may also break or crush when the rubble is being deformed so that the strength of the in-situ rubble is of interest in a numerical model as was shown by Hopkins and Hibler, 1991. The hardness derived from a drop ball test as described by Khrapaty and Wessels (1984) may be used as an index strength, though it may be difficult to relate it uniquely to standard test such as compression test (Høyland et al., 2004). As the rubble slowly approaches a slushy consistence it will no longer be possible to distinguish between original ice and the freeze bonds created in the initial phase of consolidation.

Some central but not yet well answered questions about the initial phase of ridge consolidation are how long does it last (Δt_0)? how thick does the consolidated layer become ($h_{c,0}$)? how much energy is gained from the ocean (q_{ocean})? and what is the effect of the initial ice temperature (T_{init})

and the initial ice block thickness (h_b)? In this paper we are mostly concerned with the initial phase of consolidation and will try to give some answers to some of the questions above.

2. A simple estimation of q_{ocean}

The oceanic flux (q_{ocean}) can be estimated by the following energy balance applied to the entire ridge:

$$E_{sur} - E_{ocean} = E_{lat} - E_{init} \tag{1}$$

where E_{sur} is the energy that is transported upwards into the surrounding air, E_{ocean} is the energy that comes from the surrounding water, E_{init} is the potential energy stored in the ice blocks, or the energy required to heat the ice, and E_{lat} is the energy released to freeze new ice. The left-hand side is the net energy transfer into/out of the ridge and this has to be balanced by a change in the internal energy of the ridge (right-hand side). We assume that the change in internal energy is expressed either as a temperature change (E_{init}) or a phase change (E_{lat}).

The energy loss through the surface may be estimated by the use of the measured temperature gradients in the consolidated layer and Fourier's law:

$$E_{sur} = \sum k_i \cdot \frac{\Delta T}{\Delta h} \cdot \Delta t \cdot A_{sur} \tag{2}$$

where k_i is the thermal conductivity of the sea ice (the index i is in the following used for sea ice), T the temperature, h the vertical distance, Δt the time and A_{sur} is the surface through which the energy escapes.

The initial, or the potential energy, is basically a function of the initial temperatures, T_{init} of the ice blocks and the specific heat capacity, $c_i(T)$, it may be calculated as:

$$E_{init} = \rho_i V \int_{T_{init}}^{T_f} c_i(T) dT \tag{3}$$

where V is the volume of the ice, ρ_i the density, T_{init} the average initial ice temperature, T_f is the freezing point of sea ice and $c_i(T)$ the specific heat capacity of the ice.

The latter may be calculated after Schwerdtfeger (1963). The latent heat released may be calculated by assuming that only parts of the ridge (corresponding to the macroporosity) freezes:

$$E_{lat} = \rho_i \cdot \eta \cdot l_i \cdot \Delta h_c \cdot A_{sur} \tag{4}$$

where η is the macro porosity of the ridge, l_i is the latent heat of the saline ice calculated after Schwerdtfeger (1963) and Δh_c the growth of the consolidated layer. The macro-porosity is given as the volume of non-sea ice divided by the total volume, whereas the total porosity includes the porosity of the sea ice, see Høyland (2002a) for a closer explanation of the different porosities.

The average oceanic flux (q_{ocean}) is then given as:

$$q_{ocean} = \frac{E_{sur} - E_{lat} + E_{init}}{\Delta t \cdot A_{sur}} \tag{5}$$

where Δt is the duration.

3. Experimental set-up

The ridges were produced as explained in Liferov and Høyland (2004) and two thermistorstrings were installed in R1 and R2 as shown in Fig. 2. The vertical resolution of the strings in R1 was 0.20 m and 0.10 m for the strings in R2. They were installed immediately after the ridge was produced, and the temperatures were logged periodically until the scouring experiments. During the first day every 5 minutes, thereafter every hour. Table 1 gives information about the strings. The thermistor strings and loggers are explained in Løset et al. (1998).

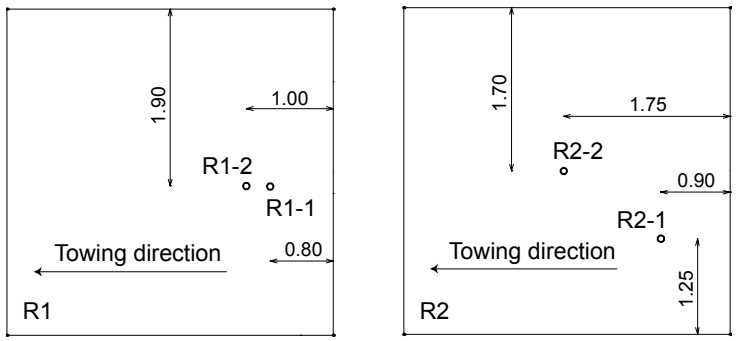

Fig. 2. The position of the thermistorstrings in R1 and R2.

Table. 1. The thermistorstrings.

Ridge	Start	Stop	*FDD*[a] (ºC·days)	Resolution (m)	Position
R1-1	13.03.02	09.04.02	-310	0.2	Side
R1-2	13.03.02	09.04.02		0.2	Side
R2-1	29.03.03	25.04.03	-253	0.1	Side
R2-2	29.03.03	25.04.03		0.1	Ridge centre

[a] $FDD = \int_{t_0}^{t} (T_a - T_f)dt$

Physical and mechanical properties of the level ice from which the ridge was made and the ridge itself was examined. The level ice in the years of 2002 and 2003 is in the following named respectively L1 and L2 and Table 2 gives an overview of the testing discussed in this paper. Cores were sampled from the consolidated layer in R1 18.04.02 and in R2 29.04.03, horizontal and vertical cores from the level ice were sampled several times during the winter 2003 and sampling from the rubble in R3 were done on two occasions; 09.04.03 (salinity and temperature) and 25.04.03 (hardness, temperature and salinity).

The salinity was measured with a conductivity measuring device and the drop ball tests were done on site and a steel ball (66 mm diameter, 1.18 kg) was dropped on the ice samples from a height ranging from 0.75 to 0.92 m. The procedure is more closely explained by Bonnemaire et al. (2003) and Vatne (2003). Mechanical drilling with a 50 mm drill bit was done to examine the porosity. Any drop of the drill was considered to be a pore and its length and position was noted. The difference between ice and pores could easily be detected as the ridge was young and the rubble not eroded. The volume of ice put into the ridge compared to the ridge volume was also used to estimate the porosity.

Table 2. Test matrix.

Ice	Salinity	Density	Temperature	Drop ball
L1	Yes	No	Yes	No
L2	Yes	Yes	Yes	Yes
R1	Yes	Yes	Yes	No
R2	Yes	Yes	Yes	No
R3	Yes	No	Yes	Yes

4. Results

Fig. 3 shows the thickness of the consolidated layer for the two ridges R1 and R2 as given by the thermistorstrings defined as given by Høyland (2002a). That is the thicknesses are given as the distance down to the lowermost node in which the temperature is below T_f, and above which all the

nodes are below T_f; in other words a minimum thickness of the consolidated layer, h_c is given and it corresponds with the upper cold front definition.

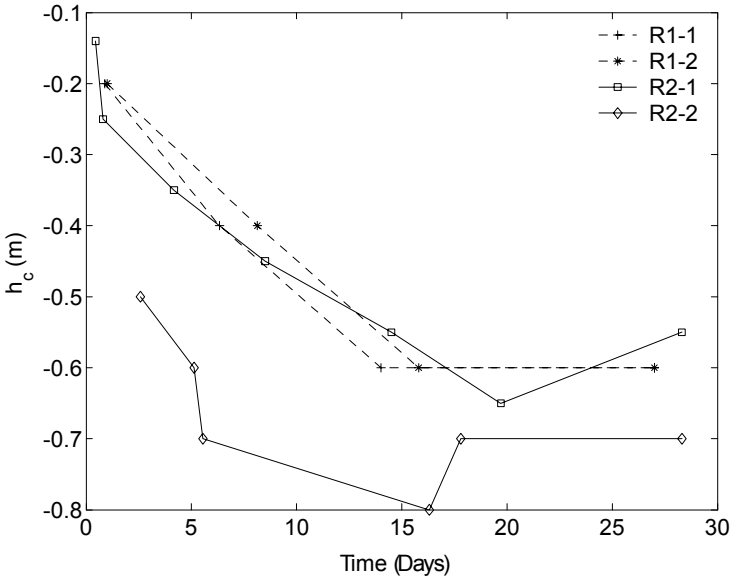

Fig. 3. The thickness of the consolidated layer in the different ridges during their period of monitoring.

The lower warm front below which the temperature is at or above T_f is plotted together with the upper in Figs. 4 and 5. The lower front is given as the maximum extension from the water line, so that it contains all the nodes (counting from the bottom) in which $T \geq T_f$. This means that the real thickness of h_c is somewhere in-between the lines giving the upper and the lower front. The transition into the main phase can be found from when the lower front reaches its maximum and turns downwards. The duration of the initial phase can be seen to vary in the different ridges and also at different places in the ridge depending on the distance to the water-keel boundary. In R2 the lower front turned after 4 days (3.5 days of monitored time + 12 hours production time) and the initial thickness was in average $h_{c,0}$ = 0.32 m, whereas the corresponding numbers for R1 were 16 hours and 0.1 m (the temperatures shows that the lower front was at 0.2 m below the water line in R1 four hours after the thermistorstring was installed, this means that the real thickness is somewhere between 0 and 0.2 m).

The porosity of R3 could be estimated from drillings, but the consistency of the two other ridges was too soft at the time of drilling to estimate the porosity. The macro porosity of the R3 ridge was measured to be 0.34.

The initial temperature of the ice (T_{init}) that was put into R1 and R2 was respectively -7.7º C and -11º C, Table 3 sums up the physical properties. The salinity of the consolidated layer in R2 was 3.6 ppt and this is less than the salinity of L2 at the day of production, but also less than the salinity of the level ice in late April. The hardness of the 2 week old pieces of rubble from R3 was 11.5 MPa,

and this is under half of that of L2. The salinity of the rubble in R3 sank from 4.5 ppt to 3.8 ppt during the 16 days between production and testing.

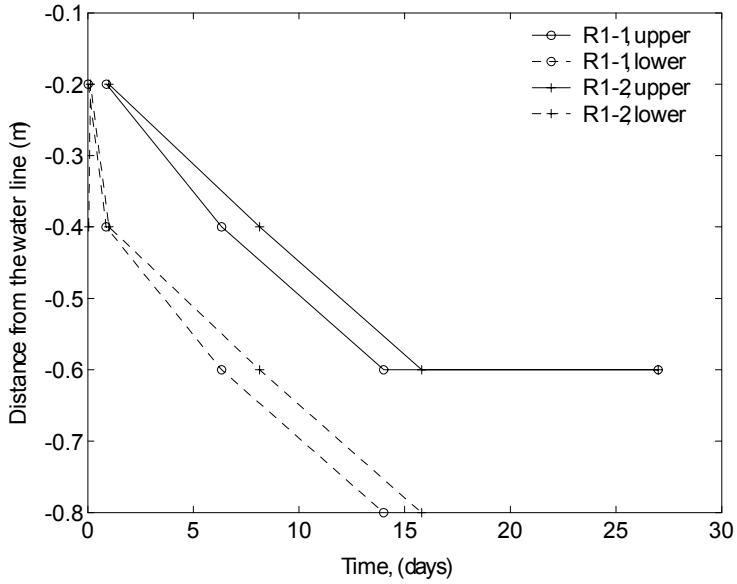

Fig. 4. The distance from the water line and down to the upper front (minimum) and the lower front (maximum) for R1 during the monitored period.

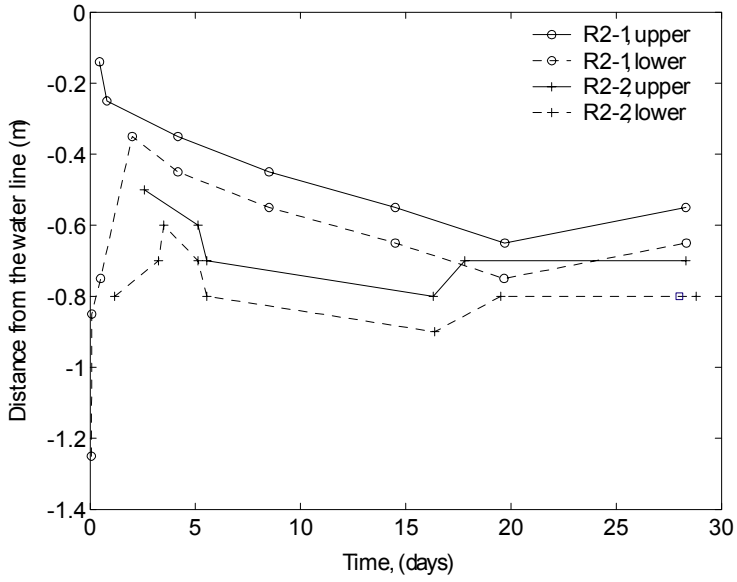

Fig. 5. The distance from the water line and down to the upper front (minimum) and the lower front (maximum) for R2 during the monitored period.

Table 3. The mechanical properties and the salinity, the index *c* means the consolidated layer, *i* means sea level ice and *r* means the rubble.

	Average	St. dev	Min	Max	n	Comment
S_c (ppt)	3.6	0.4	2.9	4.2	12	R2
S_i (ppt)	5.0	1.2	7.7	2.4	122	L2
H_r^a (Mpa)	26.1	-	19.9	37.1	41	L2, T_i = [-6.5,-11]ºC
H_r (Mpa)	11.2	2.7	7	14	16	R3, vertical
H_r (Mpa)	11.5	3.7	4	16	31	R3, horizontal
S_r (ppt)	4.5	0.2	4.2	4.9	8	R3, 09.04.03
S_r (ppt)	3.8	0.7	2.4	4.8	13	R3, 25-27.04.03

[a] H is the hardness defined in the drop ball test

5. Analysis and discussion

5.1 Consolidation and decay

5.1.1 The initial phase of consolidation

The duration of the initial phase (Δt_0) was only a few hours (4 hours + production time) in R1, whereas it was 4 days (3.5 days + production time) in R2. There was also a difference between the two strings in R2: the warm front penetrated faster and deeper into the ridge close to R2-1, which was positioned on the side of the ridge. This effect was also probably present in the year 2002, so that the initial phase may have lasted longer than the four hours predicted by the string R1-2 which was not positioned in the centre. The air temperatures were similar during the initial phase and we do not believe that they influenced on $h_{c,0}$. One reason for the lower Δt_0 in R1 was that the average initial ice temperature was higher and thus E_{init} becomes less. However, the basic difference seems to have been the keel depth. Fig. 6 shows the position of the lower front measured from the bottom of the keel during the initial phase, it shows that also in R2 the warm front quickly penetrated one metre into the ridge keel, and that the progress then slowed down. The fact that R2-2 was in the centre of the ridge may explain that this curve is lowered a bit in relation to R2-1 and the lower T_{init} in R2 may have shifted the R2 curves a bit to the right. The importance of T_{init} may be higher the larger the ridge is, and we think that in large ridges made from cold ice the initial phase may last for many days (perhaps weeks).

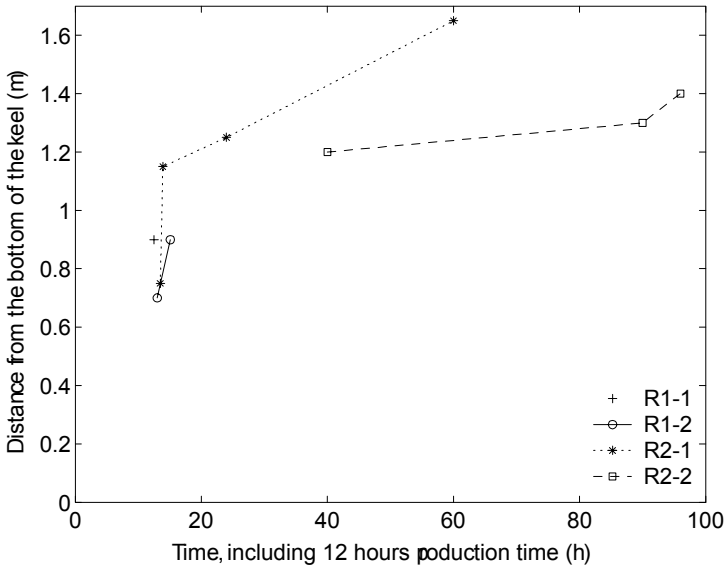

Fig. 6. The distance from the bottom of the keel and up to the lower front in R1 and R2 during the initial phase.

Table 4 shows the calculated oceanic flux for the two ridges, and during the initial phase it was about 235 W/m^2 for R1 and about 65 W/m^2 for R2 (Høyland et al. (2002) estimated the oceanic flux into R1 it to be 2 kW/m^2, but this is wrong due to a computational error). An ice ridge field was investigated in the Gulf of Bothnia the winter of 1999 and Høyland (2002b) used FEM to estimate the oceanic flux during the initial phase to be 500 W/m^2 under the assumption that it lasted one week. These values for the average oceanic flux during the initial phase of consolidation are substantially higher than what is usually estimated for level ice (2-10 W/m^2). Høyland (2002b) also investigated the ice in the Van Mijen fjord and found that an oceanic flux of 2 W/m^2 balanced the numerical ice growth model. A value of 2 W/m^2 has also been estimated by Maykut and Perovich (1987) as an average value for the Arctic basin. The oceanic flux for ridges is of interest as it affects the size of the consolidated layer, and together with the initial ice conditions (primarily the temperature and the thickness) it represents the main uncertainty in finding the maximum thickness of the consolidated layer. Marchenko et al. (2004) present a model that includes the initial ice temperatures but as it does not include any convective heat transfer from the ocean we believe that it overestimates the effect of the initial conditions.

The main reason for the higher value for R1 was the short duration of the initial phase. As given in Table 4, the model is sensitive to the initial thickness of the consolidated layer and the salinity, but the accuracy of the initial ice temperature and the ridge porosity are also important. If the initial ice temperature varies ± 2º C the oceanic flux varies 15-20 % correspondingly. The porosity of ice ridges may vary through the thickness, at least for larger ridges (Surkov and Truskov, 2003), and if we use 0.25 as the porosity for the top layer (where the initial freezing is assumed to take place) and 0.34 as average porosity for the ridge the oceanic flux increases about 15 % for R1 and about 30 %

for R2. Table 4 also shows that saline thermal properties are necessary as calculations with non-saline properties gives negative oceanic flux, which is difficult to explain. The input salinity in our three ridges was probably less than it is for naturally made ridges in the Van Mijen fjord as the block thickness of these ridges (measured in 1998, 1999, 2002 and 2003) has been between 0.15 and 0.25 m. The salinity of this thin level ice may be about 10 ppt (Weeks and Ackley, 1982) and some calculations with this salinity are also included in Table 4. In Table 5 some of the energies (MJ/m^2) from Eq.1 and ratios in-between them are given. The ratio between the energy released by ice growth and the oceanic energy argues that the smaller the ridge the larger relative oceanic heat transfer.

Table 4. The oceanic flux during the initial phase for the two ridges.

S_i (ppt)	$h_{c,0}$ (m)	Δt_0 (days)	q_{ocean} (W/m^2)
	R1		
0	0.10 (0.15)	0.7	-44 (-130)
4.5	0.10 (0.15)	0.7	221 (147)
5	0.10 (0.15)	0.7	251 (178)
10	0.10 (0.15)	0.7	523 (465)
	R2		
0	0.32	4	-28
4.5	0.32	4	58
5	0.32	4	68
10	0.32	4	182

Table 5. The different energy contributions for the two ridges (MJ/m^2).

S_i (ppt)	E_{init}	E_{lat}	E_{ocean}	E_{init}/E_{lat}	E_{init}/E_{ocean}	E_{ocean}/E_{lat}
			R1			
4.5	20.0	9.0	13.4	2.2	1.5	1.5
5	21.6	8.84	15.2	2.4	1.4	1.7
			R2			
4.5	38.5	28.8	20.0	1.3	1.9	0.7
5	41.3	28.3	23.4	1.5	1.8	0.8

5.1.2 The final thickness of the consolidated layer and the porosity

The final thickness of the consolidated layer ($h_{c,f}$) was 0.6-0.8 m in R1 and 0.65-0.9 m in R2. However, the temperatures in the lowermost node in the consolidated layer were lower in R1 than in R2. The real freezing front in R1 was probably closer to 0.7 m, whereas in R2 it was between 0.65 and 0.8 m. In other words it is difficult to find any difference between the two ridges. The higher *FDD* in the year 2002 may have been compensated by a lower initial ice block temperature (T_{init}) and thus a higher initial thickness ($hc;0$) in the year 2003. Table 6 shows the thickness of the consolidated layer predicted by an adjusted Stefan's law as given by Leppäranta and Hakala (1989).

An empirical correction coefficient (ω) is also needed to account for snow, oceanic flux and solar radiation, and this coefficient has been estimated for two places in the Van Mijen fjord to be 0.32 and 0.4 (off Camp Morton and off Svartodden, Høyland (2002a)).

The equation predicts fairly well the growth of h_c, and the colder initial ice in R2 may explain it's higher ω. The ω's are obtained from measurements of level ice growth and it is a crude approximation to apply them also to ridges, but they fit the measurements well (Høyland, 2002a). But as pointed out by Leppäranta (1993) ice growth is a stable process and this may be the reason that the simple models give good predictions for ice growth.

The measured macro porosity of 0.34 corresponds well with other results reported by e.g. Leppäranta et al. (1995) and Høyland (2002a). Høyland et al. (2002) estimated the macro porosity of R1 to be 0.34, this fits remarkably well and since the three ridges were made in the same way we assume their porosities to be equal.

Table 6. Predictions using Stefan's law. The three lower results earlier presented in Høyland (2002a).

Ridge	$h_{c,0}$	$h_{c,f}$	ω	FDD (ºC·days)	$h_{c,predicted}$
2002, R1	0.20	0.60	0.40	-310	0.69
2002, R1	0.10	0.60	0.40	-310	0.66
2003, R2-1	0.25	0.65	0.40	-253	0.65
2003, R2-2	0.50	0.80	0.45	-253	0.80
2003, average	0.32	0.72	0.45	-253	0.71
Svartodden, 1998	1.19	1.61	0.40	-985	1.65
Camp Morton, 1999	1.05	1.35	0.32	-620	1.33
Marjaniemi, 1999	0.80	1.03	0.90	-126	1.00

5.2 Physico-mechanical properties

The energy transfer from the ocean into the rubble continues during the main phase of consolidation but it is definitely less and more difficult to measure as it is no longer reflected as a change of ice-temperatures. There are little currents in this part of the fjord, but the temperature of the sea bed below the ridges were about -1.6º C, and this is reflected in the temperature measurements of the pieces of rubble from R3. The hardness tests were performed in an ice temperature range (-1.6, -2.1)º C, but no temperature dependency was found in this temperature range. The L2 level ice was as shown in Table 2 harder and colder, but the hardness of relatively warm level ice (T = -2.1º C) from the Barents Sea was 13.4 MPa (Vatne, 2003). The hardness does, as other mechanical parameters and properties of sea ice decrease with increasing temperature, and this is basically because the porosity increases with the temperature. When ice is at, or above the

freeing point the temperature is no longer an index of strength as the porosity of the ice is a function of the eroding surroundings and not the temperature.

The mechanical properties of the rubble as a whole change as energy is added and more of the ice melts, and this can be felt when drilling the same ridge several times through one season. The rubble in R3 was little eroded and the individual blocks were harder than most rubble we have experienced in nature (Høyland (2002a), Bonnemaire et al. (2003) and unpublished results UNIS). It is by this not said that the continuum strength of the rubble was higher than in an average ridge.

The salinity measurements showed a decreasing salinity with time in the rubble of R3, and this is probably because the high salinity brine in the ice blocks (S>35ppt) interacts with the sea water and lowers the salinity of the ice blocks. Salinity measurements in older ridges have shown higher salinity of pieces of rubble than of the surrounding level ice and the consolidated layer (Bonnemaire et al. (2003) and Heinonen et al. (1999)).

6. Conclusions

Three ridges have been artificially produced in the years 2002 (R1) and 2003 (R2 and R3) close to Svea in the Van Mijen fjord on Svalbard, Norway. The temperature development in R1 and R2 was monitored and physical properties have been measured in all three. The novelty of this work is the focus on the initial phase of consolidation and the main conclusions are as follows:

- The initial phase lasted 4 days for R2 and only 0.7 days for R1. The initial ice temperatures were less in R2 and this may have contributed, but we believe the principal reason was the different keel depths (respectively 2.2 and 1.4 m).
- The initial thickness of the consolidated layer was 0.32 and 0.1 m for respectively R2 and R1. We believe that the difference in initial ice temperatures was the most important factor, though the difference in keel depth may also have had effect.
- The oceanic flux during the initial phase was calculated by a simple model and it became about 63 and 235 W/m^2 for R2 and R1, and this is substantially higher than what is usually estimated for the level ice (2-10 W/m^2). It is important to include thermal properties of saline ice.
- If the cohesive strength of the rubble is linked to the freeze-bonding in-between the blocks, then the strength of the rubble will increase during the initial phase and thereafter decrease as the erosion process proceeds.

Akcnowledgement

The authors would like to thank the following people without whom the experiments could not have been done the way it was done: PhD student Per Olav Moslet, UNIS, master student Rune Nilsen, UNIS/NTNU, PhD student Basile Bonnemaire, NTNU, professor Sveinung Løset, NTNU/UNIS, PhD student Morten Bjerkås, NTNU, master student Sergeij Vernyayev, UNIS, and finally the two UNIS students Bjørn Dettwiler and Rinat Kamalov. Crucial financial and logistic support came from Store Norske Spitsbergen Mining Company (SNSK) and Statoil ASA. The Norwegian Research council and Barlindhaug Consult AS paid the salary of Pavel Liferov and the University Centre in Svalbard (UNIS) provided logistic assistance and important help.

References

Beketsky, S., Astafiev, V., and Truskov, P., 1997. Design parameters for hummocks and grounded hummocks in the Sea of Okhotsk. In Proc. of 7th Int. Offshore and Polar Eng. Conf. (ISOPE), Honolulu, Hawai, Vol. 2, pp. 487-493.

Bonnemaire, B., Høyland, K. V., Liferov, P., and Moslet, P., 2003. An ice ridge in the Barents Sea, Part I: Morphology an physical parameters. In Proc. of the 17th Int. Conf. on Port and Ocean Eng. under Arctic Conditions (POAC), NTNU, Trondheim, Norway, Vol. 2, pp. 559-568.

Croasdale, K. R., Allen, N. F. B., and Marcellus, R. W., 1990. Thermal response of ice rubble: predictions and observations. In Proc. of the 10th Int. Symp. on Ice (IAHR), Espoo, Finland, 20-24 August 1990, Vol. 1, pp. 153- 167.

Ettema, R. and Urroz-Aguirre, G.E., 1989. Friction and cohesion in ice rubble reviewed. Cold Regions Engineering, 12: 317-326.

Heinonen, J., Määtänen, M., Høyland, K. V. and Kjestveit, G., 1999. Ridge loading experiments, field experiments in winter 1999. Technical report, HSVA, Hamburg, Germany, 43 p.

Hopkins, M.A. and Hibler, III, W.D., 1991. On the shear strength of geophysical scale ice rubble. Cold Regions Science and Technology, 19: 201-212.

Høyland, K. V. (2002a). Consolidation of first-year sea ice ridges. Journal of Geophysical research, 107(C6, 10.1029/2000JC000526). 15,1-15,15.

Høyland, K. V. (2002b). Simulations of the consolidation process in first-year sea ice ridges. Cold Regions Science and Technology, 34: 143-158.

Høyland, K. V., Bjerkås, M. And Vernyayev, S., 2004. Mechanical properties of ice ridges and level ice, in-situ and laboratory testing 2003. In Proc. of the 17th Int. Symp. on Ice (IAHR), St. Petersburg, Russia, Vol. 1, pp. 69-75.

Høyland, K. V., Liferov, P., Moslet, P. O., Løset, S., and Bonnemaire, B., 2002. Medium scale modelling of ice ridge scouring of the sea bed, Part II: Consolidation and physical properties. In Proc. of the 16th Int. Symp. on Ice (IAHR), Dunedin, New Zealand, Vol. 2, pp. 94-100.

Khrapaty, N. G. and Wessels, E., 1984. A new testing technique of ice strength in compression and bending. In Proc. of the 7th Int. Symp. on Ice (IAHR), Hamburg, Germany, 1: pp. 83-91.

Leppäranta, M., 1993. A review of analytical models of sea-ice growth. Atmosphere-ocean, (31 (1)). 123-138.

Leppäranta, M. and Hakala, R., 1989. Field measurements of the structure and strength of first year ice ridges in the Baltic Sea. In 8th Int. Conf. on Offshore Mechanics and Arctic Eng. (OMAE), the Netherlands, Vol. 4, pp. 169-174.

Leppäranta, M., Lensu, M., Koslof, P., and Veitch, B., 1995. The life story of a first-year sea ice ridge. Cold Regions Science and Technology, 23: 279-290.

Liferov, P. and Bonnemaire, B., 2004. Ice rubble behaviour and strength, Part I: Review of testing methods and interpretation of results. Cold Regions Science and Technology, in press.

Liferov, P. and Høyland, K. V., 2004. Ice ridge scouring experiments, part I: Experimental set up and basic results. Submitted to Cold Regions Science and Technology.

Løset, S., Bergheim, B., Langeland, A., and Høyland, K. V., 1998. Geometry and physical properties of a stamucha found on spitsbergen. In Proc. of the 14th Int. Symp. on Ice (IAHR), Potsdam, NY, USA, Vol. 1, pp. 339-344.

Marchenko, A., Makshtas, A., Guoshnikov, Y., and Zubakin, G., 2004. Thermodynamic consolidation of sea ice ridges. In Proc. of the 17th Int. Symp. on Ice (IAHR), St.Peterburg, Russia, Vol. 2, pp. 282-288.

Maykut, G. and Perovich, D. K., 1987. The role of short wave radiation in the summer decay of a sea ice cover. Journal of Geophysical research, 92: 7032-7044.

Schwerdtfeger, P., 1963. The thermal properties of sea ice. Journal of Glaciology, (4 (36)).

Surkov, G. A. and Truskov, P. A., 2003. Parameters of hummock-forming blocks of ice. In Proc. of the 17th Int. Conf. on Port and Ocean Eng. Under Arctic Conditions (POAC), NTNU, Trondheim, Norway, Vol. 2, pp. 593-598.

Timco, G.W. and Cornett, A.M., 1999. Is φ a constant for broken ice rubble? Proc. of the 10th Workshop on River Ice Management with a Changing Climate. Winnipeg, Manitoba, Canada, pp. 318–331.

Vatne, L., 2003. Interaction between a riser armour and ice rubble. Master's thesis, The University Courses in Svalbard, UNIS / Department of Marine Engineering, NTNU. 97 p.

Veitch, B., Lensu, M., Riska, K., Koslof, P., Keiley, P., and Kujala, P., 1991. Field observations of ridges in the northern Baltic Sea. In Proc. of the 11th Int. Conf. on Port and Ocean Eng. under Arctic Conditions (POAC), St.Johns, Canada, pp. 381-438.

Weeks, W. and Ackley, S., 1982. The growth, structure and properties of sea ice. Technical Report Monograph 82-1, CRREL, USA. ? p.

4 ON ICE RUBBLE BEHAVIOUR AND STRENGTH

4.1 Introduction

This chapter presents the work on ice rubble with particular focus on its behaviour and strength. The motivation for this work within the ice ridge scour study was a lack of solid and systemized knowledge about the properties of the keels' material, i.e. ice rubble. Without having this, it would be impossible to describe the keel destruction during the scour process to correctly assess the scour depth.

A number of testing programmes was conducted both in the laboratory and in-situ during the last three decades. Ice rubble was normally described either as the Tresca or as the Mohr-Coulomb material. The cohesion and the angle of internal friction of ice rubble were a subject for investigation and discussion. Variation in the above strength parameters was, in particular for the laboratory tests, exceedingly high and there are a number of reasons for this.

In contrast with other granular materials, the lifetime of ice rubble within the first-year ice ridge is limited to a few months. During this period the ice rubble constantly evolves throughout the initial, main and the decay phases. Laboratory tests on ice rubble are normally conducted during the initial phase, which is believed to be the most sensitive with respect to the testing conditions. When modelling ice rubble, the thermodynamic similarity is of high significance in addition to geometric, kinetic and dynamic similitudes between the prototype and the model. All this, even intending, is very difficult to achieve in reality. Different interpretation of test result with subsequent comparison neither helped to meet the agreement on how to apply, e.g. the Mohr-Coulomb model to ice rubble.

This chapter consists of five papers, each composing a section. Section 4.2 gives a general overview of the tests done on ice rubble while some of the most recent tests are discussed in detail. It also describes the test results with respect to the observed behaviour. Further, it gives a discussion on the scaling aspects and summarizes the results from the different tests. Section 4.3 presents an approach to model and study ice rubble based on the findings from Section 4.2. Section 4.4 shows an application of the classical theory of elasto-plasticity to interpretation of the bi-axial tests on ice rubble. Sections 4.5-6 present the finite-element analysis of the laboratory punch tests on ice rubble. All sections are identical to the referred papers.

Publication references:

(4.2) Liferov, P. and Bonnemaire, B. Ice rubble behaviour and strength, Part I: Review of testing methods and interpretation of results. Journal of Cold Regions Science and Technology, 41: 135-151.

(4.3) Liferov, P. Ice rubble behaviour and strength, Part II: Modelling. Journal of Cold Regions Science and Technology, 41: 153-163.

(4.4) Liferov, P. and Høyland, K.V., 2003. Ice rubble properties from plane strain tests. Proceedings of the 17th International Conference on Port and Ocean Engineering under Arctic Conditions. Trondheim, Norway, Vol. 2, pp. 611-621.

(4.5) Liferov, P., Jensen, A. and Høyland, K.V., 2003. 3D finite element analysis of laboratory punch tests on ice rubble. Proceedings of the 17th International Conference on Port and Ocean Engineering under Arctic Conditions. Trondheim, Norway, Vol. 2, pp. 599-610.

(4.6) Liferov, P., Jensen, A., Høyland, K.V. and Løset, S., 2002. On analysis of punch tests on ice rubble. Proceedings of the 16th International Symposium on Ice. Dunedin, New Zealand, Vol. 2, pp. 101-110.

4.2 Ice rubble behaviour and strength, Part I: Review of testing and interpretation of results

P. Liferov[1,2] and B. Bonnemaire[1]

Abstract

The deformation behaviour and strength of ice rubble are addressed in this paper. Review of ice rubble testing and strength is given. Pure shear and punch tests on ice rubble are considered with special attention to derivation of material properties. The primary failure mode associated with initial breakage of rubble skeleton is found to dominate overall rubble strength in punch tests. Scaling of ice rubble is touched upon and a summary of scaled rubble properties is presented. The average *c/t* value was found to be around 20 kPa/m derived both from the laboratory and the in-situ tests. Unreasonably high values of φ (above 50º) seem to come from analyses where cohesive component of rubble strength was neglected when deriving the material properties.

Keywords: Ice ridge, ice rubble, strength, Mohr-Coulomb, scaling.

1. Introduction

Ice rubble plays an important role in many engineering problems, ranging from river ice engineering aspects to ice-cover interaction with offshore structures. Knowledge about the mechanical properties of ice rubble is however rather limited. Several programmes on testing these properties have been carried out since the beginning of the seventies. Both laboratory and in-situ tests were conducted.

Most of the laboratory experiments were done with different types of shear boxes. The first shear tests were done in direct shear boxes (Prodanovic, 1979; Keinonen and Nyman, 1978; Weiss et al., 1981; Hellman, 1984; Fransson and Sandkvist, 1985) followed by simple shear tests (Urroz and Ettema, 1987) and constant confining pressure tests (Sayed, 1987) and finally more sophisticated bi-axial tests (Timco et al., 1992; Løset and Sayed, 1993; Cornett and Timco, 1996). Extensive reviews of shear tests and interpretation of results are given by Ettema and Urroz (1989, 1991) and Timco and Cornet (1999). The results showed that ice rubble behaviour could generally be described by an elastic-perfectly plastic model where the plasticity is defined by the Mohr-Coulomb

[1] Norwegian University of Science and Technology
[2] Barlindhaug Consult AS

law. Tri-axial tests on ice rubble as described by Wong et al. (1990) supported the idea of using the Mohr-Coulomb yield criterion. They observed that the cohesion and the friction angle depend on the initial void ratio. Recent direct shear tests done by Yasunaga et al. (2002) agree with the above findings. Several programs on punch testing of ice rubble were also performed in the laboratory as described by Azarnejad and Brown (1998), Jensen et al. (2000, 2001) and Lemée and Brown (2002).

The variation in the reported values of ice rubble strength was very wide. Ice rubble strength appeared to be dependent on the confining pressure, strain rate, size of ice blocks, void ratio, time history, etc. Control of the boundary conditions during testing and interpretation of test results could also have been a potential source of substantial discrepancy in the measured values. Scaling of the ice rubble strength is another issue that has been addressed very little. Altogether this state of knowledge did not give reliable information for assessment of full-scale loads from first-year ice ridges and caused a need for in-situ testing.

The first in-situ testing was undertaken by Leppäranta and Hakala (1992) in the Baltic Sea. They did several punch tests on first-year ice ridges. A number of in-situ test programs has been carried out later as described by Heinonen (1999), Smirnov et al. (1999) and Timco et al. (2000). The majority of in-situ tests were punch tests. Several direct shear tests and pull-up tests were done as well. Recently, one shear-off test on artificially produced ice rubble was done by Liferov et al. (2003).

The derivation of the rubble strength from tests whose boundary conditions are not well controlled as, for example, in punch tests, is a special issue that demands particular attention. Two approaches have been used to interpret the test results, namely analytical and numerical. Among the analytical approaches both the different forms of limit equilibrium method (Leppäranta and Hakala, 1992; Azarnejad and Brown, 1998; Jensen et al., 2000) and the upper bound theorem of plasticity (Heinonen and Määttänen, 2000) were used. Regardless of the general validity of the above methods, the major problem was associated with the use of the two-parametric Mohr-Coulomb failure criterion. Simplifications were done and ice rubble was considered either as a frictionless or as a cohesionless material. In the latter case, however, excessively high values of the internal friction angle were obtained.

As the analytical approach does not take the complexity of deformation mode into account, it may yield to unreliable results. Numerical modelling of punch tests turned out to be a useful tool for judgement of the rubble strength. Finite-element modelling of punch tests was conducted by Heinonen (1999, 2002) and Liferov et al. (2002, 2003). In the latter work it was found that in laboratory punch tests the bending failure can contribute substantially and that neglecting the cohesive/adhesive strength might lead to unreliable results.

The writers are by no means the first to ponder the complicated topic of ice rubble strength. This paper is rather an attempt to address some of the unresolved questions that arise when trying to summarize and systemize the ice rubble strength based on the existing data with focus on its further application in assessment of loads from ice ridges. A discussion about interpretation of test results is essentially based upon the most comprehensive test programs conducted during the last decade with some references to earlier research.

2. Shear box tests

2.1 General

A thorough discussion about the shear box tests conducted before the 90's was done by Ettema and Urroz (1989, 1991). They addressed the meaning of internal friction angle and cohesion. An important point has been made about whether the peak angle of internal friction φ_p or the critical state friction angle φ_c have been reported in most of the studies. They also argued that unconsolidated ice rubble undergoing continuous shear deformation is essentially cohesionless and an effective angle of internal friction φ' was suggested to describe the material strength. The derivation of the ice rubble strength from the noticeable series of tests in the bi-axial compression apparatus conducted by Sayed et al. (1992), Løset and Sayed (1993) and Cornett and Timco (1995, 1996) has also been based on the assumption that ice rubble has a cohesionless nature. They used the following formulation to derive the mobilised angle of internal friction φ_m from the measured stresses:

$$\varphi_m = \sin^{-1}\left(\frac{\sigma_1 - \sigma_3}{\sigma_1 + \sigma_3}\right) \tag{1}$$

where σ_1 and σ_3 are major and minor principal stresses, respectively. The obtained values for the angle of internal friction mobilized throughout each test were somewhat illusive (Timco and Cornett, 1999). The calculated angles of internal friction that were reached during the samples loadings distinctly decreased from unrealistic 70-90° in the beginning of the test and approached stagnant constant value of about 30-45°.

An attempt to discuss initial assumptions about the material model and their influence on the derived material properties from the above tests is given further. This discussion is based on a more detailed analysis as presented by Liferov and Høyland (2003). The purpose of this discussion is to eliminate the confusion that may appear when trying to compare the rubble strength and behaviour from the tests in the bi-axial compression apparatus with other tests on ice rubble.

2.2 Reappraisal of data from Cornett and Timco

A typical view of the φ_m derived using Eq. 1 versus shear strains γ from the Constant Lateral Pressure (CLP) tests conducted by Cornett and Timco (1995) is shown in Fig. 1 as curve (a). If the classical theory of elasto-plasticity and its applications to the granular materials are kept in mind, the confusions associated with curve (a) in Fig. 1 are the following:

- It shows that ice rubble has been softening since the very beginning of the test, i.e. was becoming weaker;
- It contradicts with the measured curve (b) representing shear stresses τ versus shear strain γ and that shows that ice rubble was rather hardening as the sample was loaded, i.e. was mobilising strength. Curve (c) is the φ_m vs. γ curve that is expected to correspond to the curve (b), in Fig. 1 it coincides with the curve (b);
- The values of the φ_m are exceptionally high in the beginning of the tests (up to 90º).

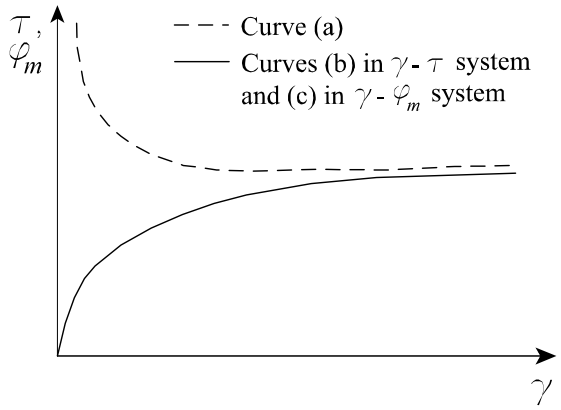

Fig. 1. Mobilized angle of internal friction and shear stress vs. shear strain.

The reason for above confusions is that the secant values of φ_m (the slope of a line drawn from the co-ordinate origin to a point on the failure envelope) rather than tangent values (the slope of the tangent to the failure envelopes at different level of normal stress) were used. The tests were conducted at relatively low stress levels and, if the cohesion is neglected while exists, the secant values of φ_m will be forced to represent the presence of shear resistance at zero normal stresses. This results in unrealistic φ_m values of 70 - 90º.

The two-parametric Mohr-Coulomb yield criterion may be uniquely given in terms of the principal stresses:

$$(\sigma_1 + a) = N(\sigma_3 + a) \tag{2}$$

where the following state parameters are used: $N = (1+\sin\varphi_m)/(1-\sin\varphi_m)$, $\sin\varphi_m = f\cdot\sin\varphi$ and φ is the angle of internal friction and f is a degree of mobilisation, $a = c/\tan\varphi$ is the attraction and c is the cohesion. The material reaches failure at $f = 1$ when the current yield surface coincides with the ultimate failure surface. Let us assume that by the end of the test when shear stiffness approached zero the rubble was in the global failure state or close to it. The corresponding stress states can be illustrated by Mohr's circles and their envelope will indicate the angle of internal friction and corresponding attraction as shown in Fig. 2 for tests 18, 23 and 24 from Cornett and Timco (1995). For these tests the τ vs. γ curves implicitly indicated that rubble was strain hardening before reaching global failure (very small τ increments corresponded to large γ increments). A common tangent to the Mohr's circles at failure defines the Mohr-Coulomb failure envelope. Stress states attained during test 18 are shown on the left from the corresponding failure Mohr's circle. The Mohr-Coulomb state line rotates around the attraction intercept and it corresponds to the friction-controlled mobilization of the ice rubble strength during the test.

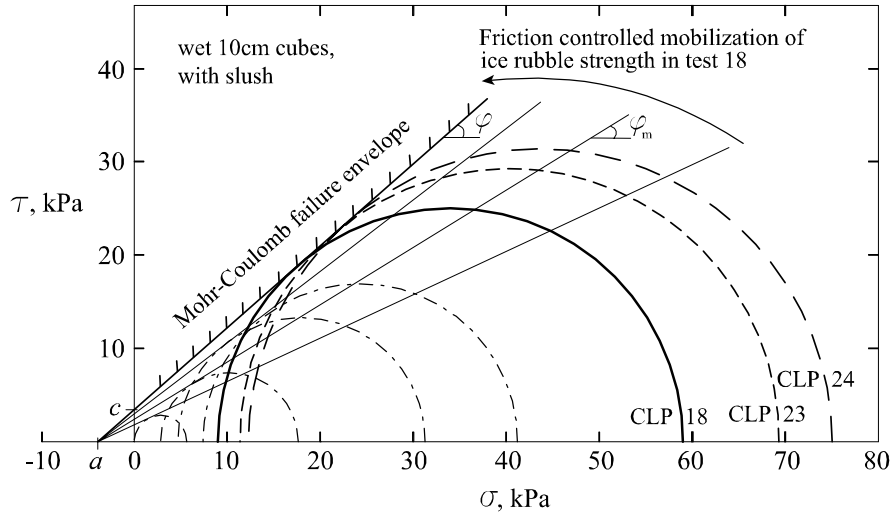

Fig. 2. Reappraisal of tests data from Cornett and Timco (1995) using two-parametric Mohr Coulomb yield criteria.

Fig. 3 shows φ_m calculated from Eq. 2 vs. γ lines for several CLP tests on different type of rubble. Values of attraction for different types of rubble and testing procedures were derived in the same way as illustrated in Fig. 2. A summary of the derived rubble properties and their comparison with those from Cornett and Timco (1995) is given in Table 1.

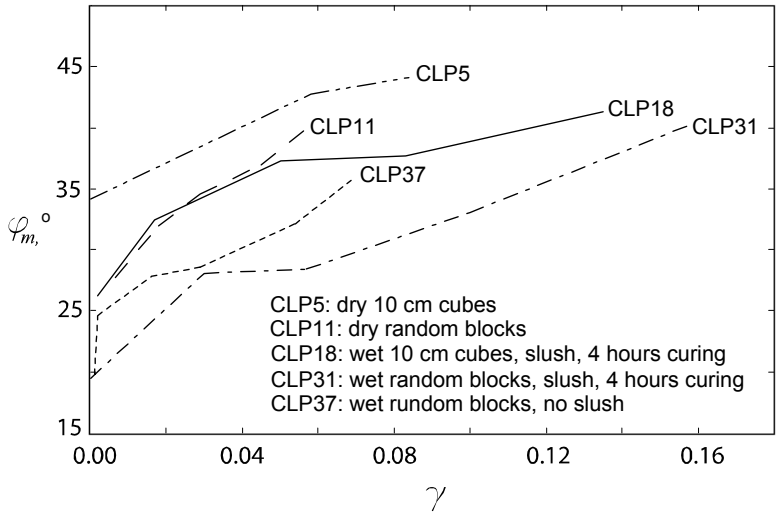

Fig. 3. Mobilized angle of internal friction vs. shear strain based on data from Cornett and Timco (1995).

Table 1. Ice rubble properties from some of the CLP tests.

	a (kPa)*	φ (º)*	φ_m (º)†
CLP 5	3.9	44	90 → 58
CLP 11	4.3	41	65 → 45
CLP 18	3.6	41	78 → 48
CLP 31	2.5	40	82 → 45
CLP 37	4.9	36	90 → 38

* Values derived in the present study

† Values presented by Cornett and Timco (1995)

The highest attraction among the analysed tests corresponds to the case where testing was done immediately upon filling apparatus with cold random ice blocks and saline solution (0.5% concentration by weight) at room temperature. Four-hours curing at -1ºC room temperature without pre-stress resulted in lower values of attraction. The reason for this could be the following: in the latter case the freeze bonds that formed immediately after filling the apparatus with water decayed during the curing process. Cornett and Timco (1995) reported that curing under pre-stress dramatically increased the initial yield strength. It is suggested herein that this increase is attributed to higher attraction. Similar tendency was also observed by Ettema and Schaefer (1986) when they studied the influence of the normal pressure on the freeze bond strength. Attraction value for the dry blocks was somewhere in-between the former two cases.

The highest angle of internal friction corresponds to the dry blocks while the lowest to wet random blocks without slush. This result looks reasonable, as the dry friction is likely to be higher than wet friction. Presence of slush increased the friction angle mobilized by the rubble at failure.

Analysis of the volumetric behaviour indicates that rubble behaved as a loose-packed material and the reported φ is indeed φ_c.

The foregoing derivations contain several assumptions and are based on hand-picked tests (caused by the writers' uncertainty as to exact test conditions and procedures). But they do indicate that use of the two-parametric Mohr-Coulomb material with a set of constant parameters a and φ helps to eliminate confusion in the choice of rubble properties to characterize its strength at all stress levels.

3. Punch tests and failure modes

Punch testing is a relatively new method to analyze rubble behaviour and strength although several punch tests were done both in-situ and in laboratories since the beginning of the 90's. Experience and knowledge associated with derivation of material properties from the punch tests is, however, still rather limited. There often remains one key question before the measured force-displacement curves can be interpreted in terms of rubble strength properties: what is the failure mechanism of ice rubble? Having an answer on this question, well-founded assumptions can be made for applications in both limit equilibrium and upper bound methods. Laboratory testing appeared to be the only practical possibility to get an insight about the failure process. Some aspects of laboratory and in-situ punch tests will be further discussed in this section.

3.1 Laboratory vs. in-situ

Laboratory and in-situ punch tests are, in fact, not absolutely similar. In the field, configuration of punch test is such that global bending of the rubble pack is avoided (forces exerted between the rubble and the consolidated layer) and the only failure mode is the so-called "punch-through" mode. In the laboratory loading is applied differently so bending is not omitted (forces exerted between the test facilities and the rubble pack). This was first observed in a series of punch tests conducted at the Hamburg Ship Model Basin (HSVA) by Jensen et al. (2001). As a matter of fact, the latter behaviour is more realistic with respect to some of the real/full-scale interactions between ice ridges and structures, e.g. icebreakers or down-bending cones. However, interpretation of force-displacement curves from lab tests becomes even more difficult due to the complex failure mechanism. Simple analytical approaches could still be used to derive the rubble strength but only if similar methods and assumptions about failure are further used in assessment of the full-scale loads on offshore structures.

Liferov et al. (2003) used finite element (FE) modelling to study the consistent behaviour of an artificial laboratory ice ridge undergoing punch test. The following basic conclusions are a

summary of the conducted parametric study on the influence of material parameters on the peak load and the failure mode of rubble:

- The peak load is to a large extent dominated by non-frictional forces;
- The cohesion and the angle of internal friction do not contribute separately to the peak load, their contribution is rather combined and it affects the local failure mode of the rubble;
- The failure of rubble in punch tests can involve global bending and therefore tensile strength of rubble is of importance.

Comparison of in-situ and laboratory force-displacement curves from punch tests is schematically illustrated in Fig. 4. The in-situ curve has either one or two force peaks where the first peak is in most cases higher than the second. In many in-situ punch tests the second peak was not observed at all. In laboratory tests there was normally found only one force peak. Maximum punch force measured in-situ was normally in order of 0.5 to 1.5 MN while in the laboratory it was below 1 kN. Geometrical scale of the lab tests (block thickness, keel depth) was typically in the order of 10 to 30. At the same time the platen displacement corresponding to the first force peak was substantially smaller in-situ. Second force peak in-situ was normally reached (when existed) at the same displacement level as the peak in the laboratory.

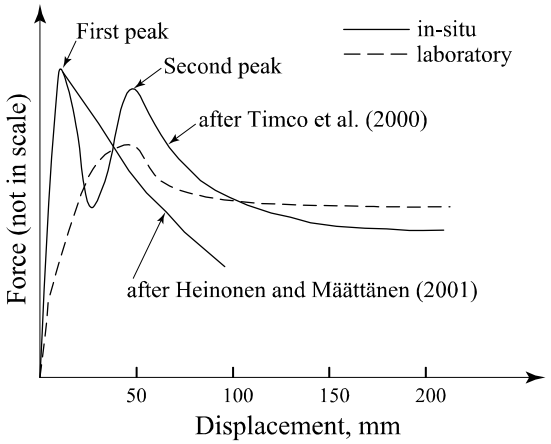

Fig. 4. Typical force-displacement diagrams for in-situ and laboratory punch tests.

There are several phenomena associated with the force-displacement curves in Fig. 4. The first peak in-situ is most likely attributed to breakage of the ice rubble skeleton. Initial strength of the skeleton is controlled by freeze bonding between separate blocks inside the rubble. In addition to the factors that affect freeze bonding, contribution of the initial failure to the global load in real situations will also depend on the aspect ratio between the structure and the rubble formation. After the initial peak, the behaviour of broken, disturbed ice rubble is dominated by contact friction,

interlocking and strain rate effective stress dependent cohesive bond that is derived from a dynamic freeze bonding mechanism (Croasdale, 1995). Smaller peaks in the descending part of the force-displacement curve (not shown in Fig. 4) could partly be induced by interlocking and breakage of individual ice blocks.

The laboratory behaviour of ice rubble in punch tests is somewhat different. There is no distinct peak at small displacement that is attributed to breakage of the rubble skeleton though there is a change in overall stiffness of rubble at some point. It is thought to be a transition point between bending and punch through failure modes as was shown by Liferov et al. (2003). Initial failure could also contribute to this change in stiffness though it is on significantly smaller level compared to that in-situ. The peak load in laboratory punch tests occurs at such high level of rubble deformation that the frictional resistance is believed to be the major (if not the only) contributor.

This principal difference in behaviour of ice rubble between the in-situ and the laboratory tests shows that thermodynamic scaling of ice rubble has not been appropriate. The consequence of it could be reduced (or in some cases increased) initial strength of the rubble skeleton in the laboratory tests. As far as the authors are aware, there were no concrete attempts so far to study this topic, although it seems to be of high importance for correct assessment of the full scale rubble strength from the laboratory experiments.

Shear box tests on mush ice performed by Hellmann (1984), though they can not be directly compared with punch tests, showed somewhat similar qualitative results with respect to the failure modes. Comparison of Hellmanns' and in-situ (with two peaks) force displacement curves is shown in Fig. 5. Hellmann divided the whole shear process into three phases and defined three shear modes: primary, secondary and tertiary:

- In the primary shear mode a steep increase in the shear force took place while the normal force remained at the original (pre-consolidation pressure) value. The highest shear force in this phase (about 60% of the max. value) was reached after less than 2 mm of displacement and was attributed to denser packing of ice particles. Herein the authors suggest that this was rather associated with breakage of the rubble skeleton as the displacement was too small to accommodate any compaction and there were observed no increase in normal pressure.
- In the secondary failure mode the peak force was reached through extensive dilatation.
- Tertiary failure mode reflects behaviour of ice rubble in the critical state.

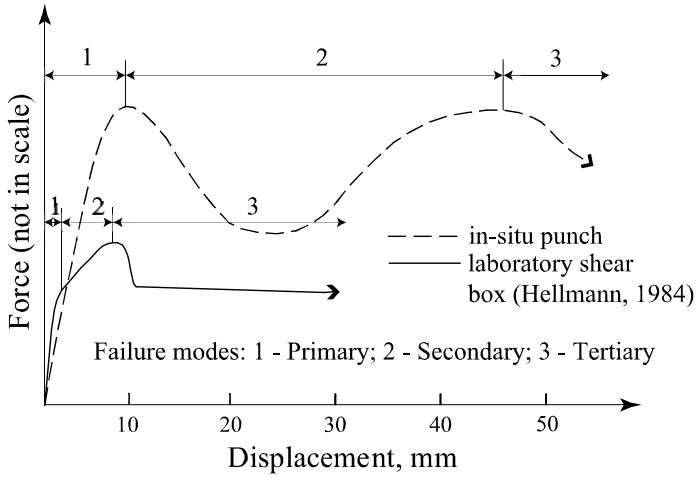

Fig. 5. Typical force-displacement diagrams for in-situ punch and laboratory shear box tests by Hellmann (1984).

The peak force in Hellmanns' tests was reached during the secondary failure in contrast to the in-situ punch tests where the peak is reached in primary failure. Difference in the imposed deformations, the boundary conditions and the pre-consolidation conditions (thermodynamic scaling in laboratory tests) can explain this dissimilarity. In the shear box the failure planes were prescribed and the normal stresses on them increased during the secondary failure in Hellmanns' tests. In punch tests, when the initial rubble skeleton is broken and the global plug begins to move down, the normal stress on the global failure surface will decrease. The frictional resistance will therefore not be fully mobilized. Degree of its mobilization will largely depend on the initial density of rubble and the boundary conditions. Proximity of the stress-free boundaries will decrease the mobilization of the frictional resistance. The secondary and the tertiary failure modes may be absent in punch tests and the global softening after the primary peak will take place. Heinonen (2002) used the FE simulations with cohesive softening material model to describe this behaviour.

3.2 Low speed vs. high speed

Remarkable observations were reported by Azarnejad and Brown (2000), Brown and Lemée (2002) and Lemée and Brown (2002). They found two different forms of rubble behaviour depending on the speed of the punch platen. At lower speeds (10-45 mm/s) the rubble failed along very clearly defined planes with minimal lateral disturbance of the ice particles. A rectangular or trapezoidal plug of undisturbed ice covering the whole rubble depth moved down with the platen. Similar behaviour was observed by Jensen et al. (2001) and it is also likely to take place at the in-situ testing. At higher speeds (45-115 mm/s), there was observed significant particle motion along the failure planes that were much less well defined. There was a wedge of rubble ice moving with the platen that in most cases was triangular but did not cover the whole rubble depth. As the platen

moved down a bulge at the bottom surface of the ice developed without a distinct plug being formed. The same type of triangular/bulb wedge can be observed in-situ in front of the narrow structures during their interaction with poorly consolidated ice ridges and ice rubble fields. This boundary wedge becomes larger as the drift speed increases. Hellmann (1984) observed that at high strain rate in his shear box tests a narrow zone of high velocity gradient was formed within the shear cylinder while the ice in the side chambers was almost at rest.

The measured peak load in fast punch tests was substantially higher (1.2 - 2 times) with the same test conditions. Derivation of rubble properties from the force-displacement curve using the Meyerhof's theory (Meyerhof and Adams, 1968) or the quasi-static finite element analysis is no longer valid for fast tests. Azarnejad and Brown (2000) suggested that the loading rate dependency of measured loads can be attributed to the following processes:

(1) Inertia component due to acceleration of ice rubble

(2) Effect of high pore pressures that do not have time to dissipate at high loading rates

(3) Loading rate dependence of freeze bond shear strength

(4) Change of failure mode.

The authors agree with the above suggestions, and attempted to investigate them more thoroughly.

(1) Inertia component due to acceleration of ice rubble. Under that definition, Azarnejad and Brown (2000) seem to have assimilated two different effects:

- Hydrodynamics effects. These are the buoyancy forces, the drag forces and free surface dynamic effects. Open water tests (load platen pushed down without rubble in the basin, see Fig. 6) were performed to evaluate these effects so fast punch tests measurements could be corrected. The load measured shows the inertia force needed to accelerate the platen (and a big ice block in some tests) the first half-second after the motion start (① in Fig. 6), an important peak corresponding to the free surface effects (② in Fig. 6), and finally a constant load corresponding to the buoyancy and drag forces (③ in Fig. 6). It can be seen in Azarnejad and Brown (2000) that the free surface effect presents a peak load 0.6 – 0.7 s after immersion of the platen. This event will excite the first mode of the water basin, i.e. a stationary wave with a wave length λ equal to the basin width. In finite water depths, the wave period T respects the following relation (Faltinsen, 1990):

$$T^2 = \frac{2\pi\lambda}{g}\left[\tanh\left(\frac{2\pi}{\lambda}h\right)\right]^{-1} \tag{3}$$

where g is the acceleration due to gravity and h the water depth. Half a period of the first mode is around 0.65 s, this coincides with the free surface peak force. The free water tests were used to

correct loads measured during the fast punch tests. This is a delicate procedure as the presence of rubble will affect these hydrodynamic effects. The amount of buoyancy from the rubble supported by the platen is variable in time. The free surface effects will be modified by the rubble (the generated waves will be different). Further, these generated waves will imply forces on all the rubble and not only the platen. After correction for hydrodynamic effects, the shear resistance of ice rubble presents on the plots a maximum force after 0.6 – 0.7 s at high speed. This may not be a coincidence, it might be a remain of the hydrodynamic effect; the correction for hydrodynamic forces was maybe not enough. Free surface effects (if important enough) might even disturb the failure mode of the ice rubble as they modify the stress field in the rubble. This should be further studied. A possibility would be to do punch tests on rubble submerged at a greater depth to avoid these effects.

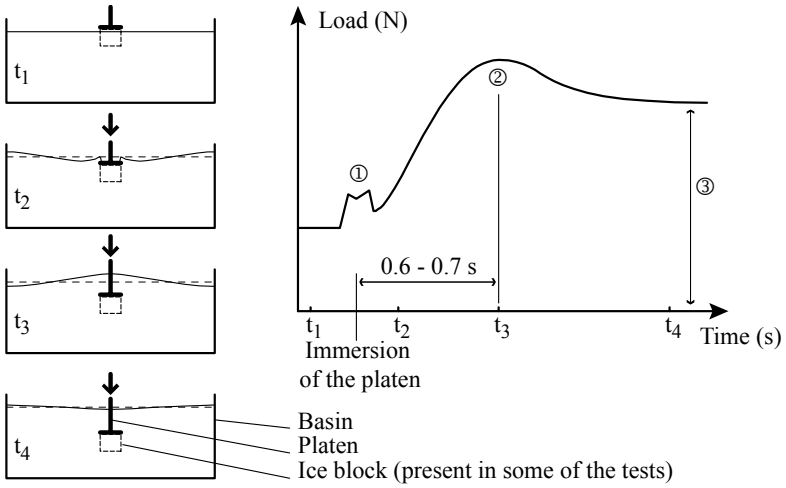

Fig. 6. Open water tests from the punch test series of Azarnejad and Brown (2000). A typical load plot is presented with representation of the basin at various times.

- Inertia force due to acceleration of ice rubble. It will be very different from those due to the acceleration from an ice block (as drawn in Fig. 6).

At low speed the inertia forces are negligible and the stress state in the rubble is statically admissible. The failure takes place along the planes where shear/tension resistance is minimal. These planes were described above to be either vertical or inclined at some angle (up to 45º) to form a trapezoidal plug. It reminds a case with a strip load on half space. The only difference is that the lower boundary is not infinite but free. The failure mechanism consisting of active Rankine, Prandtl and passive Rankine zones cannot fully develop, as the least work is associated with failure planes that lie inside the Prandtl zone and go through to the free boundary.

At high speed the situation will be different although the rubble remains to be essentially the same material (i.e. keeps the same material properties). It is assumed that there are no initial freeze-bonds or they are broken immediately upon loading the rubble at very small displacement z of the

platen. By this initial time (t_i) the rubble is assumed to be at rest. As the platen begins to penetrate further down, it induces stresses as in the low speed case (static effect) and at the same time accelerates the ice blocks below (dynamic effect). The rubble is not accelerated instantly throughout the whole thickness (as would be in case with solid ice block) but incrementally due to propagating local failure beneath the platen. A zone where the velocity at upper boundary equals to velocity of the platen (or to velocity of ice blocks above) and at the lower boundary it approaches zero will further be called as active zone. Thickness of the active zone is difficult to estimate precisely, but a guess in order of 10-15 times the ice block average dimension may be appropriate as a first approximation. Consider two alternatives for platen to penetrate through the rubble as shown in Fig. 7. In Alternative 1 the failure mechanism is assumed to be as in the quasi-static case. The internal work associated with infinitesimal displacement of the platen is composed of the plastic work along the failure planes and acceleration of the area A_1. This area is defined by the thickness of the active zone (active depth). However, there could be formed another initial failure mechanism providing less resistance for the platen to start penetration. This mechanism is illustrated as Alternative 2 in Fig. 7. The area A_3 will resist penetration of the beginning to form kinematic boundary wedge (area A_2) beneath the platen due to its inertial resistance (inertial restrain). In other words the inertia stress field superimposed on the statically admissible stress field will change failure planes that are associated with the least resistance.

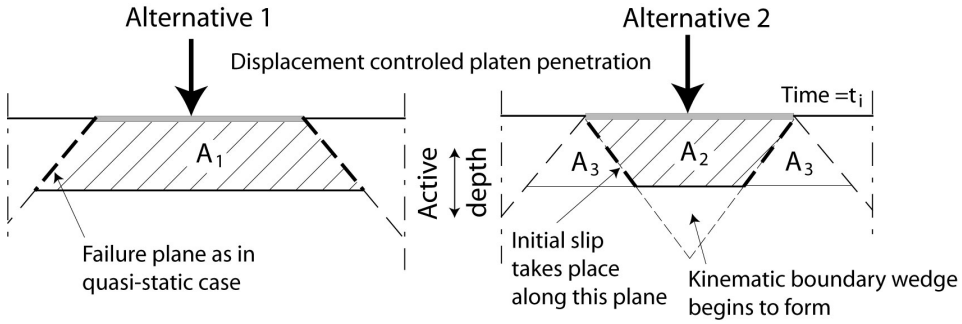

Fig. 7. Initial failure.

At time t_{i+1} (Fig. 8) when the platen has started penetration, the kinematic boundary wedge will fully develop. Its velocity will be equal to velocity of the platen. In the area around the wedge, i.e. in the active zone, ice rubble will be subjected to local deformation (both deviatoric and volumetric) and acceleration. In Fig. 8 the vertical components (simplified) of velocity and acceleration in space are shown though they can also be representative for the horizontal components.

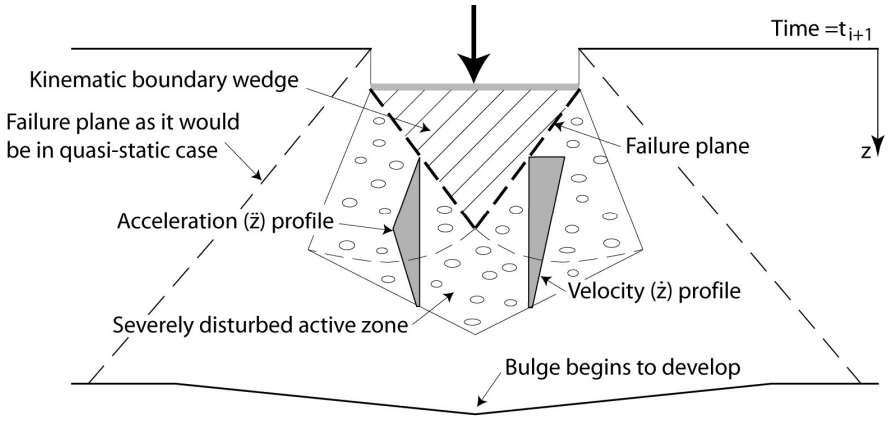

Fig. 8. Propagating failure.

At some transition point corresponding to the peak on the force-displacement curve, the bottom influence (non-restrained boundary) will become significant. Inertia component of the platen resistance will become smaller. There will be no more distinct failure at the boundary of the kinematic wedge and the active zone will become more spread with more uniform velocity profile as shown in Fig. 9.

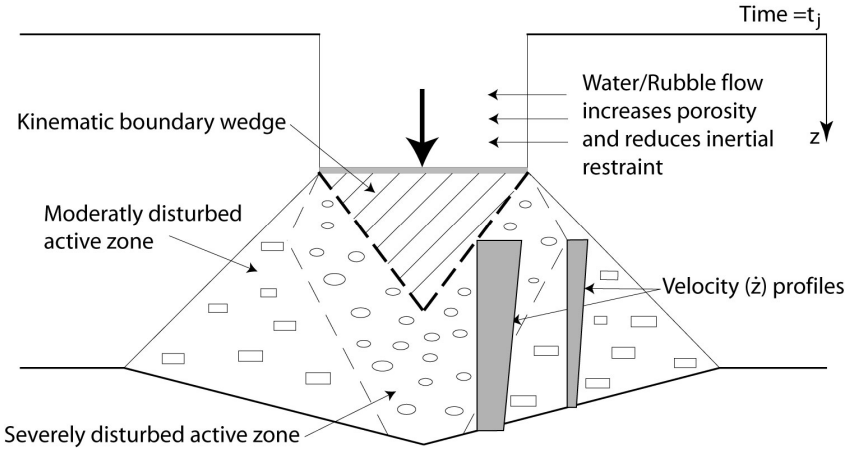

Fig. 9. Before ultimate failure.

Crude estimates of the net inertia contribution (disregarding the failure mechanism modified due to rubble inertia) based on the above assumptions give values in order of 25-40% of the peak equivalent static force. Detailed analysis of strip foundations subjected to transient loads was discussed by e.g. Das (1983). A number of methods to calculate the ultimate bearing capacity were presented. Similar methods could be used in thorough analysis of fast punch tests provided that necessary modifications are implemented due to different boundary conditions.

(2) Effect of high pore pressures that do not have time to dissipate at high loading rates. Partly this effect can be included into the free surface effect described earlier (reduced permeability and subsequently large force required to get the water up the block/plate in case of ice rubble in comparison to solid ice block). The increased loading speed can make ice rubble to behave undrained. In this case, however, the behaviour of rubble will entirely depend on its relative density:

- If it is initially loose, the effect of increased loading speed will reduce the rubble resistance. Under loading the rubble will try to contract that will cause built-up of excess pore-pressure and subsequent reduction of effective stresses.
- If dense, the effect of increased speed may be a significant increase in resistance. If permeability is small enough compared to the speed of the platen, then water is trapped and a change of volume during deformation is prohibited. Dense ice rubble will try to dilate or increase in volume during deformation. Water will prevent the volume increase by reduction in pore-pressure (suction) that will cause the effective stresses increase.

To examine whether it is a relevant situation, the following rough estimate could be done (adopted from the soil mechanics). The time needed for drainage of water is given by:

$$t_{drain} \cong 0.25 t_p = 0.25 H^2 / c_v \tag{4}$$

where t_p is a primary consolidation time, H is half of the rubble thickness and c_v is a consolidation coefficient. The drainage velocity could be estimated as:

$$v \cong 0.1 H / t_{drain} = 0.4 c_v / H \tag{5}$$

The consolidation coefficient is rather difficult to guess for such complex media as ice rubble. It will depend significantly on the temperature and the salinity of water as well as on the amount of slush in the rubble. If there is slush and the water is at the freezing point, then ice rubble can exhibit relatively low permeability. Ashton (1986) reported that although the porosity of frazil flocs that form slush is high, their structure effectively inhibits water movement in the interstices of the flocs. For example, if the consolidation coefficient is assumed to be $c_v \approx 8.3\text{E}04$ mm^2/s (average value for fine sand), at H = 200 mm the loading speed when ice rubble may experience undrained behaviour is about 166 mm/s. It is quite evident here that the consolidation coefficient is a key parameter that will define a switch between drained and undrained behaviour. More research is needed in this area to verify the relevance of undrained behaviour on the ice rubble strength at high strain rates.

(3) Loading rate dependence of freeze bond shear strength. Ettema and Schaefer (1986) conducted a number of tests to examine the influence of loading speed on the strength of a freeze-bond between two ice blocks. At the range of loading speeds between 0.44 mm/s to 0.84 mm/s they

found no influence of the loading rate on the measured freeze-bond strength. Although this may not be true for all conditions, it is believed that loading rate dependence of freeze bond shear strength has minor or nearly no influence on increased rubble resistance in punch tests at high speeds.

(4) Change of failure mode. The phenomena discussed in (1) - (3) cause change of rubble failure mode in punch tests. Their relative contribution to both change of failure mode and resistance of ice rubble under loading shall be further studied. It is perhaps also worth noting that similar phenomena could cause change in rubble failure under different boundary and loading conditions.

In summarizing punch testing of rubble and its behaviour, the following key items can be outlined:

- Punch testing of ice rubble may yield in underestimation of frictional strength due to specific type of loading and boundary conditions.
- At in-situ tests the primary failure mode that is associated with breakage of the initial rubble skeleton seems to dominate the rubble resistance.
- Laboratory test do not qualitatively reproduce in-situ tests (shape of the force-displacement curves). This could be primarily caused by neglecting accurate thermodynamic scaling and subsequent reduction of the initial skeleton strength.
- High speed punch tests result in higher (up to two times) rubble resistance. The increase in resistance is associated with change of failure mode that is provoked by different physical phenomena. Interpretation of high speed tests is far from straight forward and assumptions that are valid under quasi-static conditions (failure mechanism) can not be used any longer.

4. Scaling of ice rubble strength

Ice modelling has been studied theoretically and practically for many years. Extensive reports on the subject can be found in e.g. Michel (1978), Timco (1984) or Ashton (1986). Scaling of ice accumulations found many applications in river ice engineering. Scaling of sea ice rubble has been less addressed, and quite different problems are of concern. Some reminders on principle of scaling rubble and comparisons of measurements from different scales are given in the following.

4.1 Principles of scaling ice accumulations

Correct scaling of a problem requires respecting certain similitude laws. The number and the compatibility of these laws will depend on the complexity of the problem. The similitude between the model and the prototype should be geometric, kinetic and dynamic. Appropriate length and time scales will ensure the first two. Dynamic similarity requires correct scaling of the present forces.

This requirement can rarely be completely fulfilled; one must then concentrate on scaling the most important forces.

As a following to dynamic scaling, the ratios between relevant forces have to be the same at any scale. The Froude number, F_r, Cauchy number, C_h, and the Reynlods number, R_e, are three well known ratios. They represent respectively the ratio of inertial forces to gravity forces, elastic forces and viscous forces and can be expressed as:

$$F_r = \frac{V_c}{\sqrt{gL_c}}, C_h = \frac{\rho_c V_c^2}{E_c} \text{ and } Re = \frac{V_c L_c}{\nu_c}. \quad (6)$$

where V_c, L_c, E_c, ρ_c and v_c are characteristic speed, length, module of elasticity, density and kinematic viscosity in the model or the prototype (g is the acceleration of gravity).

Keeping these numbers constant will ensure proper scaling of these forces, but it might not be possible. For example, in a problem presenting laminar flow and low Reynolds number, Froude scaling will not be compatible with Reynolds scaling (Michel, 1978).

Scaling of shear box tests and scaling of punch tests are the two scenarios of concern here. In a shear box test, a dominant force is the internal friction, F_φ, it should be scaled properly. From dimensional analysis one can write:

$$F_\varphi = \sigma \cdot S \cdot f_{ND}\left(\frac{c}{\sigma}, \varphi\right) \quad (7)$$

where is σ the applied stress, S the contact area, c the cohesion, φ the angle of internal friction and f_{ND} a non-dimensional function. The dynamic scaling factor, λ_d, will be equal to the ratio of internal friction forces in model and prototype:

$$\lambda_d = \frac{F_{\varphi,p}}{F_{\varphi,m}} = \frac{\sigma_p \cdot S_p}{\sigma_m \cdot S_m} \cdot 1 = \gamma \cdot \lambda^2 \quad (8)$$

where p and m indices represent model and prototype scale, λ is the geometric scale ratio and γ is the stress scale ratio. This similitude provides scaling laws equal to the Cauchy scaling laws as shown in Table 2. This scaling presents two degrees of freedom (when ρ_r is fixed). So scaling of the cohesion or the material strength can be independent from the geometrical scaling. This scaling does not respect gravity force similitude; it should be applied only if this can be neglected. In shear boxes gravity force provides the initial confining pressure. It is more pronounced in cases when dry rubble is tested at low external confining pressures. Assessment of the initial confinement due to self weight as was discussed by Ettema and Urroz (1989) shows that its contribution to the overall

sample confinement is indeed quite low for a number of test programs they evaluated. The Cauchy scaling will therefore be the preferred scaling for testing of ice rubble in shear box.

Gravity forces are of larger importance in punch test. The entire set-up of punch test is such that the overall confinement (here it defines normal stresses on failure planes) is to a large extent provided by the initial confinement due to buoyancy force. Froude scaling is thus necessary and the scaling factors are presented in Table 2. There is only one degree of freedom in this scaling. Cohesion as a part of the rubble strength (if the two-parametric Mohr-Coulomb material description is assumed to be valid) has to be scaled by λ. It is shown here that Cauchy scaling is respected in Froude scaling but the reciprocal is wrong. Applying Froude similitude will ensure a proper scaling of the internal forces.

Table 2. Scaling laws for undistorted Froude scaling (from Ashton, 1986).

Variable	Units	Scaling ratio	
		Cauchy	Froude
Length	m	λ	λ
Density	kg/m^3	ρ_r	ρ_r
Mass	kg	$\rho_r\lambda^3$	$\rho_r\lambda^3$
Velocity	m/s	$\gamma^{1/2}\rho_r^{-1/2}$	$\lambda^{1/2}$
Time	s	$\lambda\rho_r^{1/2}\gamma^{-1/2}$	$\lambda^{1/2}$
Accel.	m/s^2	$\gamma(\rho_r\lambda)^{-1}$	1
Force	N	$\gamma\lambda^2$	$\rho_r\lambda^3$
Stress	Pa	γ	$\rho_r\lambda$

NB: The densities of the fluids present at different scales are often close, i.e. $\rho_r \approx 1$.

If breakage of ice pieces is of importance, the strength properties of the ice pieces should be scaled properly and Cauchy similitude should be respected, which is possible. As mentioned by Michel (1978), total similitude with unconsolidated ice pieces is possible, at least in quasi-static problems where viscous fluid forces are of lower importance. Scaling of high speed punch test for example will be more problematic.

In case of Froude similitude, to achieve proper scaling of the cohesion and non-scaling of the friction angle, attention should be given to the parameters driving these values. Geometric similitude of the rubble accumulation (size ratio of the ice blocks, porosity of the accumulation) must be achieved. The Coulomb friction between ice blocks (a non-dimensional parameter) should be the same and this can be attained by using real ice at all scales. But then to achieve the similitude, material properties must be scaled. This is a difficult goal, there exist several methods (Timco, 1984), and efforts are still put in trying to achieve better results (see for e.g. Evers and Jochmann, 1993). The grain size is often reduced by perturbing the ice growth with air bubbles; the

ice is weakened by being warmed up before testing. In majority of the tests mentioned earlier little attention was paid to this scaling. Practically this resulted in overestimation of the rubble strength.

The consolidation of the rubble should also be scaled. Very little has been addressed on that topic so far. Thermodynamic scaling of the rubble is very important to aim for similitude of the skeleton. Initial temperature of ice blocks and water as well as the ambient temperature and the time before testing are of high significance. It is also critical in case of ridge modelling where part of the rubble has to be transformed into a consolidated layer. Jensen et al. (2000) described the procedure where the ridge is cooled down to consolidate, then the ice surface is warmed up just before testing (punch test) to achieve similitude of material properties.

Finally, if trying to perform the same test at different scale in order to compare the results, one should perform the tests in the same manner. This is a problem with in-situ and laboratory punch test as was mentioned earlier.

So scaling of punch or shear tests is possible if considering unconsolidated rubble and low-speed testing. But more attention should be given in scaling material properties of the ice block and in thermodynamically scaling the rubble pack before testing.

4.2 Application to available results

Up to date there have been done substantially more tests on model rubble in the laboratory than on the real rubble in-situ. The laboratory tests were all performed at different geometrical scales. The results of these tests should thus be scaled prior to comparing them with each other as well as with those obtained in-situ. Unfortunately, when trying to review and compare available results one soon realizes that scaling was not given any special attention. Application of some of the scaling laws to the available results that is presented further can thus be considered only as an over-generalized comparison.

In accordance with Froude scaling, Weiss et al. (1981) have suggested that φ is not affected by changes in scale and that c changes proportionality with the scale factor. They first proposed that c may be proportional to the thickness of ice from which the rubble is made, which in this case generally corresponds to ice rubble piece thickness t. The combined results from their test programs indicated the following:

$$c/t = 16 \pm 8 \; kPa/m \tag{9}$$

Taking into account the omitted hydrostatic confinement as was proposed by Ettema and Urroz (1989), the result will change to:

$$c/t = 12 \pm 6 \; kPa/m \tag{10}$$

Bruneau (1997) conducted a detailed regression analysis of several ice rubble shear strength laboratory test results and reported the following simplified formula:

$$c/t = 17\ kPa/m \tag{11}$$

It is important to mention three conditions that apply to derivation of Eqs. 9-11. First of all, the cohesion reported is not associated with a single-parametric Tresca model, but with two-parametric Mohr-Coulomb model. Secondly, Eq. 11 is over-generalized and the *c/t* ratio is likely to be less taking into account the omitted hydrostatic confinement in some of the tests that this ratio is based on. It is neither clear whether Eq. 11 includes the tests conducted with high pre-consolidation pressures and periods or not. And thirdly, it is important to keep in mind that none of tests was thermodynamically scaled.

To compare to these values, results of the recent (1995-2002) laboratory tests on rubble including those discussed in Section 2.2 are summarized in Table 3. Results of the published in-situ tests on rubble are summarized in Table 4 in a similar way.

Table 3. Variation of *c/t* ratio in recent laboratory tests.

Author(s)	*c/t* (kPa/m)	φ (º)	Loading rate (mm/s)	Comments
Cornett and Timco (1995)	-na-	90 - 30†	~ 3	Based on assumption that c=0
	32 ± 7	36 - 44*		Selected tests analyzed in Section 2.1 of present paper; φ reported is φ_c
Azarnejad and Brown (1998)	2 - 2.5	47 - 61*	10 – 70 (assumed as slow tests)	Best fit analysis (Meyerhof's theory)
	13 - 19	52 - 65		Average of independent values (Meyerhof's theory)
	8 - 28	25 - 45*		FE analysis by Liferov et al. (2002)
Jensen et al. (2000)	≤ 13	25 - 40*	7	Limit equilibrium analysis, inclined failure planes
Jensen et al. (2001)	8 - 12	28 - 35*	7	FE analysis by Liferov et al. (2002, 2003)
Yasunaga et al. (2002)	60 ± 13	45 - 57*	1.6	φ reported is φ_p

* Corresponding value (i.e. corresponding to given cohesion, otherwise values of c or φ are the single-parameter Mohr-Coulomb values)

† Varying mobilized friction angle during the test runs, approached constant values of about 35 – 47 º

Although it is not entirely correct to compare the values in Table 3 directly, it may be observed that at lower strain rates the *c/t* ratio is higher. Yasunaga et al. (2002) conducted a separate series of tests to study the effect of strain rate on the shear strength of ice rubble. They reported that shear strength decreased about 2.5 times as the deformation rate increased from 0.1 to 5 mm/s and then

remained constant. Similar tendency was observed by Weiss et al. (1981). He reported that increasing loading rate from 4 to 25 mm/s resulted in decreasing *c/t* ratio from 19 to 14 kPa/m. Hellmann (1984) also found that shear stress decreased as the loading rate increased from 1.5 to 10.5 mm/s. Sayed (1987) reported that the yield shear stress increases with decreasing strain rate (6.5×10^{-5} to 1.7×10^{-3} s^{-1} ↔ 0.03 to 0.85 mm/s) and increasing temperature (-22º C to -10º C). These observations inevitably show that there likely exist some mechanisms that affect the rubble behaviour at relatively low loading rates.

There are at least two phenomena that can explain what happens in transition between very low to low loading rates, i.e. the suppression of dilatancy and the dynamic freeze bonding. Relationship between vertical and horizontal deformations in the direct shear box as presented by Yasunaga (2002) explicitly shows that dilatancy was suppressed much more at higher shear deformation rates. They also observed that rubble becomes finer (due to failure of individual ice blocks) after tests at high loading rates. Stress-displacement curves as presented by Sayed (1987) show that the frequency of stress drops (probably associated with local failure of blocks) substantially increases at higher strain rates. Strength of ice blocks with respect to the stress level in the rubble will significantly influence the contribution of this phenomenon to the overall rubble behaviour.

Another mechanism, the so-called dynamic freeze bonding, is much more difficult to observe and measure compare to the suppression of dilatancy. However, if it exists, it will depend on a number of parameters in addition to the strain rate, i.e. temperature, salinity, submergence, confinement and geometry of blocks (local contact pressures).

Table 4. Variation of *c/t* ratio, in-situ tests.

Author(s)	*c/t* (kPa/m)	φ (º)	Loading rate (mm/s)	Comments
Leppäranta and Hakala (1992)	19.6 ± 8	-na-	0.015	Limit equilibrium analysis, vertical failure planes, keel depth 3 - 15 m
Heinonen and Määttänen (2000)	8 - 21	14*	Var. (~ 20)	Upper bound analysis, inclined failure planes, best fit result, keel depth 4 - 6 m
Timco et al. (2000)	19.5 ± 5 18 ± 5	-na-	Var. (~ 30)	punch test, 6-m deep keel punch + ½ shear test, 6-m deep keel
Liferov et al. (2003)	10	32*	20	FE analysis, arbitrary combination of *c* and *φ*, keel depth 2 m
	30	47		FE analysis, independent values

* Corresponding value

Timco et al. (2000) presented the best-fit linear trend for the average cohesion as function of the keel depth as:

$$c = (0.88H_k + 3.52) \pm 2.3 \ (kPa) \tag{12}$$

Similar trend for the data presented by Leppäranta and Hakala (1992) is the following:

$$c = (0.11H_k + 2.23) \pm 0.9 \ (kPa) \tag{13}$$

For a 10 m deep keel, Eqs. 12 and 13 will results in cohesion values of 12.3 and 3.3 kPa respectively. On the other hand, the *c/t* values as presented in Table 3 show very good agreement.

Neither Cauchy nor Froude scaling were fully satisfied in any of the tests discussed above. The presented comparison provides only a general picture of how the λ-scaled rubble cohesion given corresponding friction angle derived from a number of different tests at different scales look like. The average *c/t* value is about 20 kPa/m derived both from the laboratory and the in-situ tests. Scatter in the laboratory *c/t* values is higher than in the in-situ values. This is as expected due to significant variation in the laboratory testing conditions. The φ values tend to be lower when derived from punch tests (if applicable at all). The reason for this is the specific boundary conditions as was discussed in section 3. Unreasonably high values of φ (above 50º) seem to come from analyses where cohesive component of rubble strength was neglected when deriving the material properties.

5. Conclusions

The results of the present study show that investigation of ice rubble strength, particularly in the laboratory, requires more thorough attention both with respect to scaling and subsequent derivation of material properties. The main conclusions of this study are the following:

- There were two different failure modes observed in tests on ice rubble. The primary failure mode is controlled by the initial strength of rubble skeleton, i.e. by freeze bonds between blocks inside the rubble. This mode may dominate the overall strength of rubble accumulation under certain conditions, particularly in case of relative proximity of the stress-free boundaries. Otherwise it may control the local resistance at the propagating failure in case of large rubble accumulations. Frictional resistance of the rubble will not be mobilized in this failure mode. The secondary failure mode may dominate the overall strength of rubble accumulation at propagating failure under boundary conditions that provide sufficient confinement. It is associated with substantial deformations and frictional resistance will be mobilized in this failure mode. Dynamic freeze-bonding between the blocks may define the “cohesive” component of rubble resistance in the secondary failure mode.

- When ice rubble is subjected to deformations at high speeds, the inertia stress field superimposed on the statically admissible stress field may cause increase in rubble resistance to externally applied disturbance. Hydrodynamic effects could also be of importance when testing submerged ice rubble at high speeds.
- Application of the two-parametric Mohr-Coulomb material model to describe ice rubble strength can well be sufficient provided that appropriate values of cohesion and friction angle are used. Application of the *c/t* scaling results in the value of about 20 kPa/m from the overview of available data. This value is likely to describe the rubble cohesion in the primary failure mode. In the secondary failure mode the frictional resistance dominates and the values of the mobilized friction angle can be in the order of 40-45º. The values of cohesion in the secondary failure mode are substantially less than that in the primary mode.

Part II of this paper elaborates this aspect of the modelling and simulation of ice rubble behaviour and strength.

Acknowledgements

The authors would like to thank all those who have conducted the tests and published the results of ice rubble mechanical properties.

References

Ashton, G.D., 1986. River and lake ice engineering. Water resources publications, 485 p.

Azarnejad, A. and Brown, T.G., 1998. Observations of ice rubble behaviour in punch tests. Proc. of the 14th Int. Symp. on Ice. Potsdam, USA, Vol. 1, pp. 589–596.

Azarnejad, A. and Brown, T.G., 2000. Experimental investigation of ice rubble behaviour and strength in punch tests. PERD/CHC Report 5-109, 35 p.

Brown, T.G. and Lemée, E., 2002. Experimental determination of ice rubble behaviour and strength. PERD/CHC Report 5-115, 38 p.

Bruneau, S., 1997. Development of a first-year ridge load model. PhD thesis, Memorial University of Newfoundland, St. John's, Nfld., Canada.

Cornett, A.M. and Timco, G.W., 1995. Laboratory tests on the mechanical properties of saline ice rubble. NRC Report HYD-CTR-002, 171 p.

Cornett, A.M. and Timco, G.W., 1996. Mechanical properties of dry saline ice rubble. Proc. of the 6th Int. Offshore and Polar Engineering Conf. Los Angeles, USA, Vol. 2, pp. 297-303.

Croasdale, K.R., 1995. In-situ testing of ice rubble properties. Report submitted to The National Energy Board, Canada, Calgary, Alberta.

Das, B.M., 1983. Fundamentals of soil dynamics. Elsevier Science Publishing, 399 p.

Ettema, R. and Schaefer, J.A., 1986. Experiments on freeze-bonding between ice blocks in floating ice rubble. Journal of Glaciology, Vol. 32, No. 112: 397-403.

Ettema, R. and Urroz, G.E., 1989. On internal friction and cohesion in unconsolidated ice rubble. Cold Regions Science and Technology, 16: 237–247.

Ettema, R. and Urroz, G.E., 1991. Friction and cohesion in ice rubble reviewed. Proc. of the 6th Int. Speciality Conf. Cold Regions Engineering. Hanover, USA, pp. 316-325.

Evers, K.U. and Jochmann, P., 1993. An Advanced Technique to Improve the Mechanical Properties of Model Ice Developed at the HSVA Ice Tank. 12th International Conference on Port and Ocean Engineering under Arctic Conditions, Hamburg, Germany, pp. 877-888

Faltinsen, O.M., 1990. Sea Loads on Ships and Offshore Structures. Ocean Technology Series, Cambridge University Press, 328 p.

Fransson, L. and Sandkvist, J., 1985. Brash ice properties – laboratory tests. Proc. of the 8th Int. Conf. on Port and Ocean Engineering under Arctic Conditions. Narssarssuaq, Greenland, Vol. 1, pp. 75–87.

Heinonen, J., 1999. Simulating ridge keel failure by finite element method. Proc. of the 15th Int. Conf. on Port and Ocean Engineering under Arctic Conditions. Helsinki, Finland, Vol. 3, pp. 956–963.

Heinonen, J. And Määttänen, M., 2000. LOLEIF ridge loading experiments – analysis of rubble strength in ridge keel punch test. Proc. of the 15th Int. Symp. on Ice. Gdansk, Poland, Vol. 1, pp. 63–72.

Heinonen, J. And Määttänen, M., 2001. Full-scale testing of ridge keel mechanical properties in LOLEIF-Project. Proc. of the 16th Int. Conf. on Port and Ocean Engineering under Arctic Conditions. Ottawa, Canada, Vol. 3, pp. 1435-1444.

Heinonen, J., 2002. Continuum material model with shear-cap yield function for ice rubble. Proc. of 15th Nordic Seminar on Computational Mechanics. Aalborg, Denmark, pp. 87-90.

Hellman, J.H., 1984. Basic investigations of Mush Ice. Proc. of the 7th Int. Symp. on Ice. Hamburg, Germany, Vol. 3, pp. 37-55.

Høyland, K.V., Jensen, A., Liferov, P., Heinonen, J., Evers, K.-U., Løset, S. And Määttänen, M., 2001. Physical modelling of first-year ice ridges, Part I: Production, consolidation and physical properties. Proc. of the 16th Int. Conf. on Port and Ocean Engineering under Arctic Conditions. Ottawa, Canada, Vol. 3, pp. 1483-1492.

Jensen, A., Høyland, K.V. and Evers, K.-U., 2000. Scaling and measurements of ice rubble properties in laboratory tests (2000). Proc. of the 15th Int. Symp. on Ice. Gdansk, Poland, Vol. 1, pp. 105–112.

Jensen, A., Løset, S., Høyland, K.V., Liferov, P., Heinonen, J, Evers, K.-U. and Maattanen, M., 2001. Physical modelling of first-year ice ridges, Part II: Mechanical properties. Proc. of the 16th Int. Conf. on Port and Ocean Engineering under Arctic Conditions. Ottawa, Canada, Vol. 3, pp. 1493–1502.

Keinonen, A. and Nyman, T., 1978. An experimental model-scale study on compressible, frictional and cohesive behaviour of broken ice masses. Proc. of the Int. Symp. on Ice. Lulea, Sweden, Vol. 2, pp. 335-353.

Lemée, E. and Brown, T.G., 2002. Small-scale plain strain punch tests. Proc. of the 16th Int. Symp. on Ice. Dunedin, New-Zealand, Vol. 2, pp. 1–8.

Leppäranta, M. and Hakala, R., 1992. The structure and strength of first-year ridges in the Baltic Sea. Cold Regions Science and Technology, 20: 295–311.

Liferov, P., Jensen, A., Høyland, K.V. and Løset, S (2002). On analysis of punch tests on ice rubble. Proc. of the 16th Int. Symp. on Ice. Dunedin, New-Zealand, Vol. 2, pp. 101–109.

Liferov, P., Jensen, A. and Høyland, K.V., 2003. 3D finite element analysis of laboratory punch tests on ice rubble. Proc. of the 17th Int. Conf. on Port and Ocean Engineering under Arctic conditions. Trondheim, Norway, Vol. 2, pp. 599–610.

Liferov, P., Gudmestad, O.T., Moslet, P.O., Nilsen, R., Shkhinek, K.N., Løset, S. and Håland, G., 2003. In-situ modelling of ice ridge scouring of the seabed. Proc. of the 6th Int. Conf. on Development of the Russian Arctic Offshore. St.Petersburg, Russia, pp. 249-254.

Løset, S. and Sayed, M., 1993. Proportional strain tests of fresh water ice rubble. Cold Regions Science and Technology, Vol. 7, No. 2: 44-61.

Meyerhof, G.G. and Adams J.I., 1968. The ultimate uplift capacity of foundations. Canadian Geotechnical Journal, Vol. 5, No. 4: 225-244.

Michel, B,. 1978. Ice Mechanics. Les Presses de l'Universite Laval, Québec, 499 p.

Prodanovic, A., 1979. Model tests of ice rubble strength. Proc. of the 5th Int. Conf. on Port and Ocean Engineering under Arctic conditions. Trondheim, Norway, Vol. 1, pp. 89-105.

Sayed, M, 1987. Mechanical properties of model ice rubble. Proc. Struct. Cong. '87, ASCE, New York, USA, pp. 647-659.

Sayed, M., Timco, G.W. and Lun, L., 1992. Testing ice rubble under proportional strains. Proc. of Offshore Mechanics and Arctic Engineering Conf. Calgary, Canada, Vol. IV, pp. 335-341.

Smirnov, V., Sheikin, I.B., Shushlebin, A., Kharitonov, V., Croasdale, K. R., Metge, M., Ritch, R., Polomoshnov, A., Surkov, G., Wang, A., Beketsky, S., and Weaver, J.S., 1999. Large Scale Strength Measurements of Ice Ridges: Sakhalin, 1998. Proc. of the 4th RAO Conf. St. Petersburg, 1999.

Timco, G.W., 1984. Ice Forces on Structures: Physical Modelling Techniques. IAHR Ice symposium, Hamburg, Germany, pp. 117-150

Timco, G.W. and Cornett, A.M., 1999. Is φ a constant for broken ice rubble? Proc. of the 10th Workshop on River Ice Management with a Changing Climate. Winnipeg, Manitoba, Canada, pp. 318–331.

Timco, G.W., Croasdale, K. and Wright, B., 2000. An overview of first-year sea ice ridges. PERD/CHC report 5-112, 159 p.

Timco, G.W., Funke, E.R., Sayed, M. and Laurich, P.H., 1992. A laboratory apparatus to measure the behaviour of ice rubble. Proc. of Offshore Mechanics and Arctic Engineering Conf. Calgary, Canada, Vol. IV, pp. 369-375.

Urroz, G.E. and Ettema, R., 1987. Simple shear box experiments with floating ice rubble. Cold Regions Science and Technology, 14: 185-199.

Weiss, R.T., Prodanovic, A. and Wood, K.N., 1981. Determination of ice rubble shear properties. Proc. of the Int. Symp. on Ice. Quebec, Canada, Vol. 2, pp. 860-872.

Wong, T.T., Morgenstern, N.R. and Sego, D.C., 1990. A constitutive model for broken ice. Cold Regions Science and Technology, 17: 241-252.

Yasunaga, Y., Kioka, S, Matsuo, Y., Furuya, A. and Saeki, H., 2002. The strength of the unconsolidated layer model of ice ridge. Proc. of the 16th Int. Symp. on Ice. Dunedin, New-Zealand, Vol. 2, pp. 62–68.

4.3 Ice rubble behaviour and strength, Part II: Modelling

P. Liferov

Abstract

Part I of this paper reviews ice rubble testing methods and the interpretation of test results. The present Part II elaborates on the modelling of ice rubble behaviour and strength. A pseudo-discrete continuum model is presented as a tool to study ice rubble behaviour (2D) in the primary failure mode that is associated with breakage of the initial skeleton. A non-linear Mohr-Coulomb failure criterion is proposed to describe the secondary failure mode of ice rubble.

Keywords: Ice rubble, modelling, continuum, discrete, Mohr-Coulomb.

1. Introduction

There have been a number of different methods used to predict ice ridges loads against offshore structures. These methods can generally be categorized into three groups: (1) Model tests (left beyond the scope of this paper), (2) Analytical Models and (3) Numerical Models. Timco et al. (2000) give a review of the above methods. The latter two approaches have been used over the years to predict the loads from the unconsolidated parts of the first-year ice ridges.

The analytical models considered local failure (e.g. Dolgopolov et al., 1975; Mellor, 1980), global failure (Croasdale and Cammaert, 1993) or a combination of those two (Brown et al., 1996). There are always several assumptions behind each model. The common and the most substantial of them are as follows: (a) Failure mechanism and failure surface, (b) Stress state on failure surface and (c) Ice rubble properties. To date there is no common agreement about any of these three assumptions. Sayed and Frederking (1988) have developed an analytical model of ice rubble pileup. They used a stochastic model of stress transfer in particulate media and equilibrium equations to determine the stress distributions in ice rubble. If modified for different boundary conditions, this model could be used to predict loads from ice rubble on structures. This would provide a lower bound solution in contrast to the above analytical models which are in most cases upper bound methods. The problem with choice of material properties, however, remains the same as in other analytical (and numerical) methods.

The numerical models used so far were either Finite Element (FE) or Discrete Element (DE) models. FE simulations were lately used in modelling ice rubble behaviour in punch tests

(Heinonen, 2003; Liferov et al., 2003). These simulations proved that it is possible to fit the experimental behaviour and load magnitudes, though an approach is based on continuum and homogeneous material which is not entirely correct. The ratio of the average particle size to the average rubble depth is in many cases quite low (around 10) to consider ice rubble accumulation (e.g. ice ridge keel/sail, ice rubble field) as a continuum media. Rubble properties derived from these simulations can be considered only as equivalent properties under particular assumptions.

Hopkins and Hibler (1991) used DE simulations to study the behaviour and strength of geophysical scale ice rubble in a direct shear box. They outlined that local rearrangement of blocks and breakage are competing mechanisms for the relief of local forces on the nominal failure plane. The freeze-bonding effect was disregarded in these numerical simulations and it was suggested that a model of freeze-bonding might be used to explore various forms which such mechanism might take. Sayed (1995) used DE simulations to investigate the failure of a ridge against a pier in the Confederation Bridge in Canada. This method has a number of advantages as it can deal with large deformations and discontinuities. However, the choice of parameters that describe ice rubble in the DE model could be a potential source of error if not appropriately verified.

Part I of this paper reviewed testing of ice rubble behaviour and strength. It was outlined that there are essentially two local failure modes of ice rubble as was observed in different tests. The primary failure mode is associated with breakage of the initial rubble skeleton. The secondary failure mode is associated with propagating failure and mobilization of frictional resistance. Incorporation of these experimentally observed failure modes into modelling of rubble – structure interaction can provide an opportunity to conduct more physically sound simulations and to verify the existing models.

The present paper presents an attempt to reconstitute the characteristic behaviour of ice rubble that was described in Part I. A numerical pseudo-discrete continuum model that simulates the primary failure mode is described in Section 2. Numerical simulations using the above model are presented in Section 3. An approach to constitutive modelling of the complex rubble behaviour is further addressed in Section 4.

2. Pseudo-discrete continuum model

2.1 General description

The pseudo-discrete continuum model of ice rubble deformation is a combination of a discrete particles assembly (i.e. ice rubble accumulation) and a FE analysis of this assembly. The primary rational for developing such a model was to produce a tool that would enable a numerical study of the initial failure mechanism of ice rubble. This model provides the possibility to simulate contacts between ice blocks and to account for their local failure.

The modelling procedure consists of two basic steps. First, the assembly of blocks is generated. A block generator tool as described further was developed to fulfil this task. In the second step, the generated assembly is used as a geometrical input for the FE analysis to study its behaviour under different boundary conditions.

2.2 Generation of discrete block assembly

The generation of the discrete block assembly was conducted in a custom-developed computer program called herein the block generator. This program enables to fill a closed contour (either rectangular or trapezoidal) with blocks of rectangular shape. The blocks themselves are considered as solid bodies. The geometry of each block is defined by its centre of gravity x_c, y_c and four vertices in a global co-ordinate system. An assumed porosity of the assembly is used to calculate the number of blocks needed to fill the contour. While generating the block assembly it is possible to define a sub-area within the contour (by means of top and bottom control lines) to estimate the effective porosity. The direction of gravity is perpendicular towards the attraction line that can be given different locations within the contour throughout the simulation. Fig. 1 shows a typical interface view of the program during a simulation run.

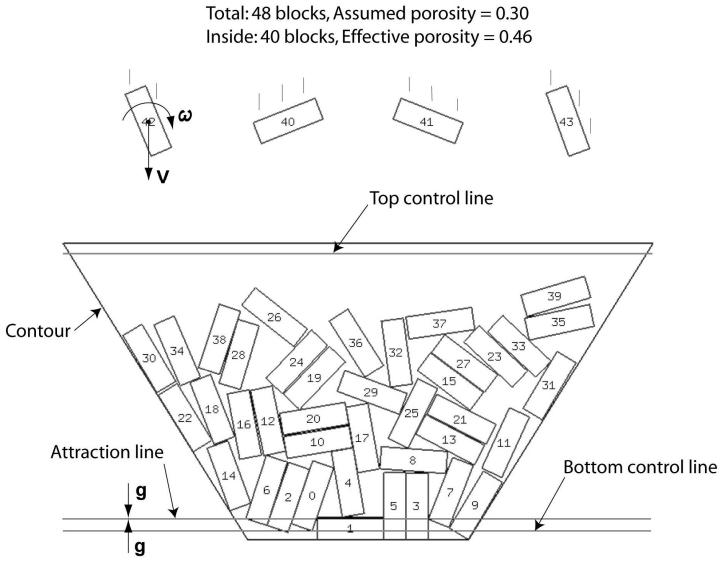

Fig. 1. Block generation in progress.

The general stepwise algorithm of the block generator is as follows:

(1) Initial position for the blocks above the contour is randomly chosen. At this stage each block is instantly given a constant linear velocity $\boldsymbol{V}$ parallel to the direction of gravity and arbitrary angular velocity $\boldsymbol{\omega}$. The program stores the instantaneous position and velocity of each of the particles in the system. A search for pairs of particles in contact starts from this point.

(2) The instantaneous assembly of blocks is calculated over a time step. At each step a search for contacts is performed. The search process is broken down in two parts: A global part with the task of finding the neighbouring pairs of particles in the system and a local part wherein a given pair of particles is checked for contact. For a system containing N_p particles, N_p^2 individual comparisons are required.

(3) Contact between the blocks occurs when the distance d between the blocks is less than EPS = 1.0E-10 m. The contact is defined by the normal $\boldsymbol{n}$ direction that is outwardly perpendicular to the side in the point/side contact. The tangential or $\boldsymbol{t}$ direction is perpendicular to $\boldsymbol{n}$. The relative velocity of the block a with respect to the block b at the centroid is:

$$\boldsymbol{V}_{a,b} = \boldsymbol{V}_a + \boldsymbol{\omega}_a \times \boldsymbol{r}_a - \boldsymbol{V}_b - \boldsymbol{\omega}_b \times \boldsymbol{r}_b \tag{1}$$

where $\boldsymbol{r}_a$ and $\boldsymbol{r}_b$ are vectors from the centers of mass of the blocks a and b, respectively, to the contact point.

A contact (may also be referred as impact) represents the momentum exchange between the two blocks. The impact type may vary from being absolutely inelastic to completely elastic. A coefficient of restitution $0 \le \varepsilon \le 1$ is introduced to handle it. It is generally given as (Marion and Thornton, 1988):

$$\varepsilon = \frac{\left|V_a - V_b\right|_{\text{before impact}}}{\left|V_a - V_b\right|_{\text{after impact}}} \tag{2}$$

Force $\boldsymbol{F}$ at contact has a unit value and defines the direction of the momentum exchange as:

$$\boldsymbol{F} = \frac{\boldsymbol{n} + \mu \boldsymbol{V}_t}{\left\| \boldsymbol{n} + \mu \boldsymbol{V}_t \right\|} \tag{3}$$

where μ is a friction coefficient and $\boldsymbol{V}_t$ is the tangential component of the relative velocity. A momentum conservation at endoergic impact (i.e. when kinetic energy is lost) gives the impulse $\boldsymbol{P}$ as:

$$\boldsymbol{P} = -\left(\frac{\varepsilon V_n}{m^{-1}{}_a + m^{-1}{}_b + \boldsymbol{r}_a^T I_a^{-1} \boldsymbol{r}_a + \boldsymbol{r}_b^T I_b^{-1} \boldsymbol{r}_b} \right) \boldsymbol{F} \tag{4}$$

where m is a mass, $\boldsymbol{V}_n$ is a normal component of the relative velocity and I is a mass tensor of inertia (in a global co-ordinate system). The impact causes change of the linear velocities as

$$\begin{aligned} \boldsymbol{V}_{a \text{ after impact}} &= \boldsymbol{V}_{a \text{ before impact}} + \boldsymbol{P} m_a \\ \boldsymbol{V}_{\text{b after impact}} &= \boldsymbol{V}_{\text{b before impact}} - \boldsymbol{P} m_b \end{aligned} \tag{5}$$

and angular velocities as:

$$\boldsymbol{\omega}_a = I_a^{-1}\boldsymbol{L}_a$$
$$\boldsymbol{\omega}_b = I_b^{-1}\boldsymbol{L}_b \tag{6}$$

where $\boldsymbol{L}$ is a moment of impulse defined as:

$$\boldsymbol{L}_{a\ \text{after impact}} = \boldsymbol{L}_{a\ \text{before impact}} + \boldsymbol{r}_a \times \boldsymbol{P}$$
$$\boldsymbol{L}_{\text{b after impact}} = \boldsymbol{L}_{\text{b before impact}} + \boldsymbol{r}_b \times \boldsymbol{P} \tag{7}$$

A series of block generation runs was conducted to achieve the realistic shape of the block assembly by varying ε and μ. Realistic shape is obviously a relative definition and is generally based on e.g. visual observations of the floating ice rubble behind the plexiglass wall in a model tank. For the final generation runs the following parameters were used: $\varepsilon = 0.35$, $\mu = 0.25$. Values of ε higher than 0.6 caused instability of the block generation for the chosen time increment. Values of μ lower than 0.10 yielded a brick wall-like formation.

2.3 Finite element model

The generated assembly of ice blocks was used as a geometrical input for the FE analysis. It was conducted using the Plaxis FE code (Plaxis, 2002). A FE model of ice rubble is shown in Fig. 2 (as example of a direct shear box simulation). The effective porosity of the generated rubble was in the order of 35 %.

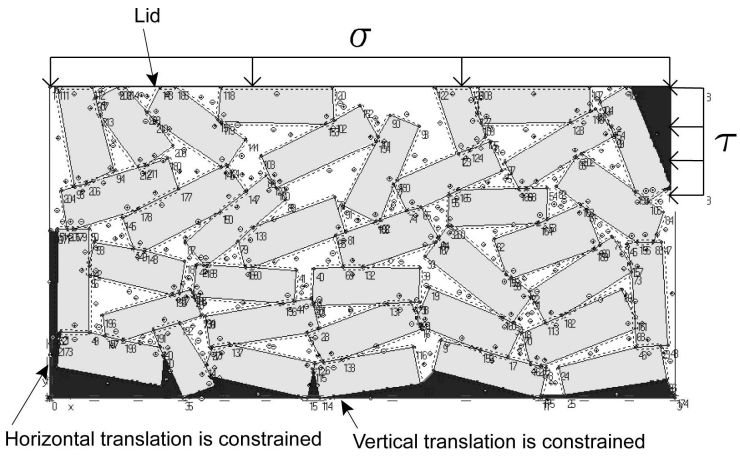

Fig. 2. The direct shear box FE model.

The model consisted of:

- *The ice blocks*. They were assigned an elastic-perfectly plastic Mohr-Coulomb material model. It is a constitutive model with a fixed yield surface, i.e. a yield surface that is not affected by plastic straining. The yield surface thus always coincides with the failure surface that is defined by six yield functions of the following form when formulated in terms of principal stresses σ_i, σ_j:

$$F = (\sigma_i + a) - N(\sigma_j + a) \tag{8}$$

where the following state parameters are used: $N = (1 + \sin\varphi) / (1 - \sin\varphi)$, φ is the angle of internal friction, $a = c/\tan\varphi$ is the attraction and c is the cohesion. For $c > 0$, the standard Mohr-Coulomb criterion allows for tension. However, the ice normally sustains smaller tensile stresses than those defined by the standard form of the failure criterion. In order to account for this, three additional yield functions are introduced:

$$F = \sigma_i - \sigma_t$$

and (9)

$$0 \le \sigma_t \le a$$

where σ_t is the tensile strength of ice.

- *The contacts between the blocks*. They were modelled using interface elements. Fig. 3 shows a close-up of contacts between ice blocks in the rubble (with the mesh shown). In the figure, the interface element is shown to have a finite thickness, but in the FE formulation the coordinates of each node pair are identical, which means that the element has a zero thickness. Each interface is assigned a 'virtual thickness' which is an imaginary dimension used to define the material properties of the interface.

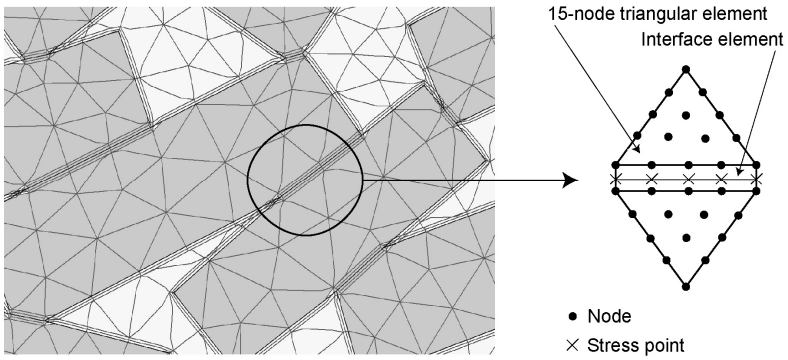

Fig. 3. Ice blocks in contact.

The Coulomb criterion is used to distinguish between elastic behaviour, where small displacements can occur within the interface, and plastic interface behaviour when permanent slip may occur. The transition between elastic and plastic behaviour of the interface is given by:

$$\sigma_n \tan\varphi_i + c_i < |\tau_i| = \sigma_n \tan\varphi_i + c_i \tag{10}$$

where τ_i is the shear stress, σ_n is the normal stress and φ_i and c_i are the friction angle and the cohesion of the interface material, respectively. The strength properties of the interfaces are linked to the strength properties of the ice blocks via the strength reduction factor for interface R_i as follows:

$$c_i = R_i \cdot c \tag{11}$$

$$\tan\varphi_i = R_i \cdot \tan\varphi \tag{12}$$

$$\sigma_n < \sigma_{t,i} = R_i \cdot \sigma_t \tag{13}$$

- *The voids between the blocks.* They were modelled using an elastic material with negligibly low stiffness. This was done in order to avoid meshing problems (use of elastic material instead of leaving voids "empty") on one hand and to prevent any considerable influence of this "filling" (assigning very low stiffness) on the other hand. Verification was conducted on identical models with and without elastic material in the voids to prove that its presence does not affect the results.

Depending on the type of simulation (e.g. direct shear box or arbitrary indentation) different boundary conditions were applied to the model. The ice rubble was in most cases modelled as a weightless material (unless different is specified), i.e. initially the rubble was in the stress-free state. It was then subjected to a load or displacement controlled deformation. Iterative calculations were carried out until the overall stiffness of the material approached zero. This was an indication of complete breakage of the initial rubble skeleton.

3. Numerical experiments

3.1 Direct shear box

The apparatus simulated in this set of numerical experiments is the two-dimensional direct shear box as shown in Fig. 2. The inner length of the shear box is 6 m and the depth is 3 m. Load controlled deformation was applied to the upper part of material. The lid was free to move vertically in order to balance the normal confining pressure σ applied to its upper surface. The horizontal pressure τ was then incrementally applied to move the upper part of the shear box. The ice rubble

used in the experiments was made up of rectangular blocks. Table 1 presents the characteristic parameters for the ice blocks that were chosen according to Kämärainen, (1993).

Table 1. Ice block properties.

Property	Value
Length, m	~ 1
Thickness, m	~ 0.3
Young's modulus, GPa	1.5
Poisson's ratio	0.3
Cohesion, MPa	0.5
Angle of internal friction, º	0-30 (var.)
Tensile strength, MPa	0.2

A parametric study was performed to investigate the effect of mechanical properties of the ice blocks and their contacts as well as the confining pressure on strength of the rubble skeleton. Three randomly generated block assemblies were used for each set of the parametric analysis. The following parameters were varied in the course of numerical experiments:

- Strength reduction factor for interfaces R_i
- Confining pressure σ
- Angle of internal friction φ
- Area of contacts between ice blocks A.

The shear strength τ (herein referred to as the maximum horizontal pressure attained during the experiment) versus R_i for two different values of angle of internal friction is presented in Fig. 4.

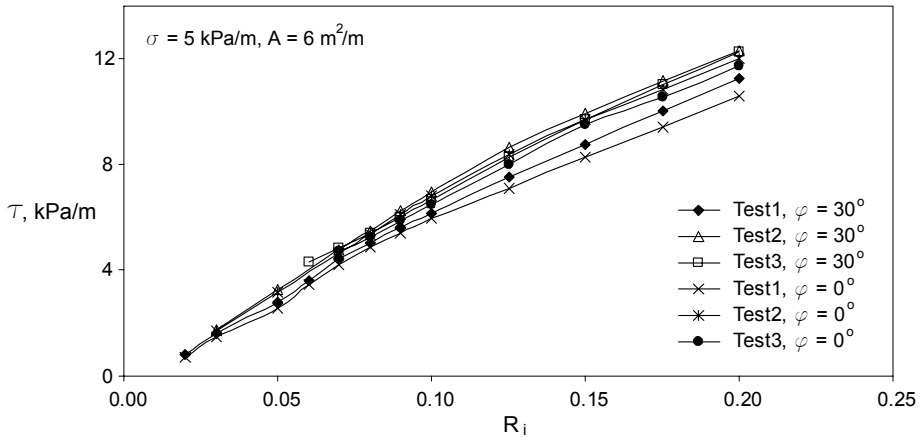

Fig. 4. Shear strength versus strength reduction factor and φ.

In the following it was assumed that the average c/t (where t is the block thickness) for ice rubble is 20 kPa/m as it was outlined in Part I of this paper. Thus, for present simulations with 0.3 m thick ice blocks the value of c is expected to be about 6 - 7 kPa. Ettema and Schaefer (1986) conducted a series of experiments on freeze-bonding between ice blocks. They reported shear strength of freeze-bonds in order of 1 - 5 kPa. The ice blocks with contact area of $4.52 \cdot 10^{-3}$ m^2 and $9.03 \cdot 10^{-3}$ m^2 were used during these experiments that corresponded to 95 · 47.5 mm and 134 · 67 mm block sizes, respectively. Rough scaling of the above results yields the freeze bond shear strength of 52 kPa. The curves (τ vs. R_i) in Fig. 4 show that τ in the order of 6 - 7 kPa corresponds to R_i of 0.08 - 0.1 that gives a freeze-bond shear strength of 40 – 50 kPa. The effect of φ on the initial failure and strength appeared to be quite negligible.

Fig. 5 shows a plot of τ vs. A. The confining pressure σ is assumed to be constant and equal to 5 kPa. The strength reduction factor is chosen as 0.09 that corresponds to freeze bond strength of 45 kPa. The shear strength increases almost linearly with increase of contact area between the blocks.

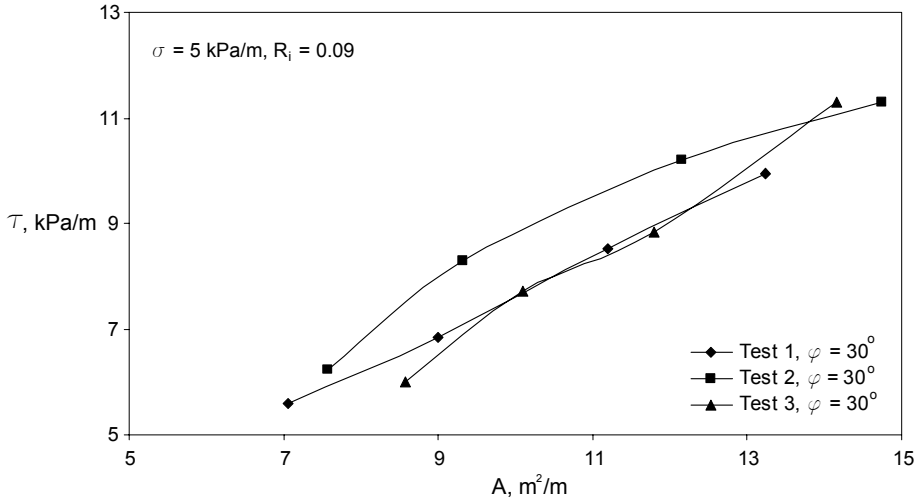

Fig. 5. Shear strength versus contact area.

Fig. 6 shows the influence of confining pressure σ on the rubble shear strength τ. The curves in Fig. 6 might also be considered as the failure envelopes of the rubble in the primary failure mode.

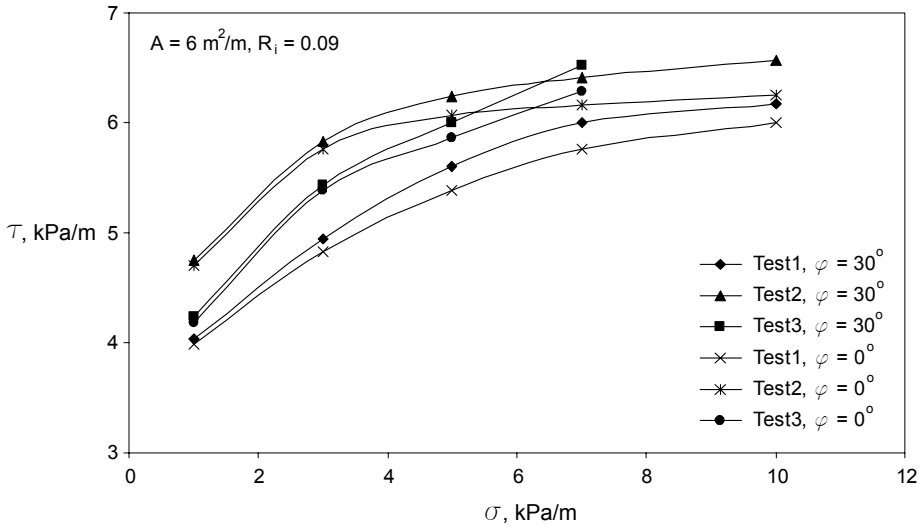

Fig. 6. Shear strength versus normal pressure.

For the range of the present analysis τ increased non-linearly with increasing σ as shown in Fig. 6. At the confining pressure σ of 1 kPa the rubble failed basically in tension, i.e. the tensile stresses at the contacts between the blocks exceeded their tensile strength. The failure mode changed with increase of σ and became a combination of tension and shear modes. Shear failure dominated at σ = 10 kPa.

3.2 Rubble indentation experiment

An experiment on indentation of rubble by a sloping face object was performed. The two-dimensional plane strain model of the experiment is shown in Fig. 7. In order to compare the pseudo-discrete and fully continuum models, identical geometry, boundary conditions and experimental procedure was used in simulations where the rubble was modelled as a fully continuum media. Herein both models are aimed to simulate the primary failure mode of the rubble.

The parameters for the ice blocks in the pseudo-discrete model were the same as in the shear box simulations and are given in Table 1. The unit area of the inter-block contacts was 11.6 m^2/m. The "continuum" rubble was modelled as a Mohr-Coulomb material with parameters shown in Table 2. The interface strength between the indenting face and the ice rubble was set to be 0.2 times the nominal strength of the rubble. In this experiment the self weight (buoyancy) of the rubble was included to account for the initial confinement.

Table 2. Ice rubble properties in the primary failure mode, continuum model.

Property	Value
Young's modulus, MPa	3
Poisson's ratio	0.3
Cohesion (c), kPa	0 – 20 (var.)
Angle of internal friction, º	6†
Tensile strength, MPa	0.4c

† Value corresponding to the ice-ice friction coefficient of 0.1

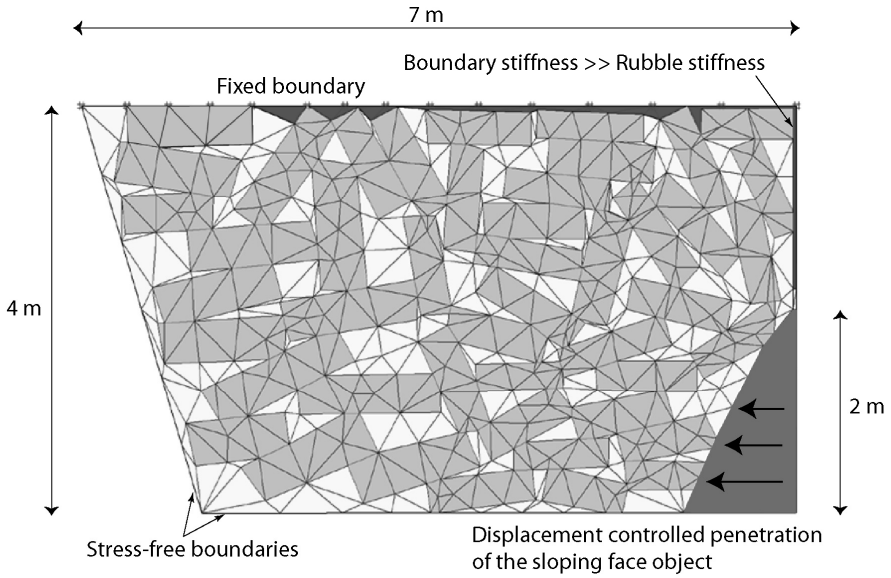

Fig. 7. Rubble indentation experiment.

The deformation and failure inside the rubble for both models are shown in Figs. 8a and b. Deformation is shown in terms of the total increments, i.e. absolute displacement increments at the step corresponding to failure. Failure zones are indicated after analysis of the stress state inside the rubble. In Fig. 8a the following zones are distinguished:

- Zone 1: Local crushing of ice blocks
- Zone 2: Majority of the inter-block failure is a shear-slip
- Zone 3: Majority of the inter-block failure is in tension
- Zone 4: Intact zone, neither inter-block nor local block failure occur.

The different failure zones in case of continuum modelling are shown in Fig. 8b.

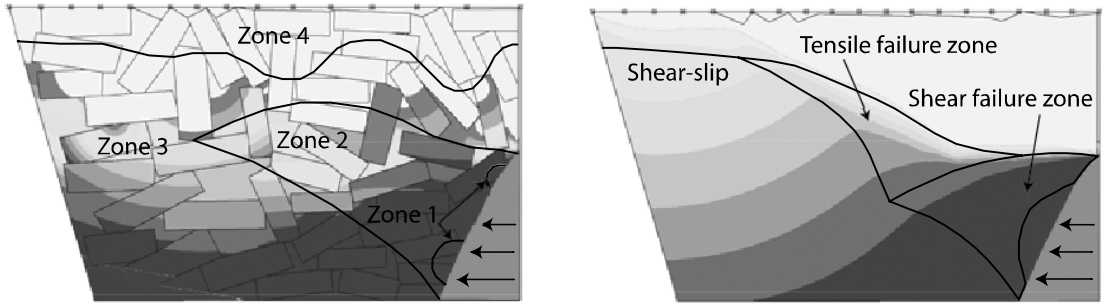

(a) Pseudo-discrete modelling (b) Continuum modelling

Fig. 8. Rubble deformation and failure.

Fig. 9 shows the correlation between the interface strength factor R_i in the pseudo-discrete model and the rubble cohesion in the fully continuum model providing equal force at failure.

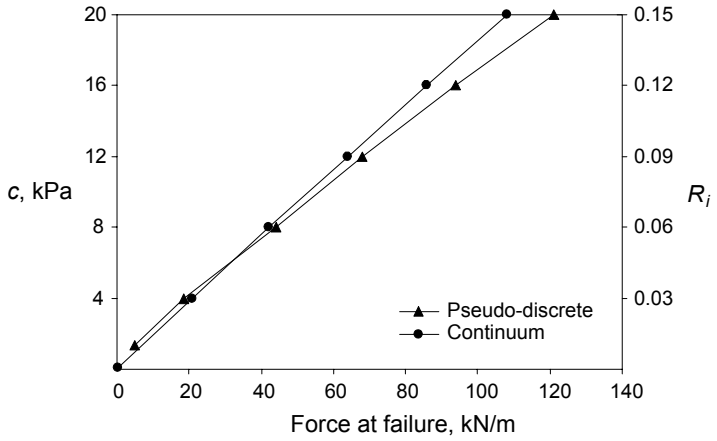

Fig. 9. c vs R_i vs. force at failure.

4. Modelling complex rubble behaviour – an approach

Ice rubble may undergo large deformations when interacting with structures. The strains within the rubble are not uniform, but diminish with distance from the loading front. In the zone of small strains the primary failure mode will dominate the shear resistance of the rubble. In the zones of large strains the secondary failure mode will govern the resistance. The secondary mode is associated with mobilization of the frictional strength that is composed of the Coulomb friction between the blocks and the dilatancy effect. The latter may be partly suppressed at high normal stresses on the failure plane. A schematic illustration of the combination of the different components to the shear resistance of ice rubble is given in Fig. 10.

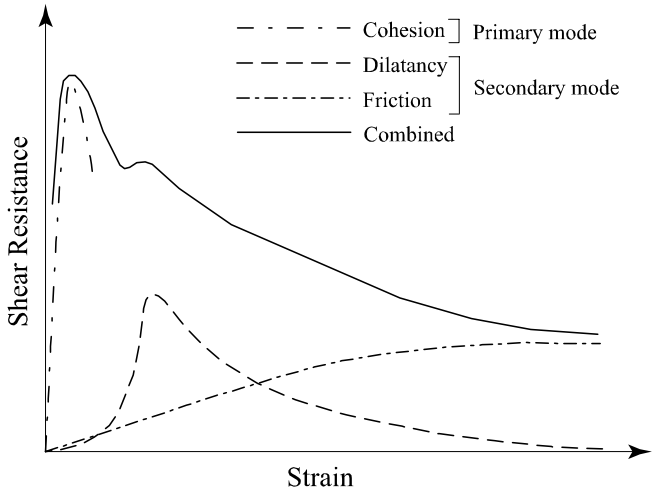

Fig. 10. Components of shear resistance, in analogy with soil behaviour.

The individual components of the shear resistance may have relative values different from what is shown in Fig. 10. Decayed, or not yet formed, freeze bonds will reduce the cohesive component. Combined dilatancy and friction will in this case provide the peak resistance. With reference to the rubble indentation experiment described in Section 3.2, a force at failure of 15 kN/m would be attained when rubble is modelled as a continuum cohesionless material with an angle of internal friction $\varphi = 45º$. This force may be considered as the shear resistance in the secondary failure mode. Equal resistance would have been attained in the primary failure mode provided that rubble skeleton has a cohesion $c = 3$ kPa.

The initial relative density with respect to the critical state density, strength of ice blocks and boundary conditions will to a large extent characterize the rubble behaviour in the secondary failure mode. Suppression of dilatancy can be accounted for by use of the non-linear Mohr-Coulomb failure envelope.

No experimental programs have been focused on studying the suppression of rubble dilatancy at increased normal stresses on the failure plane that would result in reduction of the mobilized frictional resistance. Nevertheless, a non-linearity of the Mohr-Coulomb failure envelope was observed by e.g. Sayed (1987). The measured failure envelopes showed some curvature at low normal stresses and flattened out at higher normal stresses.

Ice rubble behaviour in the secondary failure mode (i.e. when the freeze bonds are broken) can be compared with that of the rockfill material. Leps (1970) has proposed the following formulation to describe the non-linear strength envelope for rockfill and gravel materials:

$$\varphi' = \varphi'_o - \Delta\varphi' \log_{10}\left(\frac{\sigma'_{ff}}{p_a}\right) \tag{14}$$

where φ' is the secant friction angle, φ'_o is the secant angle of shearing resistance at reference stress, σ_{ff} is the effective normal stress on the failure plane and p_a is the reference stress. Slight reinterpretation of data from the DE direct shear box experiments on geophysical scale ice rubble conducted by Hopkins and Hibler (1991) shows dependency similar to the one given by Eq. 14. as illustrated in Fig. 11. They demonstrated that dilatancy of ice rubble is suppressed due to breakage of the blocks. The secant friction angle φ' is therefore reduced with increase of the confining pressure.

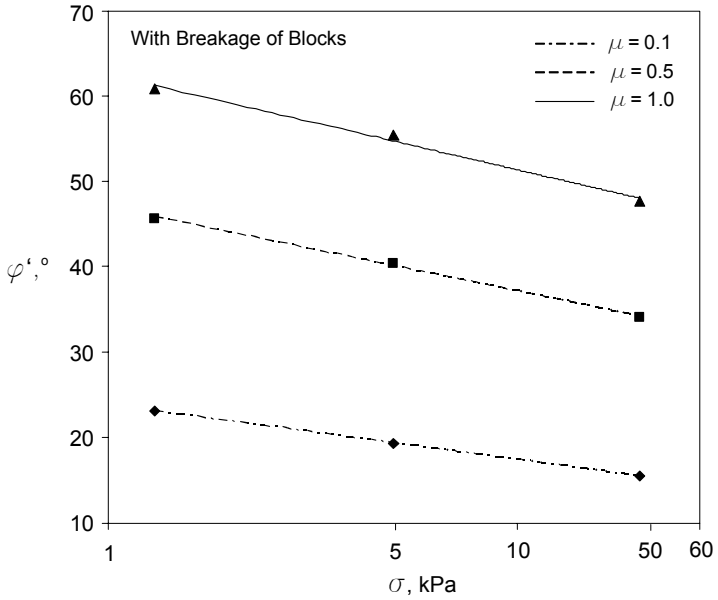

Fig. 11. Suppression of dilatancy (based on results from Hopkins and Hibler, 1991).

Assuming that the reference stress p_a is 1 kPa, Eq. 14 for ice rubble becomes:

$$\varphi'\big|_{\mu=0.1} = 23.8 - 2.8\ln\sigma \tag{15}$$

$$\varphi'\big|_{\mu=0.5} = 46.9 - 4.3\ln\sigma \tag{16}$$

Equations 15 and 16 represent the lower and the upper bounds of ice rubble strength in the secondary failure mode respectively. These results are derived from the 2D simulations and cannot be directly compared with results from the 3D physical experiments. Nevertheless, the difference in behaviour of ice rubble between 2D and 3D is not likely to be principally different, neither qualitatively nor quantitatively.

5. Conclusions

It has been demonstrated that ice rubble failure can be broken into two separate modes: primary and secondary. The primary failure mode was numerically studied with a pseudo-discrete continuum model. Failure of ice rubble took place at relatively small deformations (about an order less than the block size) and was mainly associated with the breakage of the contacts between the blocks, though some local breakage of individual blocks also occurred. The freeze-bond properties and their relation to the properties of parent ice are important for the overall strength of the rubble skeleton. The shear strength of rubble increased more or less linearly with increasing strength of the freeze bonds between the blocks. The shear strength increased non-linearly with increase of confining pressure. A change of failure mechanism from tensile to shear was observed as confinement increased.

A good correlation exists between the interface strength (i.e. freeze bond strength) in the pseudo-discrete model and the equivalent cohesion (i.e. shear strength) in the continuum model. This finding suggests the need for more efforts in studying freeze bonding under different conditions. This knowledge would enable to provide better assessment of the cohesion value that can be used in the rubble failure models.

The secondary failure mode has been described with a non-linear Mohr-Coulomb failure envelope by analogy with the rockfill material. Non-linearity of the envelope is caused by suppression of dilatancy. Accounting for this phenomenon will prevent overestimation of the rubble resistance at high normal stresses. Upon verification such envelope can be easily implemented into analytical models of ice rubble failure.

Acknowledgements

The author would like to thank Svetlana Shafrova for help with conducting the shear box experiments and Alexey Privalov for programming support in development of the block generator.

References

Brown, T.G., Croasdale, K.R. and Wright, B., 1996. Ice loads on the Northumberland Strait bridge piers – an approach. Proc. of the 6th ISOPE Conf. Los Angeles, USA, pp. 367-372.

Croasdale, K.R. and Cammaert, A.B., 1993. An improved method for the calculation of ice loads on sloping structures in first-year ice. 1st Int. Conf. on development of the Russian Arctic Offshore. St.Petersburg, Russia, pp. 161-168.

Dolgopolov, Y.V., Afanasev, V.A., Korenkov, V.A. and Panfilov, D.F., 1975. Effect of hummocked ice on piers of marine hydraulic structures. Proc. of the 3d Int. Symp. on Ice. Hanover, USA, pp. 101–109.

Ettema, R. and Schaefer, J.A., 1986. Experiments on freeze-bonding between ice blocks in floating ice rubble. Journal of Glaciology, Vol. 32, No. 112: 397-403.

Heinonen, J., 2003. Continuum material model for ice rubble – combined shear-cap yield criterion with strain softening. Proc. of the 17th Int. Conf. on Port and Ocean Engineering under Arctic conditions. Trondheim, Norway, Vol. 2, pp. 547–558.

Hopkins, M.A. and Hibler, III, W.D., 1991. On the shear strength of geophysical scale ice rubble. Cold Regions Science and Technology, 19: 201-212.

Kämärainen, J., 1993. Studies in ice mechanics. Helsinki University of Technology. Finland, 182 p.

Leps, T.M., 1970. Review of shearing strength of rockfill. ASCE Journal of Soil Mechanics and Foundations, Vol. 96, SM4: 1159-1170.

Liferov, P., Jensen, A. and Høyland, K.V., 2003. 3D finite element analysis of laboratory punch tests on ice rubble. Proc. of the 17th Int. Conf. on Port and Ocean Engineering under Arctic conditions. Trondheim, Norway, Vol. 2, pp. 599–610.

Marion, J.B. and Thornton, S.T., 1988. Classical dynamics of particles and systems. Harcourt Brace Jovanovich, Inc., 602 p.

Mellor, M., 1980. Ship resistance in thick brash ice. Journal of Cold Regions Science and Technology, Vol. 3, No. 4: 305-321.

PLAXIS, 2002. Plaxis v. 8.1. Finite Element Code for Soil and Rock Analyses. www.plaxis.nl

Sayed, M, 1987. Mechanical properties of model ice rubble. Proc. Struct. Cong. ’87, ASCE, New York, USA, pp. 647-659.

Sayed, M. and Frederking, R.M.W., 1988. Model of ice rubble pileup. Journal of Engineering Mechanics, Vol. 114, No. 1: 149-160.

Sayed, M., 1995. Numerical simulation of the interaction between ice ridges and bridge piers. Technical report TR-1995-10, National Research Council, Ottawa, Ontario, Canada.

Timco, G.W., Croasdale, K. and Wright, B., 2000. An overview of first-year sea ice ridges. PERD/CHC report 5-112, 159 p.

4.4 Ice rubble properties from plane strain tests

P. Liferov[1,2] and K.V. Høyland[3]

[1] NTNU, Trondheim, Norway
[2] Barlindhaug Consult AS, Tromsø, Norway
[3] UNIS, Longyearbyen, Norway

Abstract

Simple shear tests on ice rubble in the bi-axial compression chamber developed at the Canadian Hydraulic Centre (CHC) have been analyzed. A discussion on derivation of material properties and the testing procedures was given based on the fundamental theory of elasto-plasticity. It was shown that derivation of the ultimate material strength properties from the proportional strain tests alone might be difficult as the limit state may not have been reached in the tests discussed. The assumption that ice rubble is a cohesionless material leads to confusion when the elasto-plasticity is applied to derive the friction angle of ice rubble. The tests showed that the cohesion exists, however, its value must be clarified. The mean pressure dependence of the mobilized angle of internal friction was also observed and the possible effect of dilatancy was pointed out. The analysis of a single constant lateral pressure test showed that the angle of internal friction of the ice rubble is at least 44º corresponding to cohesion equal to 3.5 kPa.

1. Introduction

Ice rubble plays an important role in many engineering problems, ranging from the river engineering aspects to ice-cover interaction with offshore structures. The knowledge about the mechanical properties of ice rubble is however rather limited. Several programmes on testing of ice rubble mechanical properties have been carried out since the beginning of the seventies, and most of the experiments were done in laboratories with artificially produced ice rubble. Two basic types of experiments were done: shear tests and punch tests all resulting in some values of material properties. The first shear tests were done with a simple shear box (Prodanovic, 1979; Hellman, 1984) followed by the skew box tests (Urroz and Ettema, 1987) and the more sophisticated bi-axial tests (Timco et al., 1992. Løset and Sayed, 1993). Extensive reviews of these tests and interpretation of the results are given by Ettema and Urroz (1991) and Timco and Cornet (1999). The ice rubble was usually assumed to behave as an elastic-perfectly plastic material where the plasticity was described by the Mohr-Coulomb law. Only two continuum models up to date have taken into account the elasto-plastic behaviour of the ice rubble. A constitutive model developed by Wong et

al. (1990) utilized the Mohr-Coulomb yield surface while the hardening law was described by a relationship in the mean normal stress - deviatoric stress - void ratio space. Their constitutive model was based on the results of a series of tri-axial tests. Another model recently developed by Heinonen (2002) does also incorporate the cap hardening and cohesive softening effects.

Given the results from the bi-axial tests mentioned above it was decided to explore the mechanical behaviour of the ice rubble in terms of the time-independent elasto-plasticity. As an example for studying the material behaviour a series of test from the Sayed et al. (1992) was taken and analyzed in terms of the elasto-plastic Mohr-Coulomb model.

2. Theoretical background

A review of the classical theory of elasto-plasticity with emphasis on granular materials is given in this section. In particular, the attention is focused on application of the classical Mohr-Coulomb model, which has been extensively used for the ice rubble since the research on this subject started. The reason for doing such a review is the need to set up a theoretical framework for analysis/planning of the tests and for the derivation of material parameters. Before applying the Mohr-Coulomb elasto-plastic model to the behaviour of the ice rubble in plane strain tests, the following assumptions are made:

a) Time-dependent deformations are neglected
b) Ice rubble will be considered as an isotropic, homogeneous material
c) The stresses and strains within the sample are uniform.

The elasto-plastic response of the material is based on underlying elastic response, however, the magnitude of the elastic contribution can be quite small and difficult to measure. The necessary ingredients in an elasto-plastic stress strain model are summarized below:

- Total strains = elastic + plastic strains:

$$d\boldsymbol{\varepsilon} = d\boldsymbol{\varepsilon}^e + d\boldsymbol{\varepsilon}^p \tag{1}$$

- A relationship that governs the elastic contribution: $d\boldsymbol{\varepsilon}^e = \mathbf{D}^{-1} d\boldsymbol{\sigma}$, where $\mathbf{D}$ is an elastic stiffness matrix. Description and estimation of the elastic contribution is beyond the scope of this paper. It is realized, however, that there exists a possibility to evaluate the elastic parameters of the ice rubble based on the properties of ice blocks. The micro to macro mechanics approach for estimation of effective elastic properties of the granular material is extensively described in, for example, Kapustiansky et al. (1996) and Walton (1987).

- And finally the ingredients to control the plastic contribution (derivations below are inspired by Nordal (2000)):

A yield criterion is an equation in stress tensor components and state variables. Normally the criterion is denoted $F(\boldsymbol{\sigma},\kappa)=0$ and this equation must be satisfied if any plastic strain shall develop. The κ is a general letter for a state variable and may be, for example, a degree of strength mobilization f. The Mohr-Coulomb yield criterion may be uniquely given in terms of the principal stresses:

$$F=(\sigma_1+a)-N(\sigma_3+a) \tag{2}$$

where the following state parameters are used:

$N=\dfrac{1+\sin\rho}{1-\sin\rho}$, ρ is the mobilized friction angle, $\tan\rho=f\cdot\tan\varphi$ and φ is the angle of internal friction; $a=c/\tan\varphi$ is the attraction where c is the cohesion.

The *Failure Criterion* is an ultimate *Yield Criterion* and distinguishes the obtainable stress states from the unobtainable stress states. If we define a stress space σ_{ij} then the yield criterion will define a yield surface in this stress space. The initial yield surface provides the elastic limit and the failure surface is the surface, which is defined by the failure criterion. An application of the general definitions in Eq. 2 is illustrated in Fig. 1.

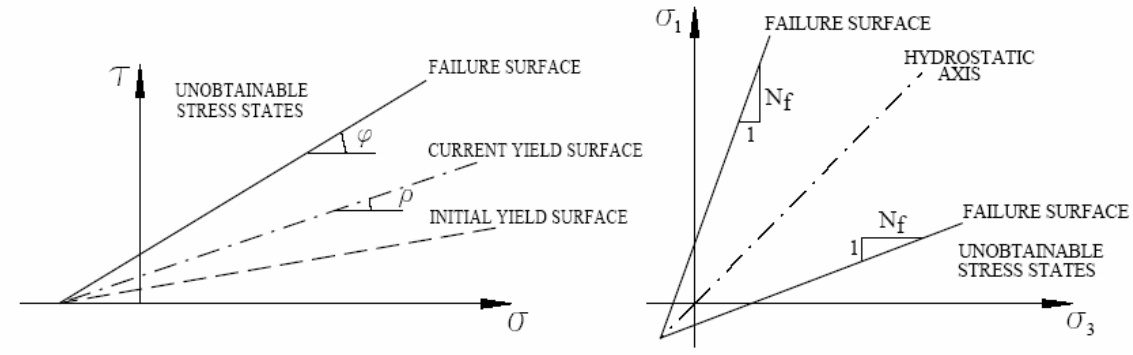

a) Yield surfaces in $\tau:\sigma$ stress space b) Yield surfaces in $\sigma_1:\sigma_3$ stress space

Fig. 1. Schematic illustration of the yield surfaces.

Further in the paper the Mohr-Coulomb yield criterion will be expressed in terms of the shear t and mean s stresses for the plane of interest:

$$F = \frac{t}{s+a} - \sin\rho = 0 \tag{3}$$

This is a shear yield criterion and it does not explain the plastic volume strain that may be measured in isotropic compression. For this purpose another type of surface can be introduced, the cap yield surface that will close the elastic region in the direction of the hydrostatic axis. However, the cap yield surface is not addressed in the present paper.

The flow rule must then be introduced to handle plastic deformations or plastic strains (irrecoverable). Plastic yielding may be associated with material flow which becomes unlimited or unconfined at failure. A general expression of an associated flow rule is given below:

$$d\boldsymbol{\varepsilon}^p = d\lambda \frac{\partial F}{\partial \boldsymbol{\sigma}} \tag{4}$$

As for any frictional material, the Mohr-Coulomb may be a fairly good yield criterion for ice rubble; however, the associated flow (i.e. normality to the yield surface) predicts plastic volume increase or a plastic dilation far above the values that can be experimentally observed. Furthermore, the plastic volume increase never stops as long as any plastic deformation takes place. Consequential, the material would expand tremendously under a process of continuous shearing. In order to avoid this unrealistic behaviour, the non-associated flow rule should be introduced and ∂F should be substituted by ∂Q in Eq.4, where Q is a plastic potential function:

$$Q = t - s\sin\psi \tag{5}$$

where ψ is the dilatancy angle.

The hardening rule defines the scalar $d\lambda$ in Eq. 4, which determines the size of the plastic strain increment. It relates the development of plastic strains to a movement of the yield surface. The movement is associated by plastic resistance and causes plastic strains to develop. The requirement of $F = 0$ during hardening may be written as (consistency equation):

$$dF = \left\{\frac{\partial F}{\partial \boldsymbol{\sigma}}\right\}^T d\boldsymbol{\sigma} + \frac{\partial F}{\partial \kappa} d\kappa = 0 \tag{6}$$

where κ is the scalar hardening parameter (degree of strength mobilization f).

The formulation of the Mohr-Coulomb criterion is well suited for isotropic strain hardening with $\sin\rho$ as a hardening parameter. The scalar measure for the amount of plastic strains is:

$$\boldsymbol{\varepsilon}^p = \sum \left| d\boldsymbol{\varepsilon}^p \right| = \sum d\lambda \sqrt{\left(\frac{\partial Q}{\partial \boldsymbol{\sigma}}\right)^2} \tag{7}$$

and hence the consistency equation may be rewritten in the following form:

$$\left\{\frac{\partial F}{\partial \boldsymbol{\sigma}}\right\}^T d\boldsymbol{\sigma} - A d\lambda = 0 \;\Rightarrow\; d\lambda = \frac{1}{A}\left\{\frac{\partial F}{\partial \boldsymbol{\sigma}}\right\}^T d\boldsymbol{\sigma} \tag{8}$$

where A is a plastic resistance number:

$$A = -\frac{\partial F}{\partial \kappa}\frac{\partial \kappa}{\partial \boldsymbol{\varepsilon}^p}\frac{\partial \boldsymbol{\varepsilon}^p}{\partial \lambda} \tag{9}$$

By this point all components needed to establish a constitutive relation between stresses and strains were defined. The elasto-plastic constitutive equation is given as:

$$d\boldsymbol{\sigma} = \mathbf{D}_{ep} \cdot d\boldsymbol{\varepsilon} \tag{10}$$

where the stiffness matrix $\mathbf{D}_{ep}$ can be written in the following form (some transition derivations are not shown):

$$\mathbf{D}_{ep} = \mathbf{D} - \frac{\mathbf{D}\left\{\frac{\partial Q}{\partial \boldsymbol{\sigma}}\right\}\left\{\frac{\partial F}{\partial \boldsymbol{\sigma}}\right\}^T \mathbf{D}}{\left[A + \left\{\frac{\partial F}{\partial \boldsymbol{\sigma}}\right\}^T \mathbf{D}\left\{\frac{\partial Q}{\partial \boldsymbol{\sigma}}\right\}\right]} \tag{11}$$

If F and Q are written in terms of stress tensor components then the gradients to the yield and potential functions are found by simple derivation. For the final determination of the coefficients of the elasto-plastic stiffness matrix the plastic resistance number A must be estimated by material testing.

3. Application for pure shear tests

The plastic resistance (or module) parameter for the case of the plane strain test and $\sin\rho$ as a hardening parameter is given as:

$$A = -\frac{\partial F}{\partial \kappa}\frac{d\kappa}{d\lambda} = -\frac{\partial F}{\partial \sin\rho}\frac{d\sin\rho}{d\lambda} = \frac{d\sin\rho}{d\lambda} \tag{12}$$

The flow rule and differentiation of the potential function with respect to stress tensor components gives the following:

$$d\varepsilon_1^p = d\lambda\left(\frac{1}{2} - \frac{\sin\psi}{2}\right);\; d\varepsilon_3^p = d\lambda\left(-\frac{1}{2} - \frac{\sin\psi}{2}\right) \tag{13a; b}$$

Thus the deviatoric plastic strain is uniquely related to the scalar $d\lambda$ as:

$$d\lambda = d\varepsilon_1^p - d\varepsilon_3^p = d\gamma^p \tag{14}$$

If the elastic shear modulus G is known or may be assumed / derived for the studied ice rubble, then the following expression can be obtained and the experimental curve for determination of the plastic resistance may finally be constructed:

$$d\gamma^p = d\gamma - d\gamma^e = d\gamma - {}^{t}\!/_{G} \tag{15}$$

The stress paths from the bi-axial experiments conducted by Sayed et al. (1992) are shown in Fig. 2. The summary of the characteristic stress and strain values needed for determination of the plastic resistance is given below in Table 1. Major σ_1 and minor σ_3 principal stresses were directly measured (Note: this may not be true if the friction at the boundaries is of significance for this particular test apparatus). The maximum shear stress τ is thus given as:

$$\tau = {}^{1}\!/_{2}(\sigma_1 - \sigma_3) = t \tag{16}$$

The value of the shear strain γ corresponding to τ was taken from the graphs presented by Sayed et al. (1992). It was further assumed that the elastic contribution is negligible and thus $d\gamma^p \cong d\gamma$ in Eq. 15. The values of the mobilized friction angle ρ were calculated using Eq. 2 based on assumption that the attraction a is zero following the approach that was used earlier in the analysis of the plain strain tests. Herein the angle ρ may indeed be regarded as an effective mobilized friction angle according to Ettema and Urroz-Aguirre (1991). It should be noted, however, that the effective friction angle concept may lead to under prediction of the strength capacity of ice rubble in case of the punch-like loading scenario (Liferov et al., 2002). Finally, the curves showing the relation between the mobilized angle of internal friction and the deviatoric plastic strains (shear strains γ) are given in Fig. 3.

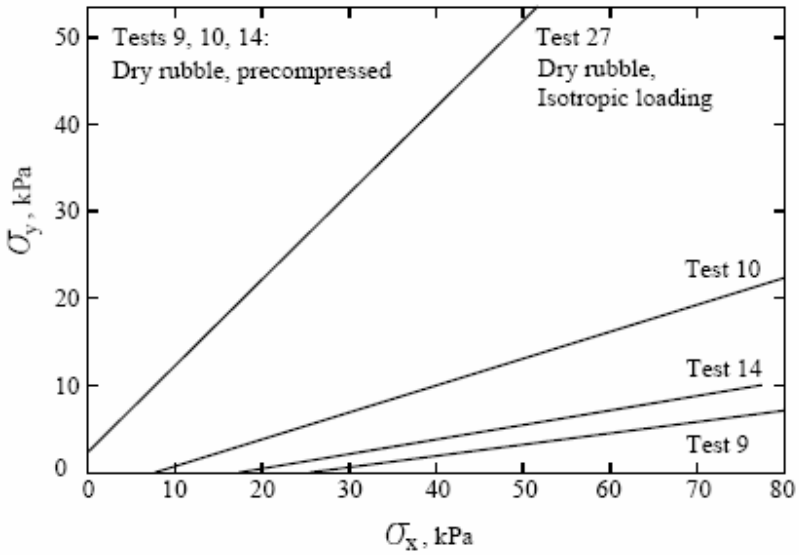

Fig. 2. Stress paths data from Sayed et al. (1992).

Table 1. Characteristic test results from Sayed et al. (1992).

σ_3, kPa (1)	σ_1, kPa (2)	τ, kPa (3)	γ (4)	$\sin\rho$ (5)
		Test 10		
0.1	9	4.5	0.003	0.98
5	26	10.5	0.004	0.68
10	43	16.5	0.028	0.62
15	59	22.0	0.043	0.59
20	72	26.0	0.085	0.57
25	88	31.5	0.100	0.56
		Test 14		
0.1	18	9.0	0.042	0.99
5	46	20.5	0.120	0.80
10	76	32.0	0.174	0.76
		Test 9		
0.1	26	13.0	0.061	0.99
5	71	33.0	0.205	0.87

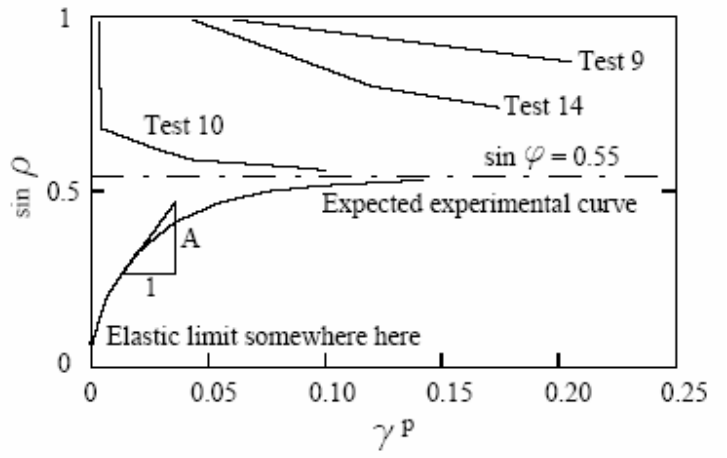

Fig. 3. Curve for determination of the plastic resistance (Note: attraction is assumed to be zero).

A curve that normally defines the plastic resistance of the material is shown in Fig. 3 below the asymptote $\sin\varphi = 0.55$ and is denoted as the expected experimental curve. The plastic parameter A is shown as a tangent to this curve and defines the plastic resistance as a function of the accumulated plastic shear strains. The experimental curves have a negative A that is a case for the softening behaviour if the elasto-plastic theory is valid for derivation of the ice rubble properties. The curves may be thought to proceed either towards the critical state or the residual state. However, the softening begins since the first step of loading and the mobilized angles of internal friction are unreasonably high. In this respect the experimental curves in Fig. 3 show that the unobtainable stresses have been reached and this is unacceptable within the theory described above. Alternatively this kind of behaviour may be attributed to the viscous phenomena. The importance of the viscous contribution for the ice rubble is basically a function of the strain rate and the temperature. Very slow loading makes the viscous effects dominant (e.g. deformation of glaciers) and fast loading also makes viscous behaviour important (e.g. penetration of a bullet through a steel plate). The stress states outside the failure surface as shown in Fig. 1 are unobtainable in a quasi-static formulation and in case when the stress path reaches the failure surface from the inside. However, if the viscous effects are taken into account and the very quick initial loading from the outside the failure surface is applied, it may be possible for the stress path to approach the failure surface from the quasi-statically unobtainable stress state. Similar concept was applied by Ioselevich et al. (1979) in their study of the loading surfaces in soils where they used the distinction between the immediate and the stable yield surfaces.

However, if the stress states reached throughout, for example, Test 10 are illustrated in form of the Mohr circles as shown in Fig. 4, it becomes apparent that the cohesion/attraction is not zero. By sketching an envelope to the Mohr circles the attraction is determined as 3.6 kPa. The corresponding mobilized angle of internal friction is 33º and the material neither hardens nor

softens. It should be noted that the envelope in Fig. 4 might be used only to determine the minimum possible attraction (assumed to be constant until the critical state is reached) of the tested material. The real attraction which is used in the Mohr-Coulomb failure criterion may be determined only if at least two ultimate Mohr circles are available. It is, however, not possible to say whether the circles in Fig. 4 are the ultimate ones or not. The shear strain versus shear stress curves from the proportional strain tests can neither provide sufficient information about the ultimate state of the material for the given ranges of stresses. If one assumes that in Fig. 4 the attraction is higher than 3.6 kPa then the ice rubble had been in the hardening state throughout test 10, i.e. the frictional resistance was being mobilized.

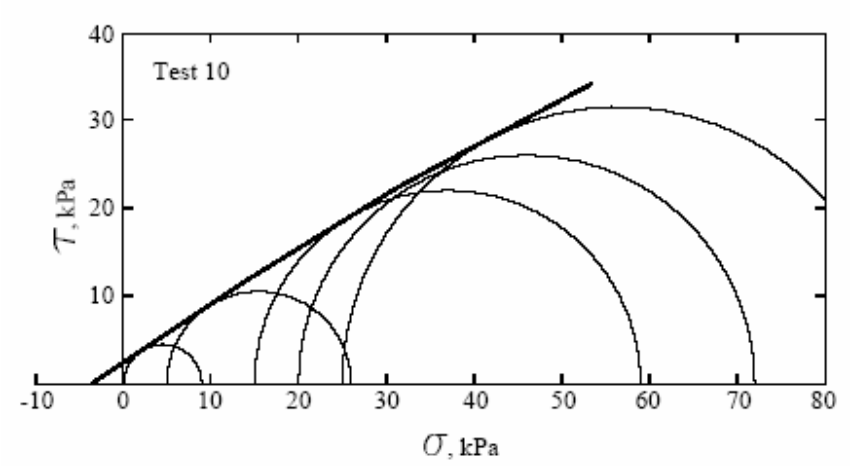

Fig. 4. Reached stress states throughout Test 10.

It is also interesting to note that for the same assumed attraction the mobilized angle of internal friction will be dependent on the mean pressure. The mobilized friction angle increases with increasing strain ratio (decreasing confinement). The same tendency was observed for the coarse soils. In granular materials with large particles the increase of mean pressure can cause the decrease of the angle of internal friction by 15-20º (Goldin and Rasskazov, 2001). This may be attributed to the breakage of the particles and the ice rubble may indeed be very susceptible to this. At low mean stresses when the ice pieces are prevented from breakage and the ice rubble is in a dense state the dilatancy effect may contribute to the mobilized ice rubble strength. The maximum mobilized angle of internal friction (peak angle) is substantially higher than the one that corresponds to the critical state. For sands the effect of the relative density of the sample and the mean pressure on the mobilized angle of internal friction was extensively studied by Bolton (1986). In an example given by Wood (1990) the maximum peak angle of shearing resistance (at low mean pressure) of the Chattahoochee river sand is 45º while the critical state angle is only 32º degrees.

In general it is difficult to distinguish whether the envelopes for tests 10, 14 and 9 are the failure envelopes or only the envelopes that reflect the state of the material to which it was brought during

the testing. The material properties (both for the elasto-plastic range and the ultimate ones) may not be reliably estimated based on the given data. The data from the constant lateral pressure (CLP) tests in the same apparatus as published by Cornett and Timco (1996) can provide better information about the material behaviour and its ultimate strength properties. An example of interpretation of the CLP test results taken from Cornett and Timco (1996) is illustrated below in Fig. 5.

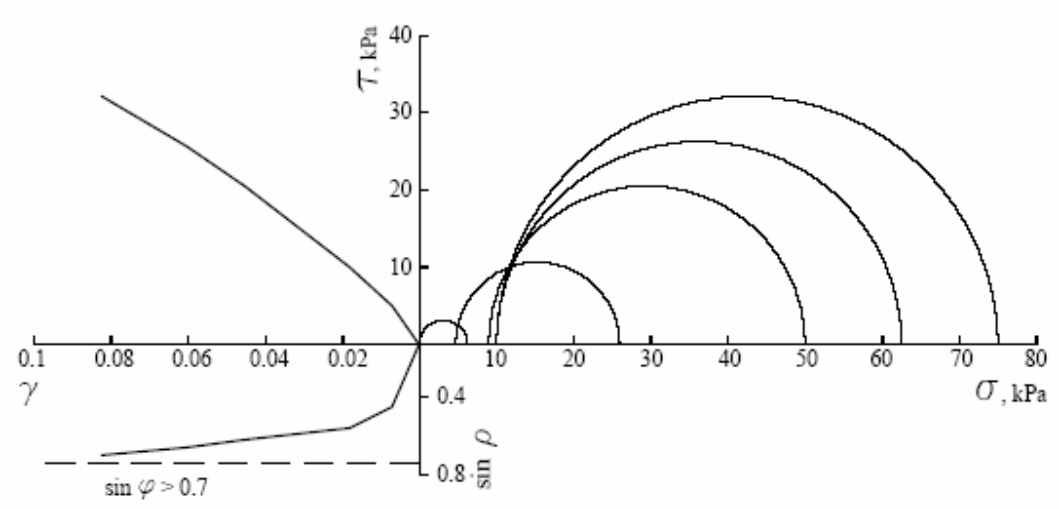

Fig. 5. CLP test no. 6, $\sigma_Y = const = 10\ kPa,\ a = 3.6\ kPa$.

The curve in Fig. 5 in the lower left corner (shear strain versus the mobilized angle of internal friction space) shows that in the given test the ice rubble resistance was not fully mobilized. The material was still in a hardening state and seemed to approach its ultimate state ($A \to 0$). The maximum friction angle that was mobilized in the test is 44º corresponding to an assumed value of attraction equal to 3.6 kPa. The obtained value of the friction angle for the ice rubble is indeed quite reasonable provided that no significant breakage of the particles took place. This may be attributed to the relatively large size of the ice blocks with respect to the size of the test chamber as well as to the shape of the ice blocks. Ivanov (1985) reports that large, poor-rounded particles may have the friction angles significantly higher than those for the small well rounded ones. If the assumed attraction of the ice rubble in Fig. 5 is 10 kPa, then the maximum corresponding value of the mobilized friction angle is 38º.

4. Conclusions

The behaviour of the ice rubble in the plain strain tests was analyzed. The analysis showed that the proportional strain tests alone might not be sufficient enough for derivation of the ice rubble properties. The analysis of the constant lateral pressure test showed that the ice rubble behaviour might be described by elasto-plastic model with shear strain hardening. The neglecting of the

cohesive component of the ice rubble shear strength may lead to the strength mobilization curves that can not be described in the framework of the conventional time-independent theory of elasto-plasticity. The mean pressure dependence of the angle of internal friction of the ice rubble cannot be verified until the ultimate state of the rubble is clearly determined and the volumetric behaviour of the ice rubble in CLP tests is further studied.

For further testing of the ice rubble it would be beneficial to choose the stress paths that follow the hydrostatic axis (pre-consolidation) until the certain limit before deviatoric loading is applied. This will allow to trace the elasto-plastic response of the material better and derive the associated material properties, including those that are needed for the non-associated flow rule.

Acknowledgement

The authors would like to thank Dr. M. Sayed for comments and review of this paper.

References

Bolton, M.D. (1986): The strength and dilatancy of sands. Geotechnique Vol. 36, No. 1, pp. 65-78.

Cornett, A.M. and Timco, G.W. (1996): Mechanical properties of dry saline ice rubble. Proceedings of the 6th Int. Offshore and Polar Engineering Conference (ISOPE'96), Vol. 2, pp. 297-303, Los Angeles, USA.

Ettema, R. and Urroz, G.E. (1991): Friction and cohesion in ice rubble reviewed. Proceedings of the 6th International Speciality Conference, Cold Regions Engineering (1991), pp. 316-325.

Goldin, A.L. and Rasskazov, L.N. (2001): Soil dams (in Russian), Moscow, 2001.

Heinonen, J. (2002): Continuum material model with shear-cap yield function for ice rubble. Proceedings of 15th Nordic Seminar on Computational Mechanics (NSCM 15), pp. 87-90, Aalborg, Denmark.

Hellman, J.H. (1984): Basic investigations of Mush Ice. Proceedings of the 7th Int. Symposium on Ice (IAHR), Vol. 3, pp. 37-55, Hamburg, Germany.

Ioselevich, V.A., Rasskazov, L.N., and Sysoev, U.M. (1979): On the development of yield surfaces in the process of plastic hardening (in Russian). Russian academy of science, Solid Mechanics series, no. 2, pp. 155-161.

Ivanov, P.L. (1985): Soils and foundations of the hydrotechnical structures (in Russian), Moscow, 1985.

Kapustiansky, S., Shkhinek, K. and Kärnä, T. (1996): A mathematical model of the ridge. Proceedings of the 13th Int. Symposium on Ice (IAHR), Vol. 1, pp. 335-345, Beijing, China.

Liferov, P., Jensen, A., Høyland, K.V. and Løset, S. (2002): On analysis of punch tests on ice rubble. Proceedings of the 16th Int. Symposium on Ice (IAHR), Vol. 2, pp. 208-216, Dunedin, New Zealand.

Løset, S. and Sayed, M. (1993): Proportional strain tests of fresh water ice rubble. Cold Regions Science and Technology, Vol. 7, No. 2, pp. 44-61.

Nordal, S. (2000): Lecture notes in the EEU/PhD course in soil modelling. Norwegian university of science and technology, Department of geotechnical engineering.

Prodanovic, A. (1979): Model tests of ice rubble strength. Proceedings of the 5th Int. POAC Conference, Vol. 1, pp. 89-105.

Sayed, M., Timco, G.W. and Lun, L (1992): Testing ice rubble under proportional strains. Proceedings of Offshore Mechanics and Arctic Engineering (OMAE'92) Conference, Vol. IV, pp. 335-341, Calgary, Canada.

Timco, G.W. and Cornet, A.M. (1999): Is φ a constant for broken ice rubble. Proceedings of 10th Workshop on river and ice measurements with a changing climate: Dealing with extreme events, pp. 318-331.

Timco, G.W., Funke, E.R., Sayed, M. and Laurich, P.H. (1992): A laboratory apparatus to measure the behaviour of ice rubble. Proceedings of Offshore Mechanics and Arctic Engineering (OMAE'92) Conference, Vol. IV, pp. 369-375, Calgary, Canada.

Urroz, G.E. and Ettema, R. (1987): Simple shear box experiments with floating ice rubble. Cold Regions Science and Technology, 14 (1987), pp. 185-199.

Walton, K. (1987): The effective elastic moduli of a random packing of spheres. J. Mech. Phys. Solids, Vol. 35, No. 2, pp. 213-226.

Wong, T.T., Morgenstern N.R. and Sego, D.C. (1990): A constitutive model for broken ice. Cold Regions Science and Technology, No. 17, pp. 241-252.

Wood, D.M. (1990): Soil Behaviour and Critical State Soil Mechanics. Cambridge University Press, 1990.

4.5 3D Finite element analysis of laboratory punch tests on ice rubble

P. Liferov[1,2], A. Jensen[2] and K.V. Høyland[3]

[1] NTNU, Trondheim, Norway
[2] Barlindhaug Consult AS, Tromsø, Norway
[3] UNIS, Longyearbyen, Norway

Abstract

A series of punch tests on ice rubble conducted at the Hamburg Ship Model Basin (HSVA) was analyzed. The tests were simulated using the PLAXIS finite element code. Both simple elastic-perfectly plastic Mohr-Coulomb and advanced hardening model with cap were used to simulate the ice rubble behaviour. The ice ridges were geometrically modelled as closely as possible to how they were really produced in the ice tank, i.e. as a part of the body consisting of the level ice/consolidated layer/ice rubble floating in the water. The material properties were chosen such that the simulated load-displacement curves fitted the experimental ones sufficiently close. Particular attention was focused on modelling the consistent behaviour of both the pushing platen and the surrounding ice sheet. The simulations showed that the bending effect and consequently the tensile strength of the ice rubble play an important role in this kind of punch tests or, more generally, in this kind of loading. Finally, the parametric study was carried out in order to investigate the influence of different ice rubble material parameters on its behaviour in the punch test.

1. Introduction

Loads from sea ice ridges on offshore structures are usually estimated by calculating the loads from the sail, the consolidated layer and the keel separately and adding them at the end. The consolidated layer is often considered to be a thick level ice sheet so that the thickness and the strength (flexural and compressive) become the vital parameters. The sail and particularly the rubble are often treated as a material that obeys the Mohr-Coulomb law. However, knowledge about the material properties of the ice rubble is rather limited although several programs on testing of ice rubble mechanical properties have been carried out since the beginning of the seventieths involving different shear box and punch tests (Leppäranta and Hakala, 1992; Timco and Cornett, 1999; Bruneau et al., 1997; Lemée and Brown, 2002). The variation in the reported values is not surprisingly wide. This may basically be attributed to difference in the test methods, stress strain paths, type of rubble, strain rate effects etc. Derivation of the material parameters from the conducted tests is another issue that demands particular attention. Two types of approaches have been used so far to derive the material

properties, i.e. analytical and numerical. In case of the shear box tests the derivation is rather straightforward and will not be discussed in this paper. In the analysis of the punch tests both approaches were used in the same manner: the experimental load-displacement curves or the limit values were fitted by adjusting the material properties (Azarnejad and Brown, 1998; Heinonen, 1999, 2002; Jensen et al., 2000; Liferov et al., 2002). The analytical approaches do not, however, take the complexity of the deformation mode into account and thus may yield to unreliable results.

The punch tests conducted in the field and in the laboratory are, in fact, not as similar as one may want them to be for the comparison purposes. In the field the ice rubble is pushed down in such a way that the bending effect is avoided. In the laboratory the ice rubble is loaded more realistically such that the bending effect is not omitted by artificial boundary conditions. In this respect it is worthwhile to mention the stress path method. Basically, the method tells that the material is likely to be tested under the same stress path, as it will be subjected to in the real-life loading situation. It is therefore very important to refer to the type of experiment and assumptions which were used to derive the rubble properties prior to applying them in a particular problem. In the present study the punch tests were modelled using the Finite Element Method (FEM) based 3D PLAXIS code (PLAXIS, 2000). The simulations were focused on analysis of the consistent behaviour of the artificial ice ridge in the punch down testing. The attention was further concentrated on how and which ice rubble parameters may influence the ultimate load that can be reached in the finite element modelling of the punch tests.

2. Experimental

Ridge production

The model ice sheets were produced according to the procedure described by Evers and Jochmann (1993). The salinity of the water in the basin was 8.5 ppt. The ridges were prepared by pushing level ice against a transverse beam as described by Høyland et al. (2001).

Punch tests

The goal of the experiments was to investigate the deformation mode of the ridges and to estimate the mechanical properties of the modelled ridge as well as to find out more about the mechanical behaviour of the rubble in the punch-loading scenario. The test program involved several experiments and it is described in Jensen et al. (2001). Herein only the large circular platen punch tests conducted at the centre line of the ice tank will be briefly described as only they were simulated numerically. A principal sketch of this test is given in Fig. 1. The large circular load platen had a diameter of 0.7 m and was loaded by 175 kg of steel weights. Penetration force *(Fz)* and displacements of the platen (*Z1)* and of the surrounding ice *(Z2)* were measured. The penetration speed was about 7 mm/s.

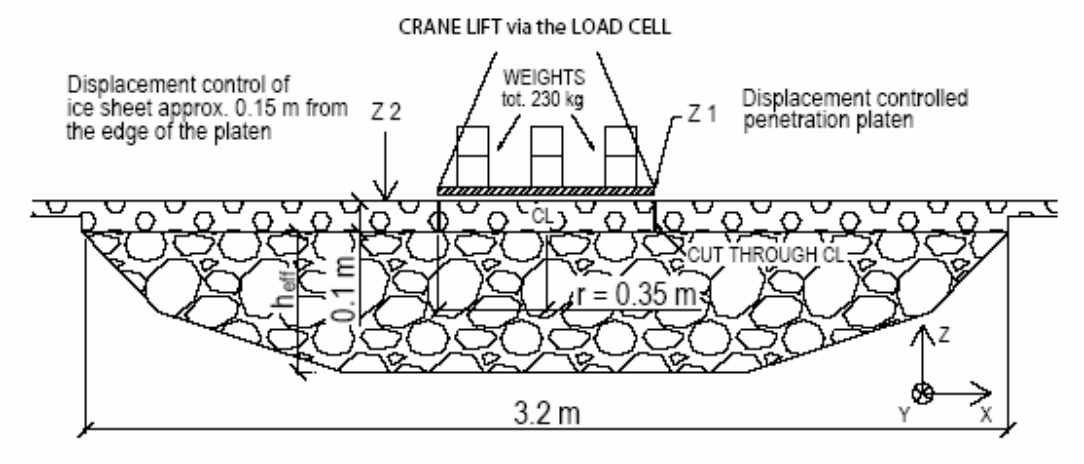

Fig. 1. Set-up of the ridge punch tests in the ice tank.

The ridges were prepared in order to measure only essential mechanical properties of the ridge keel. Basically, the preparation work comprised the following two steps: the sail was removed and the consolidated layer (CL) was cut free from the surrounding ice along the perimeter of the platen. During testing the platen was lowered until it was clear that failure had developed and then it was lifted up and lowered again.

3. Simulations

FE model

The finite-element model simulating the punch tests described above is shown in Fig. 2. As the simulated problem is neither axi-symmetrical nor plane-strain, it was decided to conduct the entirely 3D modelling. The model consisted of the 15-node second order 3D wedge elements. The wedge elements are composed of 6-node "unstructured" triangles in-plane (*X*-*Z* plane) and 8-node quadrilaterals in *Y*-direction. The quasi-static approach was used in the simulations and the iterative calculations were carried out until the prescribed displacement level was reached.

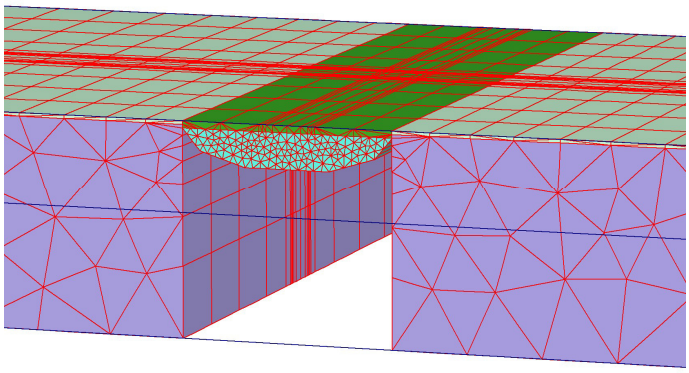

Fig. 2. Finite-element model of the simulated punch tests.

Boundary conditions and loading

The initial stress state inside the ice rubble was neglected, i.e. the ice rubble was considered as a weightless material. The ice sheet was modelled resting on the underlying elastic layer whose properties were calibrated such that it perfectly modelled the water for the particular needs. In the part of the cross-section where the ice rubble existed the elastic layer underneath was deactivated as it could impose unrealistic boundary conditions at the bottom of the keel, i.e. $\sigma_z \neq 0$ and $\tau_{xy,xz} \neq 0$. In this area the buoyancy force was modelled as an imposed traction load applied to the bottom of the consolidated layer and proportional to the displacement of the ice sheet in *Z*-direction. As the ice became fully submerged the buoyancy load was set to a constant value. The displacement of the platen was prescribed to a value that was recorded during the experimental testing. The material properties of the ice rubble were then adjusted in order to fit the recorded load-displacement curve.

Material models

Level ice and consolidated layer were modelled as an elastic material. Their Youngs' moduli were estimated from the 3-point bending tests performed by (Jensen et al., 2001). Their values are given in Table 1.

Table 1. Youngs' moduli of the level ice and the consolidated layer.

Level Ice	Consolidated Layer
$E_{LI} = 11.7$ *MPa*	$E_{CL} = 17.1$ *MPa*

Two types of material models were used for the ice rubble: the elastic-perfectly plastic Mohr-Coulomb model and the hardening model with cap. A brief description of the material models and their specific features is given further.

- *Mohr-Coulomb model*

An elastic-perfectly plastic model is a constitutive model with a fixed yield surface, i.e. a yield surface that is not affected by plastic straining. The yield surface does thus always coincide with the failure surface, which is defined by six yield functions of the following form when formulated in terms of principal stresses σ_i, σ_j :

$$F = (\sigma_i + a) - N(\sigma_j + a) \tag{1}$$

where the following state parameters are used:

$N = \frac{1+\sin\varphi}{1-\sin\varphi}$, φ is the angle of internal friction; $a = c/\tan\varphi$ is the attraction where c is the cohesion.

The plastic potential functions are used to control the plastic volumetric strains:

$$Q = \frac{1}{2}(\sigma_i - \sigma_j) + \frac{1}{2}(\sigma_i + \sigma_j)\sin\psi \tag{2}$$

where ψ is the dilatancy angle.

For $c > 0$, the standard Mohr-Coulomb criterion allows for tension. However, the ice rubble may sustain smaller tensile stresses than those, which are defined by the standard form of the failure criterion. In order to account for this type of behaviour, three additional yield functions must be introduced:

$$F = \sigma_i - \sigma_t \text{ and } 0 \le \sigma_t \le a \tag{3, 4}$$

where σ_t is the allowable tensile stress in the ice rubble.

The elastic (stiffness) properties of the model are defined by the Young's modulus E_{50} and the Poisson's ratio μ. E_{50} is a secant modulus taken at the 50 % mobilized strength. The material model described above is illustrated in Fig. 3 in the shear stress versus normal stress space.

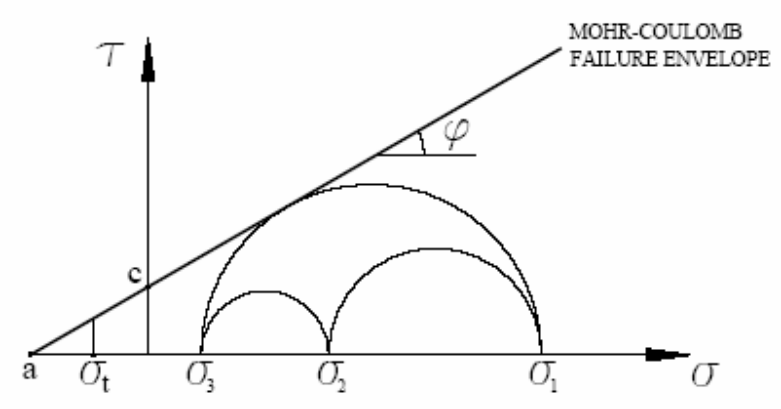

Fig. 3. Mohr-Coulomb model with tension cut-off (allowable tensile strength).

- *Hardening model with cap*

In contrast to an elastic perfectly-plastic model, the yield surface of the hardening model is not fixed in a principal stress space, but it can expand due to plastic straining (isotropic hardening model). The failure occurs when the yield surface touches the Mohr-Coulomb failure surface, which is described above. Both shear and compression hardening are implemented in the model used. Comprehensive description of the present material model is given in PLAXIS (2001). The present model is illustrated in Fig. 4. Note that the magnitude of the yield cap is determined by the pre-consolidation stress p_p, which means that for the given assumption (initial stress state inside the ice rubble is neglected) the initial length of the ellipse on both axes is zero.

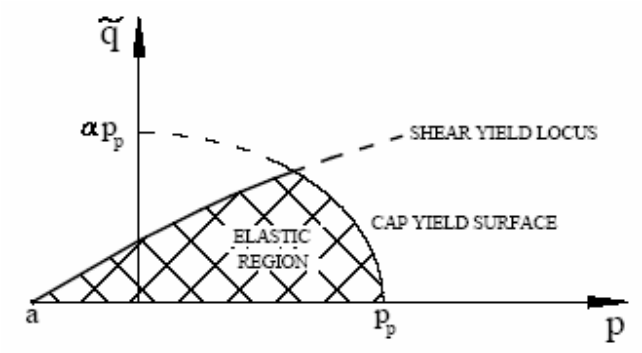

Fig. 4. Hardening model with cap (the notations used are given below).

$\tilde{q} = \sigma_1 + (\delta - 1)\sigma_2 - \delta\sigma_3$ (special stress measure for deviatoric stresses); $\alpha \leftrightarrow 1 - \sin\varphi$;

$\delta = (3 + \sin\varphi)/(3 - \sin\varphi)$; $p = (\sigma_1 + \sigma_2 + \sigma_3)/3$.

The elastic region can be further reduced by means of the allowable tensile strength. In the principal stress space both the shear locus and the yield cap have a hexagonal shape of the classical Mohr-

Coulomb failure criterion. The shear yield locus can expand up to the ultimate Mohr-Coulomb failure surface while the cap yield surface expands as a function of the pre-consolidation stress, which in the present case computed from the reached stresses inside the ice rubble.

4. Results

General

The goal of the modelling was to fit the experimental curves by the simulated ones. Both the shape of the curves and their ultimate values were fitted. Nevertheless, no particular efforts were put into "refining" the fitting and the attention was rather focused on the parametric study that follows below. One test on a large ridge (h_{eff} = 50 cm) and one test on a small ridge (h_{eff} = 40 cm) were chosen for the modelling corresponding to ridges 2001 and 2002 as described in Jensen et al. (2001). The results of the simulations are shown in Figures 5a, b and 6. The material parameters used in the simulations are given in Table 2.

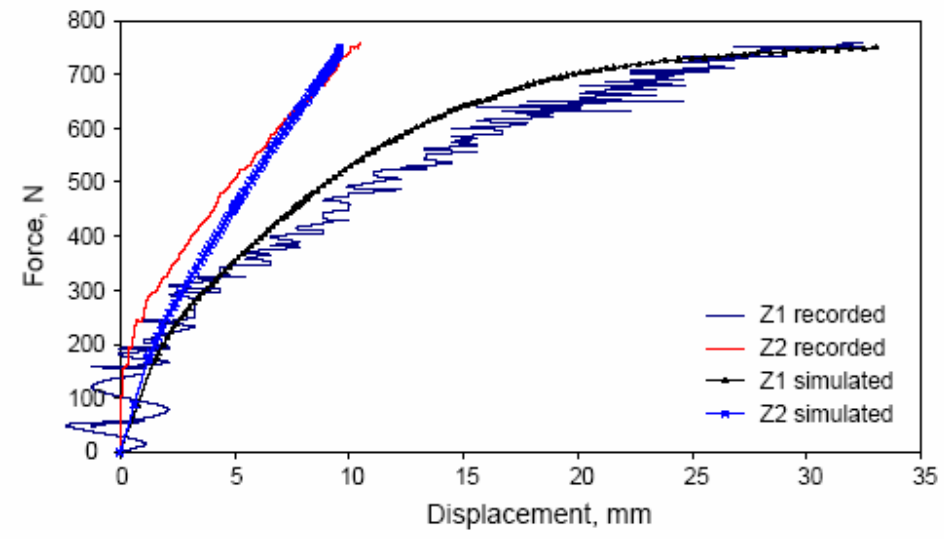

Fig. 5a. Load-displacement curve, large ridge, c = const.

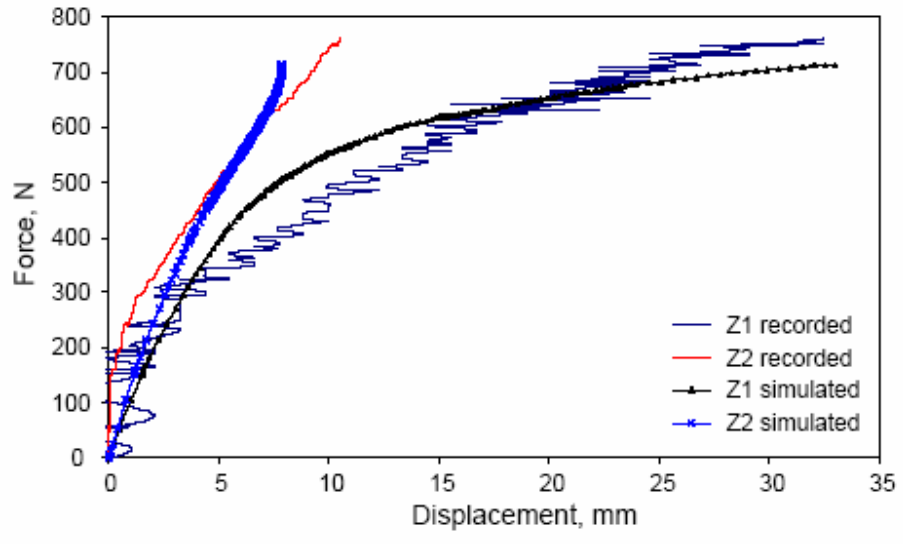

Fig. 5b. Load-displacement curve, large ridge, $c \neq$ const.

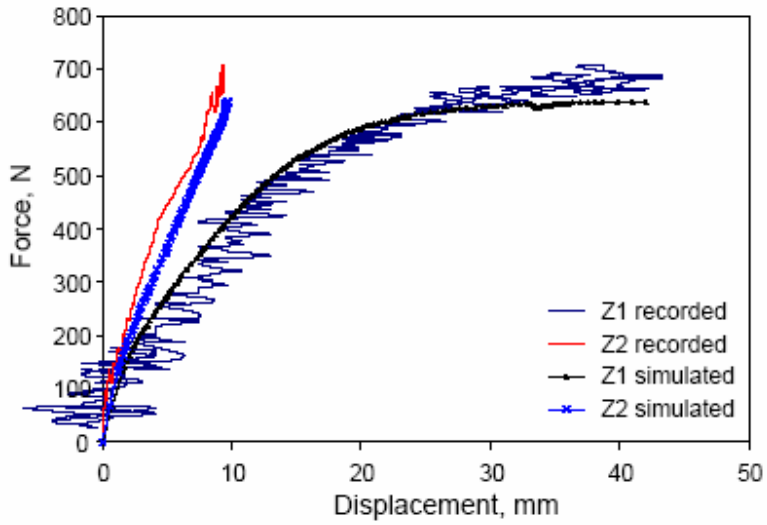

Fig. 6. Load-displacement curve, small ridge (Note: Recorded force includes the buoyancy load that is 40 kN at 40 mm displacement).

Table 2. Material parameters used for the curve fitting (Mohr-Coulomb model).

	E_{50}, kPa	μ	c, kPa	φ, °	ψ, °	σ_t, kPa
Large1	1100	0.3	0.45	35	0	0.25
Large2	1100	0.3	Linearly varying 1.2 (top) – 0 (bottom)	35	0	$a = c/\tan\varphi$
Small	1100	0.3	0.50	35	0	0.25

Two stiffness regions separated at about 1-2 mm displacement were obtained as a result of the simulations as shown in Figs. 5 and 6. This coincides well with the experimental records. The

analysis of the material state at the transition point (large ridge, c = const) shows that in the first high stiffness region the ice rubble fails in tension in the lower part of the ridge (Fig. 7). The ice rubble underneath the platen is not deviatorically disturbed. After this the slip surface begins to develop through the keel (Fig. 8) and the stiffness drops approaching zero at failure (Fig. 9). The cross sections on figures below show the cut through the middle of the ridge perpendicular to its CL. The plastic Mohr-Coulomb stress points are indicated with red dots and the tension cut-off points are indicated with white dots.

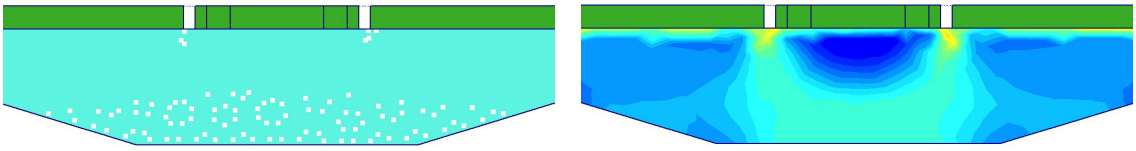

(a) Plastic/Tension cut-off points (b) Relative shear stresses

Fig. 7. Stress state inside the ice rubble at 1.5 mm displacement of the platen.

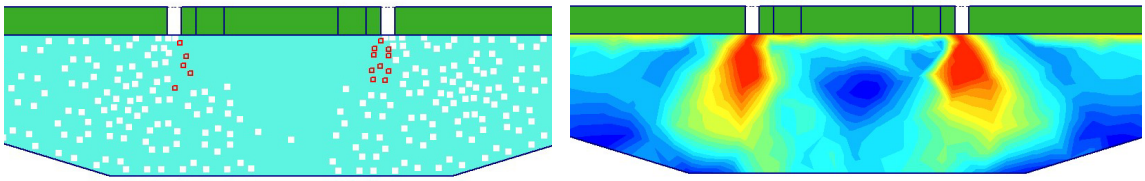

(a) Plastic/Tension cut-off points (b) Relative shear stresses

Fig. 8. Stress state inside the ice rubble at 6 mm displacement of the platen.

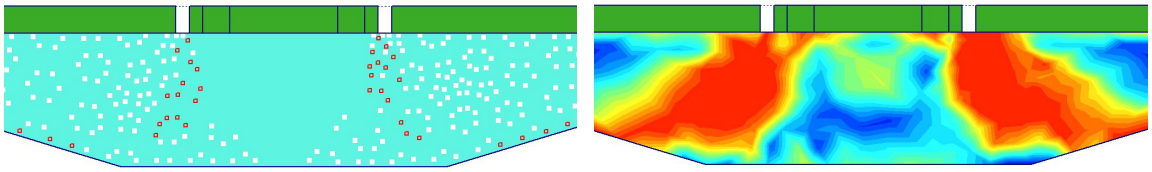

(a) Plastic/Tension cut-off points (b) Relative shear stresses

Fig. 9. Stress state inside the ice rubble at failure.

The relative shear stresses give an indication of the proximity of the stress point to the Mohr-Coulomb failure envelope. The relative shear stress, τ_{REL}, is defined as:

$$\tau_{REL} = \tau / \tau_{MAX} \tag{5}$$

where τ is the maximum reached value of shear stress. The parameter τ_{MAX} is the maximum value of shear stress for the case where the Mohr's circle is expanded to touch the Coulomb failure envelope keeping the intermediate principal stress constant.

Several simulations were also conducted applying the hardening model with cap. However, as there are more input parameters for this model compare to the basic Mohr-Coulomb, the "fitting" of the single experimental load – displacement curve is much more arbitrary and unreliable with respect to the chosen model parameters. The results of the simulations are therefore not presented in this paper. Nevertheless, the simulations were analyzed with respect to the volumetric plastic strains in the ice rubble. It was found that the plastic volumetric strains are concentrated at the contour of the "bulb" beneath the platen.

Parametric Study

The parametric study was conducted in order to investigate the influence of the material parameters on the peak load (bearing capacity) and the failure mode of the ice rubble. The geometry of the large ridge was used in the modelling. The results of the study with respect to the peak load are presented below in Figs. 10, 11 and 13.

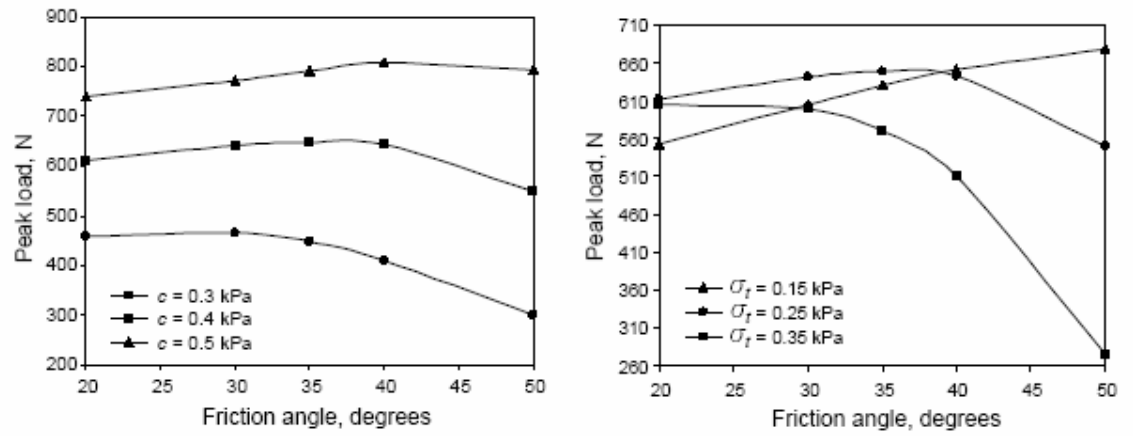

(a) $E = 480$ kPa; $\mu = 0.3$; $\sigma_t = 0.25$ kPa; $\psi = 0°$

(b) $E = 480$ kPa; $\mu = 0.3$; c= 0.4 kPa; $\psi = 0°$

Fig. 10. Peak load versus the angle of internal friction.

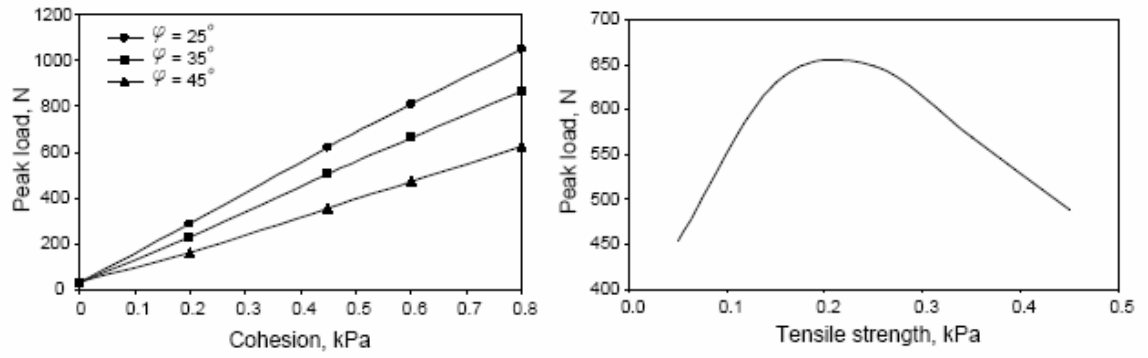

(a) Cohesion (E = 1100 kPa; μ = 0.3; $\sigma_t = c / \tan\varphi = a$ kPa; ψ = 0°).

(b) Allowable tensile strength (E = 480 kPa; μ = 0.3; c = 0.4 kPa; φ = 35°; ψ = 0°).

Fig. 11. Peak load versus cohesion and allowable tensile strength.

The curves presented in Figs. 10 and 11 basically tell the following:

- The peak load is to a large extent dominated by cohesion.
- The cohesion and the angle of internal friction do not contribute separately to the peak load; their contribution is rather combined and it affects the local failure mode.
- The failure of the ice rubble under the punch loading is quite complex as it involves bending and therefore the tensile strength of the ice rubble is of importance.

The curve on Fig. 11b shows a distinct transition between two failure modes as a function of the allowable tensile strength of the ice rubble. When the tensile strength is less than 0.2 kPa the propagating tensile failure from the bottom upwards was observed. At higher values of the tensile strength the failure in tension was omitted and the friction angle controlled resistance dominated. The peak load was attributed to the transition case where none of the mechanism dominates. Fig. 10 shows that the peak load decreases as a certain value of the friction angle is reached and this transition value depends on the cohesion and the allowable tensile strength. Moreover, Fig. 11a shows that for the same values of cohesion in the classical Mohr-Coulomb failure criteria the higher peak loads corresponds to smaller values of the angle of internal friction. The physical explanation of this tendency is given by recalling the illustration of the Mohr-Coulomb failure criteria and focusing on the area close to the axes intercept as shown in Fig. 12. Significant part of the ice rubble is in the stress zone, which is denoted as the area of interest in Fig. 12. In fact, in the area on the left side of the τ axis, i.e. in the tension zone, the increase of the friction angle from φ_1 to φ_2 causes the reduction of the stress space inside the failure surfaces. Thus, the strength of the ice rubble is reduced particularly in its lower part.

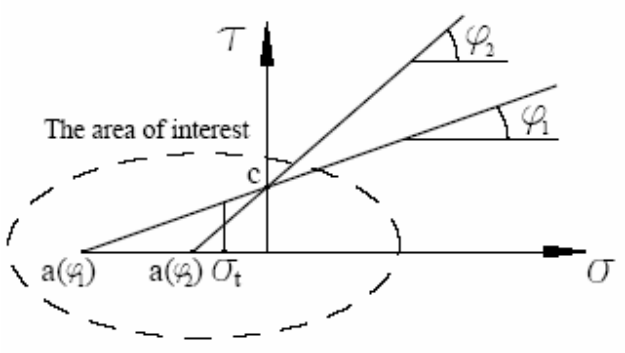

Fig. 12. Close-up on the near axes intercept area in the Mohr-Coulomb model.

The influence of the dilatancy angle and the Young's modulus of the material was also investigated and the results are shown in Fig. 13.

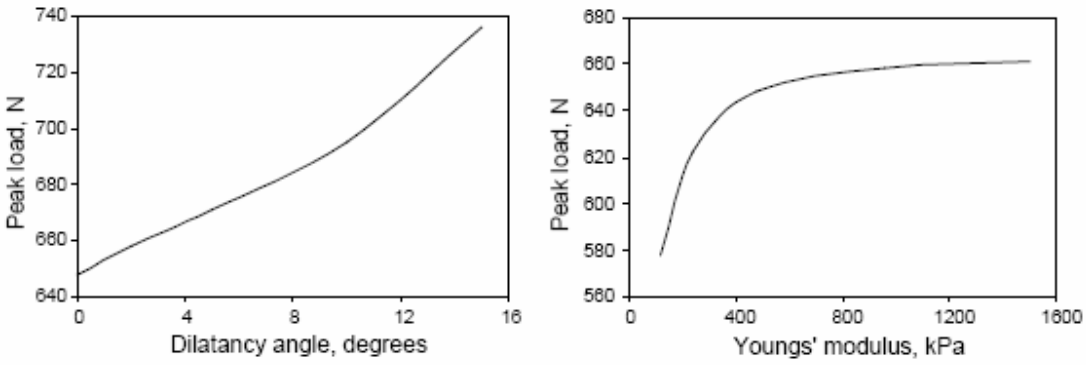

(a) Dilatancy angle (E = 480 kPa; μ = 0.3; c = 0.4 kPa; σ_t = 0.25 kPa; φ = 35°)

(b) Young's modulus (μ = 0.3; c = 0.4 kPa; σ_t = 0.25 kPa; φ = 35°; ψ = 0°).

Fig. 13. Peak load versus the dilatancy angle and the Young's modulus.

5. Conclusions and recommendations

The paper describes a series of finite-element simulations of the punch tests on ice rubble. The simulations were conducted in order to investigate numerically the behaviour of ice ridge under punch loading and to study the influence of ice rubble material parameters on the failure mode and the peak load. It was found that the failure mechanism consisted of the combination of bending and punch through effects. The analysis of stress state inside the ice rubble from the experimental curve fitting simulations showed the following:

- Initial loading caused the bending of the ice sheet (including the ice ridge) and the ice rubble failed in tension in the lower part of the keel. This corresponds to the initial high stiffness region on the load-displacement curve.

- Further the slip line (failure plane) started to propagate through the rubble and the stiffness began to drop approaching zero at failure.

The additional failure surface was added to the standard Mohr-Coulomb failure criterion in order to control the tensile strength of the ice rubble. The parametric study showed that the strength parameters of the material do not contribute independently to peak load. Basically, it was found that strength of the ice rubble in the punch test is largely dominated by cohesion and tensile strength. The local failure mode is rather complex and depends on combination of the material properties. It was also shown that increase of the friction angle may cause decrease of the attained peak load when the bending of the ice formation is not prevented. It may also be pointed out that the cohesion of the simulated ice rubble could be in order of 0.5 kPa while its tensile strength is about 0.25 kPa and they are constant for the material. These values correspond to the assumed angle of internal friction of 35º and they provide the best fit of the experimental curves.

Derivation of ice rubble properties from the punch tests and their analysis is of importance with respect to similar type of loading in the real life situations. However, application of the results obtained from punch tests to another type of loading may not be correct, particularly where the ice rubble is subjected to higher confinement and subsequent deviatoric loading. Another tests (e.g. different types of shear tests) are needed to investigate the frictional behaviour of ice rubble. Finally, it should be noted that application of the Mohr-Coulomb model (as any kind of model) and its parameters must be carefully thought through with respect to the method of analysis used and the anticipated boundary conditions.

Acknowledgement

The research activities carried out at the Major Research Infrastructure ARCTECLAB were granted by the Human Potential and Mobility Programme from the European Union through contract HPRI-CT-1999-00035.

References

Azarnejad, A. and Brown, T.G. (1998). Observations of ice rubble behaviour in punch tests. Proceedings of the 14th International Symposium on Ice (IAHR), Potsdam, USA, Vol. 1, pp. 589–596.

Bruneau, S.E., McKenna, R.F., Croasdale, K.R. and Crocker G.C. (1996). In-situ direct shear of ice rubble in first year ridge keels. Proceedings of the 49th Canadian Geotechnical Conference, St. John's September 1996.

Evers, K.-U. and Jochmann, P. (1993). An advanced technique to improve the mechanical properties of model ice developed at the HSVA ice tank. Proceedings of the 12th International Conference on Port and Ocean Engineering under Arctic Conditions (POAC), Hamburg, Germany, Vol. 2, pp. 877 – 888.

Heinonen, J (1999). Simulating ridge keel failure by finite element method. Proceedings of the 15th POAC Conference, Vol. 3, pp. 956–963.

Heinonen, J. (2002). Continuum material model with shear-cap yield function for ice rubble. Proceedings of 15th Nordic Seminar on Computational Mechanics (NSCM 15), pp. 87-90, Aalborg, Denmark.

Høyland, K.V., A. Jensen, P. Liferov, J. Heinonen, K.-U. Evers, S.Løset and M. Määttänen (2001). Physical modelling of first-year ice ridges – Part I: Production, consolidation and physical properties. Proceedings of the 16th International Conference on Port and Ocean Engineering under Arctic Conditions (POAC), Ottawa, Canada, Vol. 3, pp. 1483-1492.

Jensen, A., Løset, S., Høyland, K.V., Liferov, P., Heinonen, J, K.-U. Evers and M. Maattanen (2001). Physical modelling of first-year ice ridges – Part II: Mechanical properties. Proceedings of the Conference on Port and Ocean Engineering under Arctic conditions (POAC), Vol. 3, Ottawa, Canada (2001), pp. 1493–1502.

Jensen, A., Høyland, K.V. and Evers, K.-U (2000). Scaling and measurements of ice rubble properties in laboratory tests (2000). Proceedings of the 15th International Symposium on Ice (IAHR), Gdansk, Poland, Vol. 1, pp. 63–72.

Lemée and Brown (2002). Small-scale plain strain punch tests. Proceedings of the 16th International Symposium on Ice (IAHR), Dunedin, New-Zealand, Vol. 2, pp. 1–8.

Leppäranta, M. and Hakala, R. (1992). The structure and strength of first-year ridges in the Baltic Sea. Cold Regions Science and Technology 20: 295–311.

Liferov, P., Jensen, A., Høyland, K.V. and Løset, S (2002). On analysis of punch tests on ice rubble. Proceedings of the 16th International Symposium on Ice (IAHR), Dunedin, New-Zealand, Vol. 2, pp. 101–109.

PLAXIS (2001): Plaxis 3D Tunnel. Finite Element Code for Soil and Rock Analyses. Material models manual, www.plaxis.nl.

Timco, G.W. and Cornet, A.M. (1999): Is φ a constant for broken ice rubble. Proceedings of 10th Workshop on river and ice measurements with a changing climate: Dealing with extreme events, pp. 318-331.

4.6 On analysis of punch tests on ice rubble

P. Liferov[1,2], A. Jensen[2], K.V. Høyland[3] and S.Løset[1]

[1] NTNU, Trondheim, Norway
[2] Barlindhaug Consult AS, Tromsø, Norway
[3] UNIS, Longyearbyen, Norway

Abstract

Punch tests on ice rubble conducted at the University of Calgary and at the Hamburg Ship Model Basin (HSVA) were analyzed. They were simulated using the PLAXIS finite element code. Special care was taken of the loading and the boundary conditions of the ice rubble and in particular of the buoyancy force and the in-plane friction forces. Simple Mohr-Coulomb material was used to simulate the ice rubble. The material properties were chosen such that peak values of the experimental and the simulated load – displacement curves were roughly the same. The simulations showed that the bending effect and consequently tension play an important role in punch tests. The effect of the material parameters on the bearing capacity of the rubble in punch tests was also analyzed. Cohesion seems to be the major contributor to the bearing capacity of the ice rubble, as the frictional resistance is not well mobilized in the punch tests.

1. Introduction

Sea ice ridges are formed by compression or shear in the ice cover. They are porous ice features consisting of ice, water, air and snow. The part above the water line is called the sail and consists of ice, air and snow, whereas the keel below the water line consists of ice and water. The pores in the upper part of the keel freeze up during the cold season and form a refrozen or consolidated layer. Thus, a ridge is often divided in three parts: the sail, the consolidated layer (the upper part of the keel) and the unconsolidated (or much less consolidated) ice rubble. Material parameters of the first-year ridges are not well known yet (Croasdale et al., 1999). Knowledge about properties of the ice rubble (in the following we will use this term for the lower part of the keel only) is even more limited. It is also worthwhile to mention that the ice rubble, like geotechnical materials can exhibit very different properties from one material to another. Several programs on testing of ice rubble mechanical properties have been carried out since the beginning of the seventies. Most of the experiments were done in laboratories with artificially produced ice rubble. Two basic types of experiments were done: shear tests and punch tests all resulting in some values of material properties. First shear tests were done with a simple shear box (Prodanovic, 1979; Hellman, 1984)

followed by the skew box tests (Urroz and Ettema, 1987), the plane-strain apparatus tests (Løset and Sayed, 1993) and the more sophisticated bi-axial tests (Timco et al., 1992). Extensive reviews of these tests and interpretation of the results are given by Timco and Cornet (1999) and Ettema and Urroz (1991). However, there exists a very wide variation in the reported values. One of the reasons comes from the difference in tested materials as the fresh water ice cubes from the commercial machines and the saline nature-like ice rubble will definitely exhibit different properties. Another reason comes from the influence of test method and test conditions, particularly the boundary conditions. Altogether this does not give the appropriate values for the assessment of the full-scale loads from the first-year ice ridges. This has caused a need for the in-situ testing and for a possibility to relate them to the same type of tests done in the laboratory.

The first attempt on the in-situ testing was undertaken by Leppäranta and Hakala (1992) in the Baltic Sea where they did several punch tests on the first-year ice ridges. More recently punch tests have been performed in-situ by Heinonen and Määttänen (2000) and Bruneau et al. (1998). Several punch test programs were also carried out in the laboratory (Azarnejad and Brown, 1998; Jensen et al., 2001, 2000). Punch tests have the definite advantage that it is possible to do them both in-situ and in the laboratory on ice rubble that is in its natural state. Interpretation of the test results, i.e. the derivation of material properties from the recorded force and displacement curve is among the major disadvantages of the punch tests. A numerical analysis seems to be the only way to analyze these tests in a proper way.

In the present study the punch tests were simulated using the Finite Element Method (FEM) based PLAXIS code (PLAXIS, 2000). FEM-based approach for the analysis of punch tests was originally used by Heinonen (1999). As the FEM is based on the continuum mechanics, the ice rubble is considered as a continuum media. There is no doubt about the discrete nature of the ice rubble and that its effect increases with decrease of the rubble formation/particle size ratio. However, the FEM has proven to be very efficient and accurate in the soil mechanics and as long, for example, as the substitution of the ice rubble with the continuum media gives the results that fit the experiments the FEM can be used in the ice rubble mechanics. Moreover, FEM may be very useful and efficient in modelling of the ice rubble/structure or, for example, ice rubble/soil interaction. The main question is thus to estimate the range of the material parameters that substitutes the ice rubble and evaluate the effect of their variation on the load level that the ice rubble formation may exert on the structure.

2. Simulated tests and models

The major purpose of this study was to analyze the behaviour of the ice rubble in the laboratory punch tests and to derive the material parameters from the experimental records. Two different

punch tests were chosen for simulation. Let us refer to Azarnejad and Brown (1999) and PERD/CHC Report 5-109 (2000) for the description of the tests conducted at the University of Calgary. These tests are further called CHC tests. The next series of tests were conducted at the HSVA in Hamburg and is described by Jensen et al. (2000, 2001). These tests are further called HSVA tests. Only the 2D plane strain test from the HSVA series was simulated. The principal models of the tests are shown in Fig. 1.

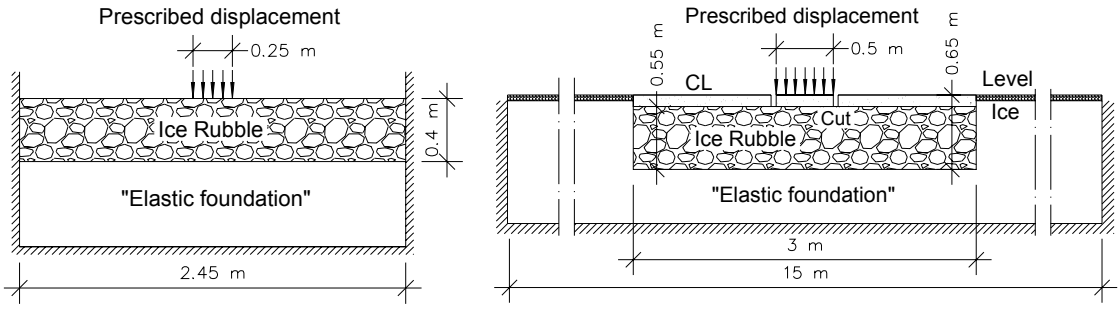

a) CHC b) HSVA

Fig. 1. Principal models of the CHC and HSVA punch tests.

The same modelling approach was used for both tests. Particular care was taken of the buoyancy force acting on the submerging ice rubble. This was done due to fairly significant contribution of the buoyancy force associated with the movement of the platen and the ice under the platen to the measured peak force during the punch tests. The ice rubble was modelled as an elastic-plastic material lying (e.g. floating) on an "elastic" foundation. The "elasticity" of the foundation was justified such that it exactly simulated the buoyancy force acting on the submerging rubble. The porosity of the ice rubble was assumed to be 0.3 and this value was used for evaluation of the buoyancy force. The buoyancy load acting in each vertical cross-section of the ice rubble was modelled as a linearly increasing load until the upper bound of this section was submerged. After this the buoyancy load was constant. The Mohr-Coulomb material was used to simulate the ice rubble.

CHC tests

The quasi-static approach was used in the simulations and thus these tests may be considered for simulations of the low-speed tests only. The effect of the friction between the rubble and the in-plane tank walls on the failure mode was not taken into account in the model (plane strain conditions). However, taking into account that the roughness of the middle part of the in-plane walls was not artificially increased, we may assume that the plain strain conditions were more or less satisfied in the area where the plug failure took place. This is particularly true for the zero-age tests. Displacements were also quite substantial and thus the dynamic friction coefficient may be used in the estimation of the contact friction forces. The effect of the out-of-plane boundaries was

studied by specifying different strength properties of the ice rubble/out-of-plane tank wall interface. The iterative calculations were carried out until the limit load was reached. The elastic properties of the ice rubble were kept constant in all simulations. The Youngs' modulus of the ice rubble was set to 150 kPa in order to fit the level of experimental displacements.

HSVA test

The 2D test at HSVA was modelled fairly much in the same way as the CHC tests except for that at HSVA the ice rubble was a part of the modelled nature-like ice ridge, see Fig. 1b. The stiffness of the level ice and consolidated layer was estimated from 3-point bending tests performed by (Jensen et al., 2001). The derived Young's modules are given in Table 1.

Table 1. Youngs' moduli of the level ice and the consolidated layer.

Level Ice	Consolidated Layer
E_{LI} = 11.7 MPa	E_{CL} = 17.1 MPa

3. Results of simulations

The friction force between the ice rubble and the in-plane boundaries (e.g. two tank walls in a paper plane) was roughly estimated for both tests. The stresses in the x_3-direction (normal to in-plane), σ_{33}, are not zero. Their magnitudes at the final iteration stage were estimated in each stress point. Then the average stress acting in the x_3-direction, $\tilde{\sigma}_{33}$, was estimated as:

$$\tilde{\sigma}_{33} = \frac{1}{n}\sum_{i=1}^{n}\sigma_{33}^{i} \tag{1}$$

where n is a number of the stress points.

Then the contact friction force F_{CF} may be roughly estimated assuming that it is linearly proportional to the average stress $\tilde{\sigma}_{33}$ via the contact friction coefficients. The assumed friction coefficients are given in Table 2.

Table 2. Assumed contact friction coefficients.

Ice - Perspex	Ice – "rough" Perspex	Ice – Lexan glass	Ice – tank wall at the HSVA
0.3	0.4	0.2	0.5

CHC tests

Punch tests on the 0.4 m thick ice rubble were simulated. The cut around the platen was not simulated. The real (experimental) out-of-plane width of the platen was 0.5 m. The simulated load – displacements curves show the results for the model where the out-of-plane dimension is one meter. The contact friction force F_{CF} was estimated to be in a range of 41 N. Taking into account the buoyancy of the platen F_{PB} which equals to 22 N (Azarnejad and Brown, 1998), the load F in the simulated tests corresponding to the "Peak-Initial" load in the original experimental tests may be estimated as:

$$F = 0.5 \cdot F_{CURVEs} + F_{CF} + F_{PB} \tag{2}$$

where F_{CURVEs} is the ultimate simulated load (Note: tank width in the original experiments was 0.5 m). The example of the load – displacement curves from the CHC tests is given in Fig. 2. It shows the influence of cohesion on the ultimate load that the rubble can take.

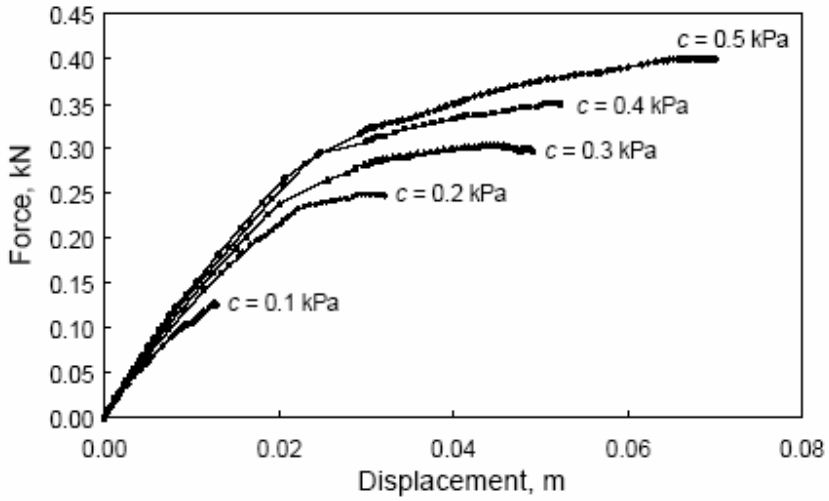

Fig. 2. Load – displacement curves; $\varphi = 40^{\circ}$.

The effect of the variation of the angle of internal friction is shown in Table 3 (cohesion equals to 0.3 kPa for this set of simulations).

Table 3. Effect of the angle of internal friction on the bearing capacity.

Angle of internal friction	25°	30°	35°	40°	45°
Ultimate load, N	272	281	292	302	309

From the analysis of the stress state inside the rubble under loading it became clear that the lower part of the rubble is in tension. According to the Coulomb envelope this is allowed when the shear

stress (radius of Mohr circle) is sufficiently small. However, the ice rubble may also fail in tension instead of in shear. Such effect was analysed by specifying the allowable tensile strength (tension cut-off) of the ice rubble. The results of this effect are shown in Table 4 (cohesion equals to 0.3 kPa and the angle of internal friction equals to 40° for this set of simulations).

Table 4. Effect of the angle of internal friction on the bearing capacity.

Tension cut-off, kPa	0	0.05	0.1	0.2	0.3
Ultimate load, N	265	286	298	301	302

Simulations also showed that the strength of the interface between the rubble and the out-of-plane tank walls has minor influence on the ultimate load. The influence of the ice rubble properties on the inclination of the failure planes was also observed. The angle of the "failure cone" α does slightly increase as the cohesion increases. With increase of the angle of internal friction the "cone" angle increases significantly. Fig. 3 shows the plots of the total strains of two simulations.

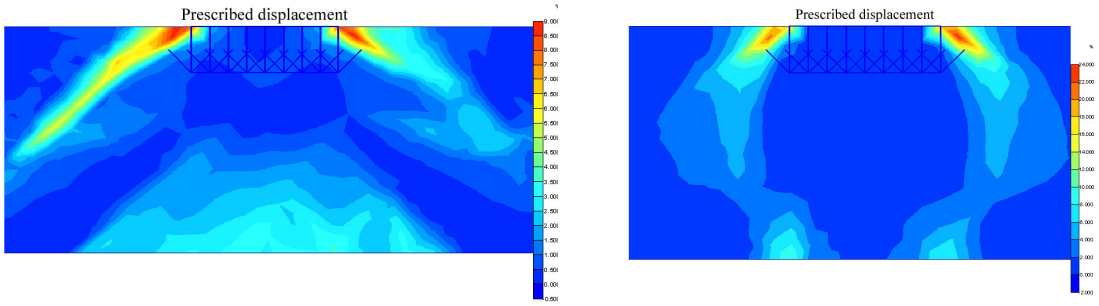

a) $\varphi = 45^{\circ}; c = 0.3$ kPa b) $\varphi = 25^{\circ}; c = 0.3$ kPa

Fig. 3. Influence of the angle of internal friction on the failure cone angles.

The stress state inside the ice rubble is illustrated in Figs. 4a-c $(\varphi = 40^{\circ}; c = 0.3\ kPa)$. Fig. 4a shows the plot of the relative shear stresses. The relative shear stresses give an indication of the proximity of the stress point to the failure envelope. The relative shear stress, τ_{REL}, is defined as:

$$\tau_{REL} = \tau / \tau_{MAX} \tag{3}$$

where τ is the maximum value of shear stress (i.e. the radius of Mohr's stress circle). The parameter τ_{MAX} is the maximum value of shear stress for the case where the Mohr's circle is expanded to touch the Coulomb failure envelope keeping the intermediate principal stress constant. Figs. 4b and 4c show the plots of the normal stresses acting on the planes A-A and B-B as indicated on Fig. 4a.

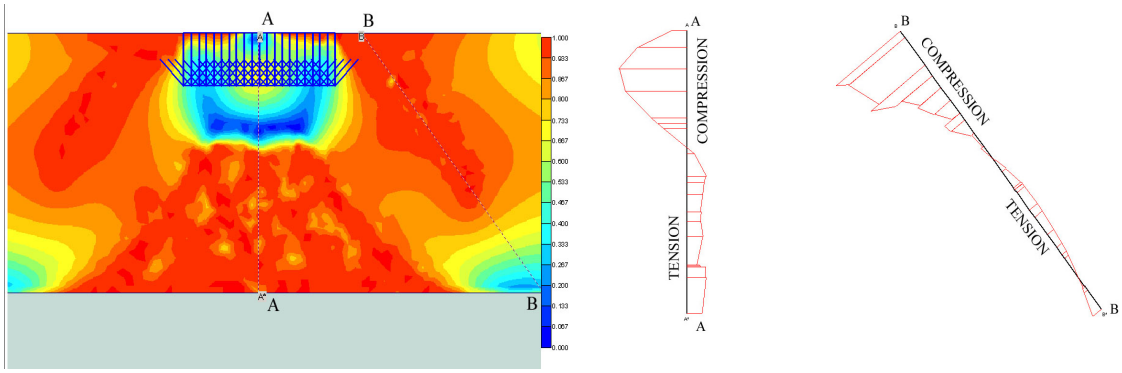

a) Relative shear stresses b) Section A - A c) Section B - B

Fig. 4. Indication of the stress state inside the ice rubble.

HSVA test

Here the intention was to simulate the particular test and try to estimate the ice rubble parameters that satisfy the peak load and the corresponding displacement of the pushing platen, which was 1.5 m wide in the out-of-plane direction. The failure pattern observed during the experiment was the secondary but not less important input for the simulation. The displacement of the ice sheet one meter away from the centreline of the platen was also traced during the simulation. As in the CHC tests simulations, the simulated load – displacements curves (Fig. 5) show the results for the model where the out-of-plane dimension is one meter. The contact friction force F_{CF} in case of the HSVA 2D test is estimated from the simulations by the procedure described above to be in a range of 50 N. The buoyancy of the platen F_{PB} at the moment of peak load is 4.5 N. Thus, the load F in the simulated test corresponding to the failure load in the original experiment may be estimated as:

$$F = 1.5 \cdot F_{CURVE} + F_{CF} + F_{PB} \tag{4}$$

where F_{CURVE} is the simulated load at the failure of the rubble.

The characteristic points from the experimental curves (Jensen et al., 2001) are given in Table 5. Ice rubble properties corresponding to the presented curves are given in Table 6. The modulus of elasticity of the HSVA ice rubble is six times that of the CHC rubble. We have so far no explanation for this very significant difference though the modulus of elasticity mainly affects the magnitude of deformations.

Table 5. Characteristic points at failure from the experimental curves.

	Failure load, N	Platen displacement, mm	Ice sheet displacement, mm
Experimental	657	28	7
Simulated, *F*	653	28	11

Table 6. Ice rubble properties.

Young's modulus, kPa	Cohesion, kPa	Tension cut-off, kPa	Angle of internal friction, °
900	0.35	0.15	28

The failure palette inside the ice rubble is shown in Figs. 6a and 6b in terms of the total strains and the relative shear stresses respectively.

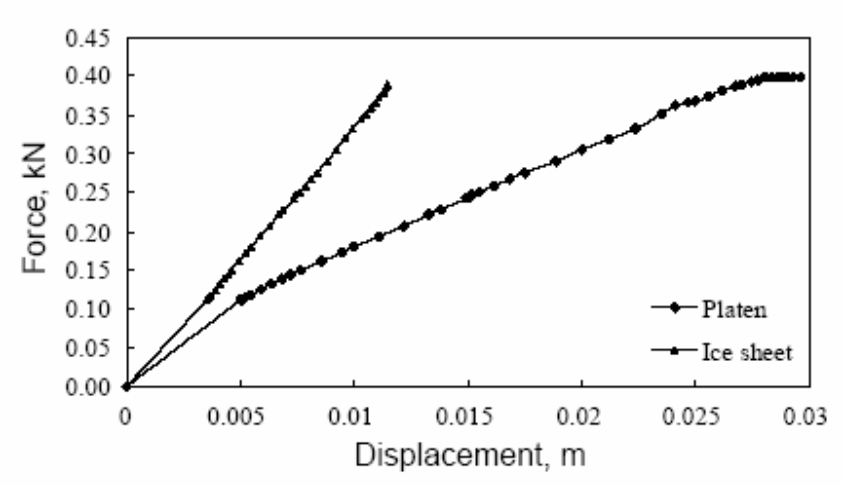

Fig. 5. Load – displacement curves.

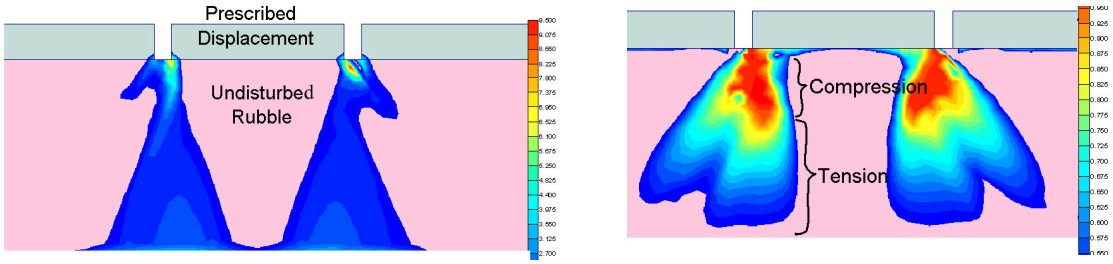

a) Total strains. b) Relative shear stresses.

Fig. 6. Failure palette inside the ice rubble.

4. Discussion on test results

In both tests the failure mechanism consisted of the combination of the "plate bending" and pushing through effects. In the HSVA 2D test the bending effect was somewhat higher than in the CHC tests. In the CHC tests the out-of-plane boundary conditions have minor influence on the failure zone and on the ultimate load. However, the in-plane boundaries may significantly contribute to the total measured load. The influence of the cohesion on the bearing capacity of the rubble is the same as it was observed by Heinonen (1999). The frictional resistance of the ice rubble against the pushing load was minor compared to the "cohesive" component. It becomes apparent from Figs. 4b,c and Fig. 6b that the frictional resistance cannot be mobilized along the entire failure plane because of the extensive tensile zone in the lower part of the rubble. Punch tests may not be good enough for the appropriate estimate of the frictional resistance of the ice rubble. It would be beneficial to carry out both the punch and the shear box tests on the same material in order to estimate the effect of testing method on the measured material parameters.

The calculations carried out by Azarnejad and Brown (1998) using the Meyerhof's theory seem to give higher values for the angle of internal friction and lower values for cohesion in their best fit analysis. The independently calculated cohesion (assuming the angle of internal friction to be zero) is fairly close to what the simulated results show. The typical values of the "Peak-initial" load from the CHC experiments (PERD/CHC Report 5-109, 2000), the corresponding simulated rubble parameters and the results obtained by Azarnejad and Brown (1998) are given in Table 7 (low speed tests, rubble thickness is 0.4 m).

Table 7: Ice rubble properties from the CHC tests.

Age, hours	"Peak – initial", N	Rubble properties, simulated	Best fit analysis	Average of independent values
0	110 - 130	$c = 0.1 - 0.2$ kPa $\varphi = 25 - 45^{\circ}$	Not given	Not given
1	180 - 240	$c = 0.2 - 0.35$ kPa $\varphi = 25 - 45^{\circ}$	$c = 0.026 - 0.030$ kPa $\varphi = 47.5 - 61.5^{\circ}$	$c = 0.288 - 0.435$ kPa $\varphi = 58.9 - 73.6^{\circ}$

The load – displacement curves from the HSVA 2D test simulation shown in Fig. 5 and the failure palette show fairly the same rubble behaviour as it was observed and recorded during the experiments. Two stiffness regions were observed. In the first high stiffness region most of the tensile failure in the lower part of the rubble takes place. The estimates of the rubble parameters from the current simulations show values that are in the same range as estimated by Jensen et al. (2000) for the HSVA-made ice ridges.

Acknowledgement

The authors would like to thank Dr. Garry Timco who has kindly provided us with the unpublished data from the punch tests conducted by Azarnejad and Brown (1998) at the University of Calgary. We would also like to thank Prof. Karl Shkhinek for extensive review and valuable comments.

References

Azarnejad, A. and Brown, T.G. Observations of ice rubble behaviour in punch tests. In Proceedings of the 14th International Symposium on Ice (IAHR), Vol. 1, Potsdam, USA (1998) 589–596.

Bruneau, S.E., Crocker, G.B., McKenna, R.F., Croasdale, K., Metge, M., Ritch, R. and Weaver, J.S. Development of techniques for measuring in-situ ice rubble strength. In Proceedings of the 14th International Symposium on Ice (IAHR), Vol. 2, Potsdam, USA (1998) 1001–1007.

Croasdale, K. A study of ice loads due to ridge keels. In Proceedings of the 4th International Conference on Development of Russian Arctic Offshore (RAO), Vol. 1, St.Petersburg, Russia (1999) 268–274.

Ettema, R. and Urroz, G.E. Friction and cohesion in ice rubble reviewed. In Proceedings of the 6th International Speciality Conference, Cold Regions Engineering (1991) 316–325.

Heinonen, J. Simulating ridge keel failure by finite element method. In Proceedings of the 15th POAC Conference, Vol. 3 (1999) 956–963.

Heinonen, J. and Määttänen, M. LOLEIF ridge-loading experiments-analysis of rubble strength in ridge keel punch test. In Proceedings of the 15th International Symposium on Ice, Vol. 1 (2000) 63–72.

Hellman, J.H. Basic investigations of Mush Ice. In Proceedings of the 7th International Symposium on Ice (IAHR), Vol. 3 (1984) 37–55.

Jensen, A., Løset, S., Høyland, K.V., Liferov, P., Heinonen, J, K.-U. Evers and M. Maattanen. In Proceedings of the Conference on Port and Ocean Engineering under Arctic conditions (POAC), Vol. 3, Ottawa, Canada (2001) 1493–1502.

Jensen, A., Høyland, K.V. and Evers, K.-U. Scaling and measurements of ice rubble properties in laboratory tests. In Proceedings of the 15th International Symposium on Ice (IAHR), Vol. 1, Gdansk, Poland (2000) 63–72.

Leppäranta, M. and Hakala, R. (1992): The structure and strength of first-year ridges in the Baltic Sea. Cold Regions Science and Technology 20: 295–311.

Løset, S. and Sayed, M (1993): Proportional strain tests of fresh water ice rubble. Cold Regions Science and Technology 7(2): 44–61.

PERD/CHC Report 5-109. Experimental Investigation of Ice Rubble Behaviour and Strength in Punch Tests. National Research Council of Canada, March (2000).

PLAXIS Finite Element Code for Soil and Rock Analyses. Reference manual. www.plaxis.nl (2000).

Prodanovic, A. Model tests of ice rubble strength. In Proceedings of the 5th International POAC Conference, Vol. 1, (1979) 89–105.

Timco, G.W. and Cornett, A.M. Is φ a constant for broken ice rubble? In Proceedings of 10th Workshop on river and ice measurements with a changing climate: Dealing with extreme events (1999) 318–331.

Timco, G.W., Funke, E.R., Sayed, M. and Laurich, P.H. A laboratory apparatus to measure the behaviour of ice rubble. In Proceedings of Offshore Mechanics and Arctic Engineering (OMAE'92) Conference, 7-11 June (1992).

Urroz, G.E. and Ettema, R. Simple shear box experiments with floating ice rubble. Cold Regions Science and Technology 14: 185–199 (1987).

5 SUMMARY, CONCLUSIONS AND RECOMMENDATIONS FOR FURTHER WORK

5.1 Summary and conclusions

In-situ modelling of the first-year ice ridge scour

Two in-situ medium scale ice ridge scour tests and one keel shear-off test have been carried out in the Van Mijen fjord on Spitsbergen. Ice ridges with dimensions of up to 4.0 × 4.0 × 2.45 m have been artificially made by cutting the level ice into pieces to produce ice rubble. The ridges were left to consolidate for up to four weeks. The consolidation process in the ridges was monitored by means of thermistor strings and mechanical drilling. Two of the three ridges have then been pulled towards the beach scouring the seabed that consisted of clayey sediments (ice scour tests). The ice ridge for the shear off test was built up in a pre-excavated trench in hard moraine. During pulling the keel of the ice ridge was sheared off by the sidewall of the trench. The pulling force, displacements, failure of the keel and resulting plough marks were measured. The most important results are as follows:

- Two ice ridge scour tests revealed, under given conditions, the steady state scour process, i.e. when the scour depth does not change significantly along the scour track. This agrees well with recent laboratory tests on ice scour and, that is most important, with observations from seabed mapping in the areas that are of interest for the oil industry.
- Experiments showed that there are two main competing mechanisms that result in the steady state scour: the heave of the ridge and the destruction of the keel. Another mechanism, the compaction of the keel, could also be of importance though it is less in magnitude.
- The magnitude of the keel destruction was in the order of the scour depth and the heave of the ridge.
- Keel failure appeared to be not simultaneous, but progressive.
- The shear-off test has been specially designed to test the keel in the shear mode under natural conditions. The strength properties of the keel in terms of the Tresca and the Mohr-Coulomb material models were evaluated.

- The rubble first becomes stronger as freeze bonds develop during the initial phase. Then it gradually decays due to erosion from the surrounding currents and the internal energy flux between the water in the pores and the pieces of ice.

Review and analysis of ice rubble behaviour and strength

Tests on ice rubble that were conducted during the last three decades have been reviewed and compared with respect to their characteristic behaviour, mechanical properties and scaling. Particular attention has been focused on *why* do the different tests result in different values for the rubble strength and *what* could bring better agreement in this field. The main conclusions of this study are as follows:

- There were observed two different failure modes in a number of different tests on ice rubble. The primary failure mode is controlled by the initial strength of rubble skeleton, i.e. by freeze bonds between blocks inside the rubble. This mode may dominate the overall strength of rubble accumulation under certain conditions, particularly in case of relative proximity of the stress-free boundaries. Otherwise it may control the local resistance at the propagating failure in case of large rubble accumulations. Frictional resistance of the rubble will not be mobilized in this failure mode. Secondary failure mode may dominate the overall strength of rubble accumulation at propagating failure under boundary conditions that provide sufficient confinement. It is associated with substantial deformations and frictional resistance will be mobilized in this failure mode. Dynamic freeze-bonding between the blocks may define the "cohesive" component of rubble resistance in the secondary failure mode.
- When ice rubble is subjected to deformations at high speeds, the inertia stress field superimposed on the statically admissible stress field may cause increase in rubble resistance to externally applied disturbance. Hydrodynamic effects could also be of importance when testing submerged ice rubble at high speeds.
- Application of the two-parametric Mohr-Coulomb material model to describe ice rubble strength can well be sufficient provided that appropriate values of cohesion and friction angle are used.
- Application of the *c/t* scaling results in the value of about 20 kPa/m from the overview of available data. This value is likely to describe the rubble cohesion in the primary failure mode. In the secondary failure mode the frictional resistance dominates and the values of the mobilized friction angle can be in the order of 40-45º. Higher frictional mobilization is not likely due to the suppression of dilatancy. The values of cohesion in the secondary failure mode are substantially less than that in the primary mode.

- The behaviour of the ice rubble in the plain strain tests was analyzed. The analysis showed that the proportional strain tests alone might not be sufficient enough for derivation of the ice rubble properties.
- The analysis of the constant lateral pressure test showed that the ice rubble behaviour might be described by elasto-plastic model with shear strain hardening. The neglecting of the cohesive component of the ice rubble shear strength may lead to the strength mobilization curves that can not be described in the framework of the conventional time-independent theory of elasto-plasticity.

Numerical modelling of ice rubble (A): failure modes

A pseudo-discrete continuum model has been developed to simulate the micro-mechanical behaviour of ice rubble. This model enabled to study numerically the primary failure mode of ice rubble. The secondary failure mode has been described with a non-linear Mohr-Coulomb failure envelope. The most important results of this work are as follows:

- Failure of ice rubble in the primary mode was mainly associated with the breakage of the contacts between the blocks though some local breakage of individual blocks also occurred.
- The shear strength of rubble increased more or less linearly with increasing strength of the freeze bonds between the blocks.
- The shear strength increased non-linearly with increase of confining pressure. A change of failure mechanism from tensile to shear was observed as confinement increased.
- There was shown a good agreement between the interface strength (i.e. freeze bond strength) in the pseudo-discrete model and the equivalent cohesion (i.e. shear strength) in the continuum model.
- Non-linearity of the Mohr-Coulomb failure envelope is caused by suppression of dilatancy. Accounting for this phenomenon will prevent overestimation of the rubble resistance at high normal stresses.

Numerical modelling of ice rubble (B): simulations of punch tests

Finite element analysis has been used to simulate the laboratory punch tests on ice rubble and to derive the material properties. The simulations were conducted in order to investigate numerically the behaviour of ice rubble under punch loading and to study the influence of ice rubble material parameters on the failure mode and the peak load. The main conclusions are the following:

- It was found that the failure mechanism consisted of the combination of bending and punch through effects. The analysis of stress state inside the ice rubble from the experimental curve fitting simulations showed the following:
  - Initial loading caused the bending of the ice sheet (including the ice ridge) and the ice rubble failed in tension in the lower part of the keel. This corresponds to the initial high stiffness region on the load-displacement curve.
  - Further, the slip surface (failure plane) started to propagate through the rubble and the stiffness began to drop approaching zero at failure.
- The additional failure surface has been added to the standard Mohr-Coulomb failure criterion to control the tensile strength of ice rubble.
- The parametric study showed that the strength parameters do not contribute independently to peak load. Basically, it was found that strength of the ice rubble in the punch test is largely dominated by cohesion and tensile strength.
- Direct comparison of the laboratory and the in-situ punch tests is not entirely correct and requires accounting for the complex deformation modes under certain boundary conditions at the laboratory testing.
- It was also shown that increase of the friction angle may cause decrease of the attained peak load when the bending of the ice formation is allowed.
- The cohesion of the simulated ice rubble was in order of 0.5 kPa while the tensile strength in order of 0.25 kPa. These values correspond to the assumed angle of internal friction of 35º and provided the best fit of the load-displacement curves from physical experiments.

5.2 Recommendations for further work

The following topics seem promising when extensions of the present work are being considered:

In-situ modelling of the first-year ice ridge scour

- The subscour soil deformations could be studied during the in-situ ice ridge scour tests. This would enable to create evidence from a relatively large-scale experiment in the field where the lack of experimental data is substantial.
- A pipeline could be places both on and into the seabed to study its response to the ice ridge scour event.

Ice rubble testing

- Scaling of ice rubble in the laboratory tests should be given a lot more attention. Thermodynamic scaling is of particular importance.
- Experiments on freeze bonding between the blocks in ice rubble would provide valuable source for numerical models that deal with inter-particle contacts.

Numerical modelling of ice rubble

- A pseudo-discrete continuum model of ice rubble could be further developed by utilizing recent advances in the finite element calculations such as the meshless and the Arbitrary-Lagrangian-Eulerian methods. This would enable to account for large displacements within the rubble and to continue simulations after the global stiffness has approached zero.
- More work should be done on verification of different numerical models of ice rubble. Analysis of tests on ice rubble, e.g. full-scale and laboratory punch tests, could be done using different numerical and analytical approaches.

Numerical modelling of the first-year ice ridge scour

- Simulations of the full scale ice ridge scour are needed based on the carefully evaluated material parameters for the full-scale ice ridges.
- An approach to model the first-year ice ridge scour process could be developed by integrating findings from the in-situ ice ridge scour tests described in Chapter 3 with numerical simulations and review of ice rubble properties addressed in Chapter 4.